AD-A182 608 TECHNOLOGY DEVELOPMENT FOR MILLIMETER WAVE PHASED ARRAYS(U) MASSACHUSETTSUUNIV AMHERST DEPT OF ELECTRICAL AND COMPUTER EN D W SCHAUBERT ET AL MAY 87 1/2

UNCLASSIFIED RADC-RR-87-42 F19628-84-K-0022 F/G 9/1 NL

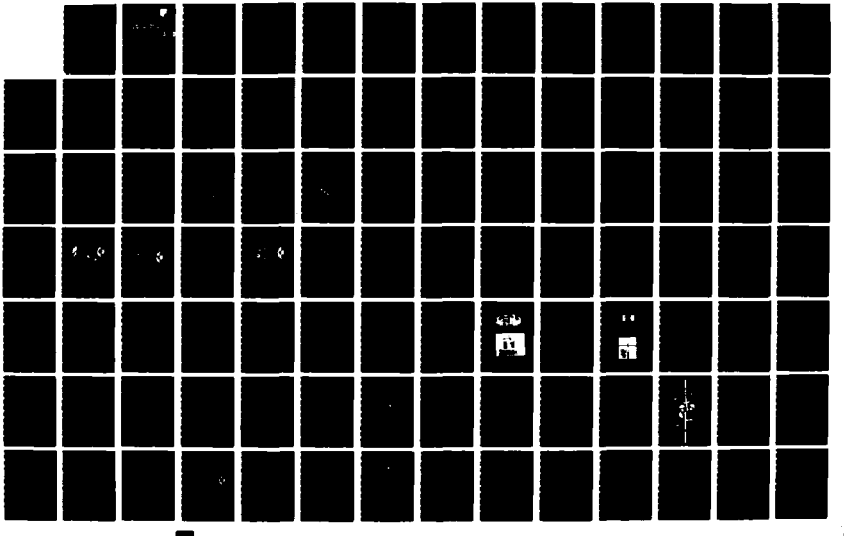

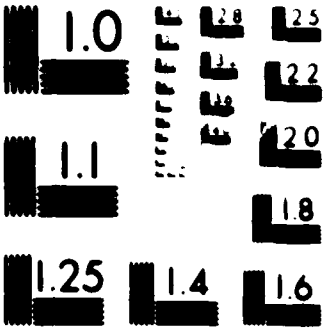
1.0
1.1
1.25
1.4
1.6
1.8
2.0
2.2
2.5

(12)

RADC-TR-87-42
Final Technical Report
May 1987

TECHNOLOGY DEVELOPMENT FOR MILLIMETER WAVE PHASED ARRAYS

University of Massachusetts

Daniel H. Schaubert, K. Sigfrid Yngvesson, David M. Pozar
and Robert W. Jackson

ROME AIR DEVELOPMENT CENTER
Air Force Systems Command
Griffiss Air Force Base, NY 13441-5700

This report has been reviewed by the RADC Public Affairs Office (PA) and is releasable to the National Technical Information Service (NTIS). At NTIS it will be releasable to the general public, including foreign nations.

RADC-TR-87-42 has been reviewed and is approved for publication.

APPROVED: Daniel T. McGrath

DANIEL T. McGRATH, Capt, USAF
Project Engineer

APPROVED: Allan C. Schell

ALLAN C. SCHELL
Director of Electromagnetics

FOR THE COMMANDER: John A. Ritz

JOHN A. RITZ
Directorate of Plans & Programs

If your address has changed or if you wish to be removed from the RADC mailing list, or if the addressee is no longer employed by your organization, please notify RADC (EEAA) Hanscom AFB MA 01731-5000. This will assist us in maintaining a current mailing list.

Do not return copies of this report unless contractual obligations or notices on a specific document require that it be returned.

UNCLASSIFIED

SECURITY CLASSIFICATION OF THIS PAGE

AD-A182 409

REPORT DOCUMENTATION PAGE

Form Approved OMB No. 0704-0188

1a. REPORT SECURITY CLASSIFICATION UNCLASSIFIED	1b. RESTRICTIVE MARKINGS N/A
2a. SECURITY CLASSIFICATION AUTHORITY N/A	3. DISTRIBUTION/AVAILABILITY OF REPORT Approved for public release; distribution unlimited
2b. DECLASSIFICATION/DOWNGRADING SCHEDULE N/A	
4. PERFORMING ORGANIZATION REPORT NUMBER(S) N/A	5. MONITORING ORGANIZATION REPORT NUMBER(S) RADC-TR-87-42
6a. NAME OF PERFORMING ORGANIZATION University of Massachusetts 6b. OFFICE SYMBOL (If applicable)	7a. NAME OF MONITORING ORGANIZATION Rome Air Development Center (EEAA)
6c. ADDRESS (City, State, and ZIP Code) Department of Electrical & Computer Engineering Amherst MA 01003	7b. ADDRESS (City, State, and ZIP Code) Hanscom AFB MA 01731-5000
8a. NAME OF FUNDING/SPONSORING ORGANIZATION Rome Air Development Center 8b. OFFICE SYMBOL (If applicable) EEAA	9. PROCUREMENT INSTRUMENT IDENTIFICATION NUMBER F19628-84-K-0022
8c. ADDRESS (City, State, and ZIP Code) Hanscom AFB MA 01731-5000	10. SOURCE OF FUNDING NUMBERS PROGRAM ELEMENT NO. 61102F; PROJECT NO. 2305; TASK NO J3; WORK UNIT ACCESSION NO. 43

11. TITLE (Include Security Classification)
TECHNOLOGY DEVELOPMENT FOR MILLIMETER WAVE PHASED ARRAYS

12. PERSONAL AUTHOR(S)
Daniel H. Schaubert, K. Sigfrid Yngvesson, David M. Pozar, Robert W. Jackson

13a. TYPE OF REPORT	13b. TIME COVERED	14. DATE OF REPORT (Year, Month, Day)	15. PAGE COUNT
Final	FROM Jan 84 TO Oct 86	May 1987	142

16. SUPPLEMENTARY NOTATION
N/A

17. COSATI CODES			18. SUBJECT TERMS (Continue on reverse if necessary and identify by block number)	
FIELD	GROUP	SUB-GROUP		
17	02		Phased Arrays	Conformal Antennas
09	05		Printed Circuit Antennas	Millimeter Wave Antennas
			Monolithic Arrays	Surface Waves

19. ABSTRACT (Continue on reverse if necessary and identify by block number)

This project investigated architectures, radiators, FET amplifiers and oscillators that could be used in monolithic millimeter wave phased arrays. These investigations contribute to an understanding of the performance of integrated phased arrays. For example, scan blindness associated with surface waves and competition with active components for limited substrate surface area lead to designs with more than one substrate. It has been shown that feed lines can couple electromagnetically to microstrip paths through apertures in an intervening ground plane, and this allows using the beat substrate for each function. Injection locked oscillators using FETs in microstrip and coplanar waveguide circuits were developed as phase controlled sources for transmitter or local oscillators.

20. DISTRIBUTION/AVAILABILITY OF ABSTRACT	21. ABSTRACT SECURITY CLASSIFICATION	
☐ UNCLASSIFIED/UNLIMITED ☐ SAME AS RPT. ☒ DTIC USERS	UNCLASSIFIED	
22a. NAME OF RESPONSIBLE INDIVIDUAL Daniel T. McGrath, Capt, USAF	22b. TELEPHONE (Include Area Code) (617) 337-4036	22c. OFFICE SYMBOL RADC (EEAA)

DD Form 1473, JUN 86 *Previous editions are obsolete.* SECURITY CLASSIFICATION OF THIS PAGE

UNCLASSIFIED

Table of Contents

Chapter 1 - Introduction 1

Chapter 2 - Monolithic Phased Array Architectures 3

2.1 Design Considerations for an Integrated Phased Array 4

2.2 The Scan Blindness Phenomenon 6

2.3 Possible Architectures for Integrated Phased Arrays 11

References - Chapter 2 29

Chapter 3 - Elements for Integrated Phased Arrays 32

3.1 Aperture Coupled Patch 33

3.2 Printed Dipoles Fed by Slotline and Coplanar Waveguide 43

3.3 Summary 53

References - Chapter 3 54

Chapter 4 - Active Circuits for Monolithic Phased Arrays 56

4.1 Coplanar Waveguide Amplifier 56

4.2 Variation of Amplifier Gain with Scan Angle 61

4.3 Phase Shifting Injection Locked Oscillators 63

References - Chapter 4 77

Chapter 5 - Prototype Arrays 78

5.1 Microstripline-Fed Slot Array 78

5.2 20-GHz Linear Array 85

5.3 2x2 Microstrip Patch Array 85

5.4 Aperture Coupled Prototype Array 85

Chapter 6 - Theoretical Developments 105

6.1 Analysis of the Scan Characteristics of an Infinite Phased Array of Microstrip Patches with Idealized Probe Feeds 106

6.2 Analysis of the Scan Characteristics of an Infinite Array of Aperture Coupled Microstrip Patches 109

6.3 A Current Sheet Model of the Scan Characteristics of a General Printed Phased Array 112

6.4 Analysis of Finite Phased Arrays of Printed Dipoles and Microstrip Patches 112

6.5 Analysis of the Aperture Coupled Patch Element 121

6.6 Full Wave Analysis of the Microstrip Open, Gap and Coplanar Waveguide Short 123

References - Chapter 6 131

Chapter 7 - Summary 133

Chapter 1

INTRODUCTION

The University of Massachusetts has conducted a 33-month study under a project entitled Technology Development for Millimeter Wave Phased Arrays. The objectives of this project can be summarized as follows:

Investigate various element designs and feed-active element configurations for monolithic EHF phased arrays. This includes:

- Theoretical analysis of elements.
- Measurement of elements on high-ϵ_r substrates.
- Scaled frequency measurement of devices in monolithic transmission lines.
- Fabricate and test prototype subarray.

This final report describes the findings of the project. Many specific results already have appeared in the literature and the reader is referred to those publications for more detailed descriptions. A list of eight publications and eight presentations resulting from this project are included as Appendix 1. A list of six students who have received support for graduate study from this project is included as Appendix 2.

Chapter 2 contains a discussion of various considerations that affect the architecture of a monolithic phased arrays. Considerations such as scan blindness and available surface area lead one to consider architectures that separate the radiating aperture from the active feed network, and considerations of heat dissipation and manufacturability or servicability lead one to consider modular architectures with feed networks arranged in shelves. Chapter 3 describes some microstrip element designs that have been studied because of their applicability to integrated phased arrays. The aperture coupled patch was developed prior to this project, but was studied extensively during the project. Printed dipoles fed by

slotline or coplanar waveguides have been developed and studied to determine their basic characteristics. An interesting variation of the coplanar waveguide-fed dipoles can radiate circular polarization.

Chapter 4 contains a description of our work on active circuits in monolithic transmission lines. Among the major developments here were FET amplifiers designed in coplanar waveguide for 10 and 20 GHz and injection locked oscillators that can be used as sources with variable phase. An FET oscillator designed for 5 GHz has yielded output powers of 30 milliwatts controllable in phase over a range of approximately 150° with less than 0.5 milliwatts of injected power. An X-band version that doubles the 5-GHz injection signal has yielded nearly 1 milliwatt controllable in phase over almost 360°.

Chapter 5 describes four prototype arrays that were developed during the project. The four prototypes were an 8-element linear array of microstripline fed slots at C-band, an 8-element linear array of microstrip patches at 20 GHz, a 2x2 array of microstrip patches at 20 GHz, and an 8-element linear array of aperture coupled patches at C-band. The last array was a scaled frequency model of an array for 20 or 25 GHz. An attempt to build hybrid circuit phase shifters for the scaled frequency array is described also.

Chapter 6 contains a brief description of some of the analyses that were developed during the project. These included analysis of (1) the scan characteristics of an infinite array of patches with idealized probe feeds, (2) the scan characteristics of an infinite array of aperture coupled patches, (3) general characteristics of printed arrays using current sheets, (4) finite arrays of printed dipoles and patches, (5) an aperture coupled patch, and (6) open-end and gap discontinuities in microstripline and coplanar waveguide shorts.

Chapter 2

MONOLITHIC PHASED ARRAY ARCHITECTURES

This section will discuss a number of considerations for the design and development of monolithic phased arrays. Much of the material of this section has appeared in the literature [1]-[21], and in earlier RADC reports; the interested reader is referred to these sources for more detail.

A phased array antenna offers a number of significant features to the systems designer, including rapid beam scanning, pattern control, and compatibility with adaptive and beamforming systems. The limiting factor in the deployment of phased array systems, of course, is cost, and ironically the cost of such systems seems to increase with time. There exists, then, a strong interest in the monolithic or integrated phased array; as such a design would use the technology of integration—the same technology that has brought us computing power at such a low cost.

The integrated phased array thus offers the potential of a low cost, reliable, and versatile millimeter wave scanning antenna. The concept is generally considered to be limited to millimeter wave systems because only at these frequencies would the antenna be small enough for wafer-scale (probably a number of wafers) integration to be practical. Although no full-scale integrated phased arrays have yet been built, developmental work is underway for a variety of systems. The integrated phased array is sometimes described as "monolithic," implying that the radiating elements, as well as the active circuitry and feed networks, are integrated on one substrate. As this chapter will show, a number of electrical and mechanical problems arise with such a geometry, and this has led to the consideration and development of new printed antenna elements and ways of feeding such elements, and to new ways of configuring radiating elements and active circuitry.

The next two sections will discuss some general issues that pertain to the design of integrated phased arrays, including the scan blindness phenomenon. The remainder of this chapter will then present a number of possible configurations for integrated arrays, and their relative merits will be discussed. Most of these geometries will be presented with experimental and/or theoretical data on their performance. The interested reader is referred to references [1]-[21] for more detail.

2.1 Design Considerations for an Integrated Phased Array

Design criteria for millimeter wave integrated phased arrays can be categorized according to electrical or mechanical considerations:

Electrical Considerations:

- Prefer GaAs (or similar) substrate for active devices (high ϵ_r).
- Prefer low ϵ_r substrate for antenna elements.
- Maximum scan range is limited by grating lobes, and the scan blindness effect.
- Bandwidth limited by element type, substrate and thickness.
- Spurious radiation from feed substrate may degrade main beam, sidelobe level, or polarization.
- Circular or dual polarization may be needed.

Mechanical Considerations:

- 10^3-10^5 elements may be required.
- Substrate area must exist for radiating elements, feed networks, and active circuitry.
- Heat transfer from active devices is necessary.
- Design must be capable of reliable fabrication.

A number of the above electrical problems arise from the apparent requirement of using a high dielectric constant substrate for both the radiating elements and the active

circuitry. For example, microstrip antennas have better bandwidth and less surface wave excitation for low dielectric constant substrates, but the likely semiconductor substrates have a relatively high dielectric constant. In a sense, then, it is a conflicting requirement to have a single substrate for the distinct functions of radiating (loosely bound fields) and circuitry (tightly bound fields). As we will see in the next section, a number of new printed antenna feed methods have been developed to resolve this basic problem by using separate substrates for the radiating elements and the active circuitry.

Substrate space is another prime concern, since a scanning array requires RF power distribution networks, control and bias circuits, phase shifter circuits, and possibly amplifier circuits, in addition to radiating elements. The amplifiers may be needed to compensate for increased circuit losses at millimeter wave frequencies. As will be discussed below, a number of array configurations use more than a single substrate to provide more space, as well as some other advantages. In such cases, a method is needed to couple from one substrate to another. Viaholes (plated through holes) can sometimes be used, but in general it is desired to avoid such direct connections because of very low yields, and because such connections are usually very inductive at high frequencies. As an alternative, some proximity coupling schemes are discussed below.

A large integrated phased array will probably consist of a number of subarrays. Such subarrays, for example, might be fabricated on a single "chip", perhaps with one phase shifter/amplifier circuit feeding all the antenna elements associated with that chip. All of the subarray "chips" could then be mounted on a "motherboard" to supply RF, bias, and control lines. Interconnections here also pose a problem.

Circular or switchable (dual) polarization is required for a number of applications, and of course such requirements complicate the design. Dual polarization is probably the

most difficult case to accommodate, as this essentially requires two separate orthogonally polarized elements, or at least a single element (such as a square microstrip patch) that can be switched between two polarization states. Circular polarization is somewhat easier to obtain, by using a circularly polarized element or a polarizer to convert linear polarization to circular.

2.2 The Scan Blindness Phenomenon

Another problem associated with some types of phased arrays, including printed phased arrays, is scan blindness. This term refers to a condition where, for certain scan angles, no real power can be transmitted (or received) by the array. Scan blindness has been experimentally and theoretically observed in a number of different types of arrays, and is generally related to the resonance of some type of trapped mode. In the case of a printed array, such a mode is present in the form of a surface wave of the loaded (by the antenna elements) dielectric substrate. References [15] and [16] give a more thorough discussion of this effect.

As the substrate is made electrically thicker (higher frequency, dielectric constant, or thickness), the angle at which scan blindness occurs moves closer to broadside. This blindness angle thus effectively limits the scanning range of the array. Figure 2.1 shows the blindness angle of an infinite microstrip patch array on a GaAs substrate versus substrate thickness. Such a substrate $0.04\lambda_o$ thick, for example, would have a blindness angle of about 60^o, which would probably limit the useful scan range of the array to less than 50^o due to the rapid increase of the reflection coefficient near the blindness angle. The data of Figure 2.1 assumes an element spacing of $\lambda_o/2$—the blindness angle moves closer to broadside for larger spacings [16]. Also shown in Figure 2.1 is the approximate bandwidth of the patch element, which shows that a tradeoff exists between the bandwidth of the

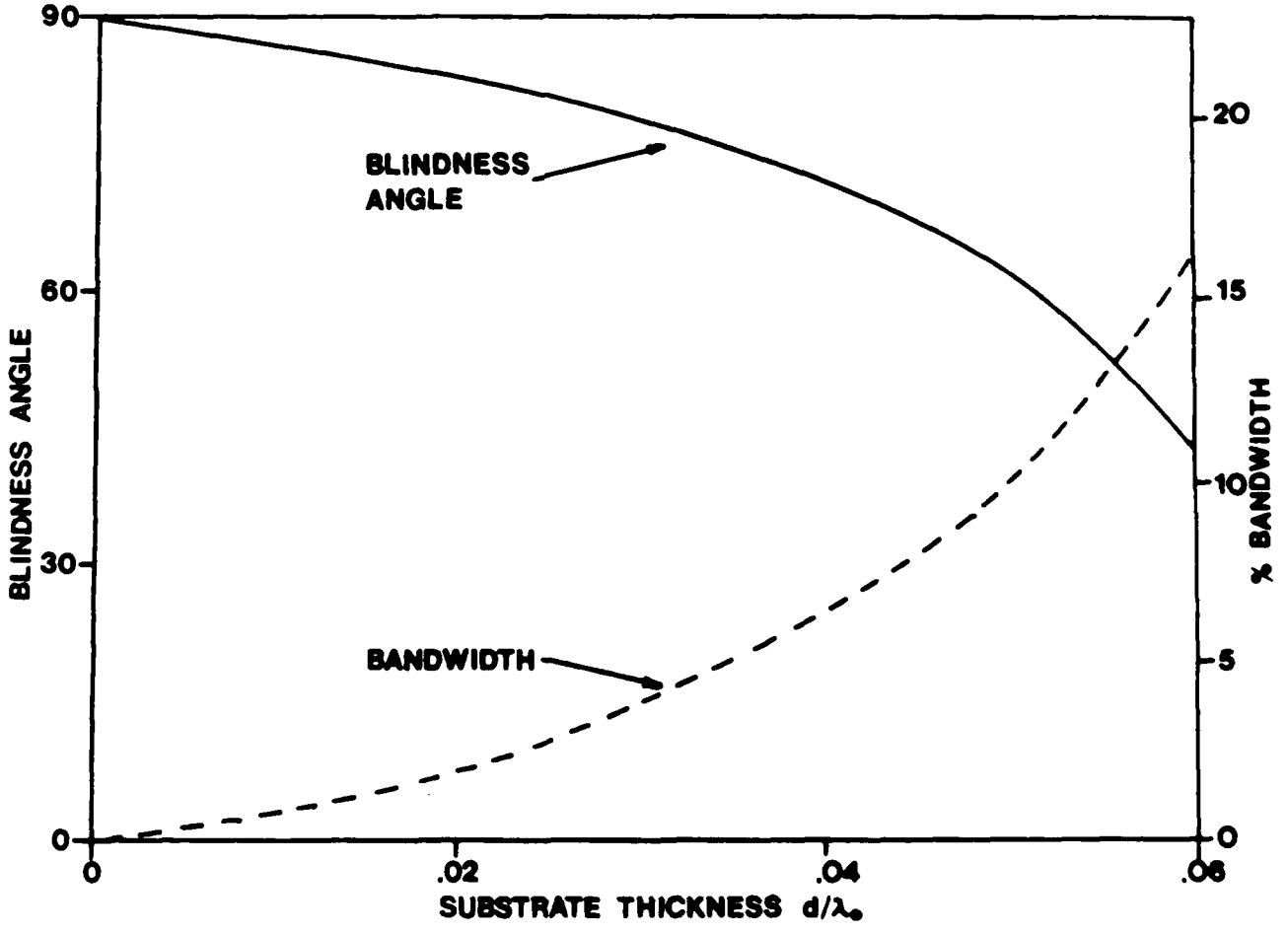

Figure 2.1 Scan blindness angle and bandwidth for a patch array with $\lambda_o/2$ spacing on a GaAs substrate versus substrate thickness.

array and its maximum scan range. For the reason mentioned above, the blindness angle of Figure 2.1 should probably be reduced by at least 10° to get the realistic scan range.

The relation of the scan blindness angle to the substrate parameters (thickness, dielectric constant) and the array element spacing is given by the following equation:

$$(\beta_{sw}/k_0)^2 = (u + \frac{m}{a/\lambda})^2 + (v + \frac{n}{b/\lambda})^2.$$

This result was derived in [16]. In this equation, β_{sw} is the propagation constant of a surface wave mode of the grounded dielectric slab, m and n are integers that can range from $-\infty$ to $+\infty$, a and b are the E- and H-plane element spacings, and u=$sin\theta cos\phi$, $v = sin\theta sin\phi$ are direction cosines for scanning at the angle θ, ϕ. Strictly speaking, β_{sw} in the above equation should be the surface wave propagation constant of the dielectric slab in the presence of the antenna elements. In practice, however, the use of the unloaded propagation constant yields essentially the same result.

Figure 2.2 shows the normalized surface wave propagation constants versus substrate thickness for a GaAs material. The lowest order mode, the TM_o mode, has a zero cutoff frequency and so is propagating for any substrate thickness; it is this mode which usually leads to scan blindness. The data of Figure 2.2 show that β_{sw} increases monotonically with substrate thickness, and that β_{sw} is always greater than k_o, the propagation constant of free space.

The above equation represents a family of circles on the u-v scan plane, as shown in Figure 2.3 (the dotted circles). Also shown in this Figure are the usual grating lobe circles (the solid circles); the data plotted in Figure 2.3 is for a=b=$\lambda/2$. The circles repeat periodically as the integers m,n change. These integers correspond to discrete Floquet modes above the periodic surface of the array; in the absence of grating lobes, only the

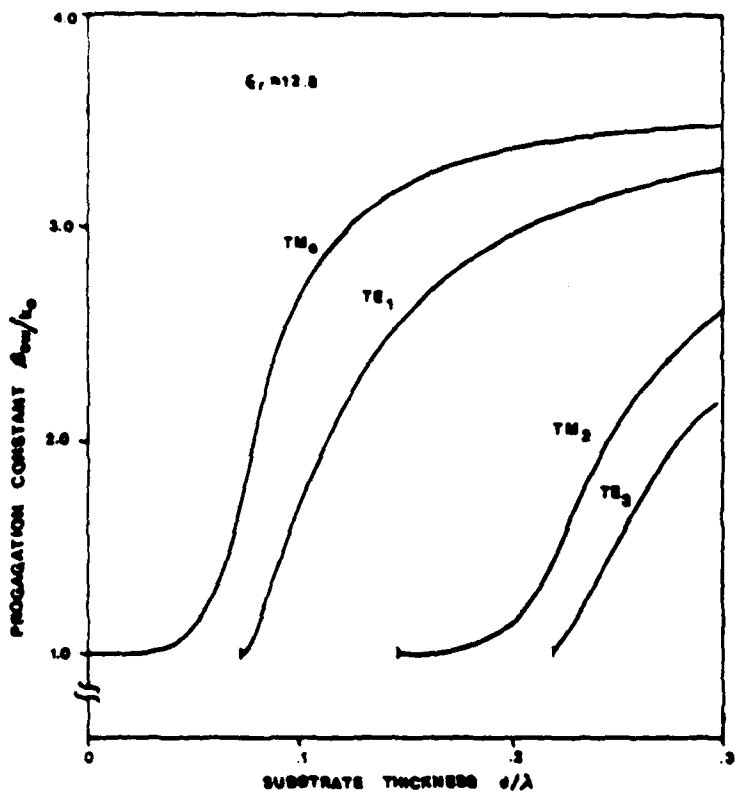

Figure 2.2 Normalized surface wave propagation constants for a GaAs substrate versus substrate thickness.

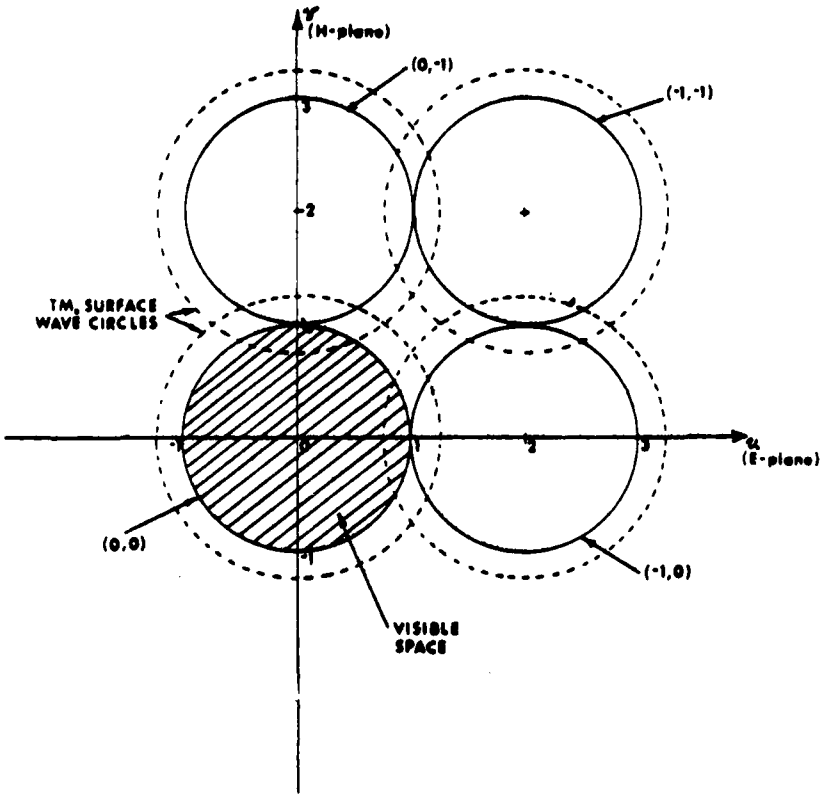

Figure 2.3 A surface wave circle diagram for an infinite array of printed antennas.

m= n=0 Floquet mode is propagating real power. This region is indicated by the hashed unit disk centered at the origin of the u-v plane, and corresponds to visible space. When one of the surface wave circles (dotted circles) enters the visible space region, a scan blindness can occur along the locus of the intersection. This usually is the result of interaction with the m=0, n=-1, or the m=-1, n=0 Floquet mode.

This "surface wave circle diagram" is thus seen to be a useful graphical aid for determining the effect of element spacing and surface wave propagation constant on the blindness position. In general, a blindness will occur at the above described location, unless for some reason the coupling between the surface wave field and the relevant Floquet mode is zero. Such is the case for the TM_o mode for H-plane scanning. This type of blindness will occur for large arrays of printed antennas, but it should be noted that other blindnesses are also possible, due to other effects (such as feed networks). The effect of dielectric constant on the blind spot position is shown in Figure 2.4, where it is seen that lower dielectric constant materials are preferred.

2.3 Possible Architectures for Integrated Phased Arrays

Because of the compatibility of printed antennas with monolithic integrated circuits, it seems that microstrip patches and printed dipole antennas are well suited to integrated array applications, and so the geometries discussed below all use these elements.

A Single Layer Substrate

The type of geometry that probably first comes to mind when considering an integrated phased array is the single layer substrate shown in Figure 2.5, where radiating patches, active circuitry, and the necessary feed networks are all contained on the same substrate. A major problem with this approach is that there may not be enough room on the substrate for all of the components. To avoid grating lobes, antenna elements must be

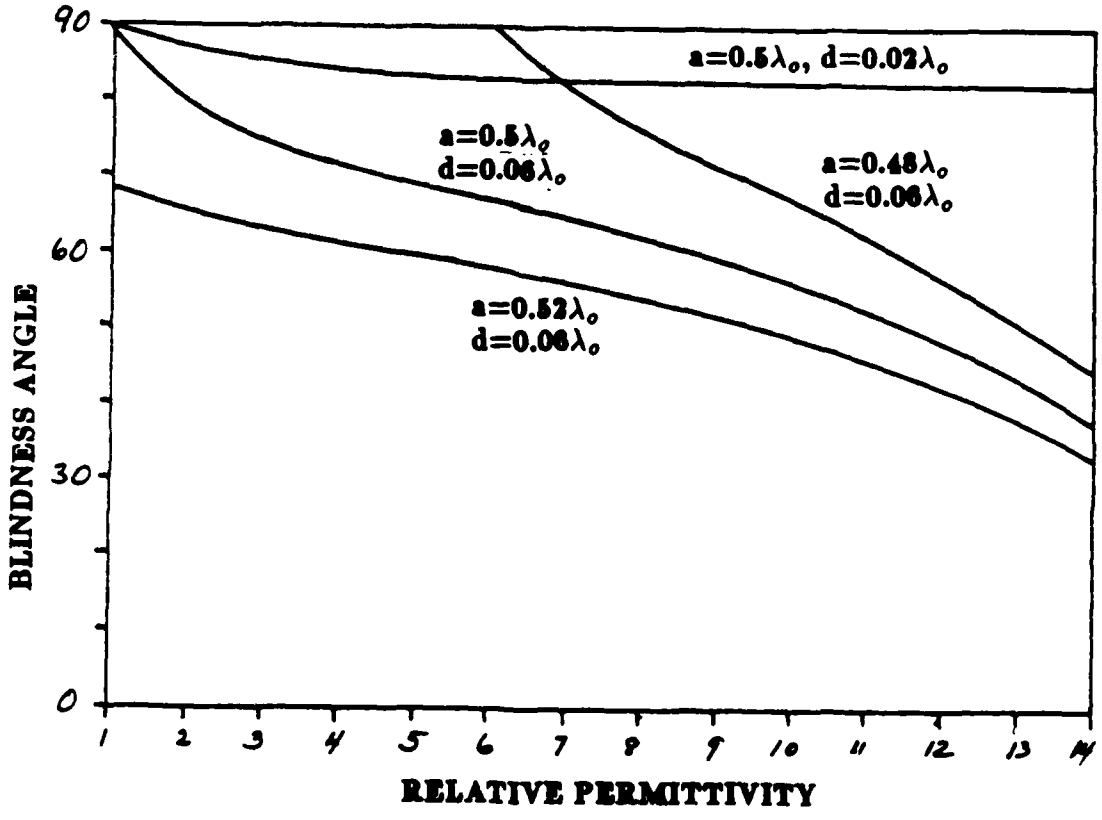

Figure 2.4 Scan blindness angle versus substrate permittivity for various elements spacings (a), and substrate thickness (d).

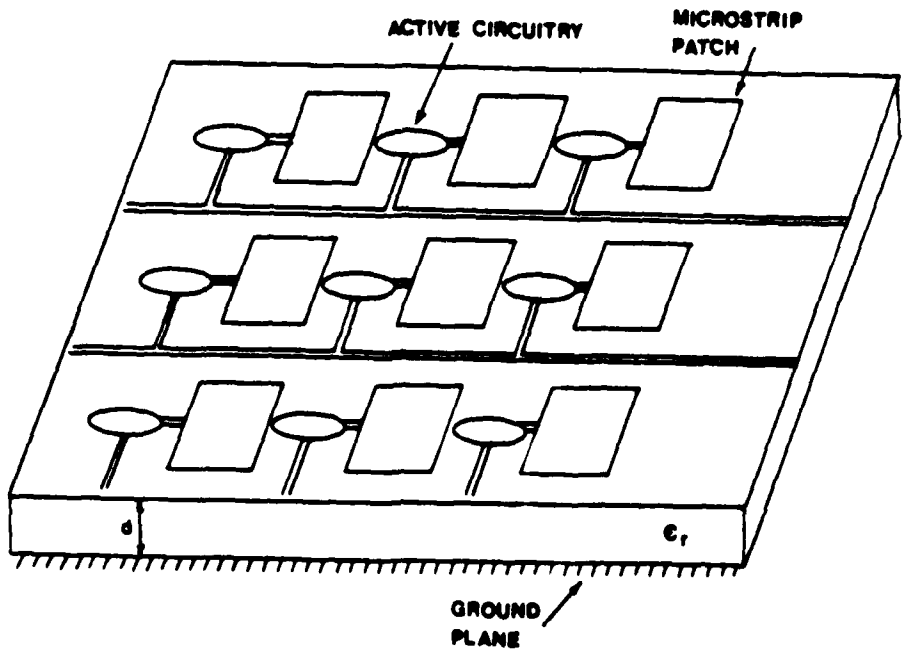

Figure 2.5 Geometry of an array of microstrip patches integrated on a single semiconductor substrate.

spaced about $\lambda_o/2$ apart, so if the phase shifter circuitry, RF feed network, and bias lines can be fit in at all, the spurious coupling between these components may be severe.

Another problem with this geometry is the scan blindness/bandwidth tradeoff which was discussed above. Figure 2.6 shows the reflection coefficient magnitude versus scan angle for an infinite array of rectangular microstrip patch antennas [15]. The element spacing is $0.5\lambda_o$, and the substrate is GaAs $0.06\lambda_o$ in thickness. A number of trends common to printed phased arrays are evident from this Figure. First, observe that in all planes (E-plane, H-plane, and a 45° diagonal plane) the array elements may be matched at broadside scan, but a unity reflection coefficient magnitude is reached as the array is scanned towards endfire. In addition, we see a unity reflection coefficient magnitude in the E-plane at 45° - this is a scan blindness. The unity reflection coefficient magnitude means that all generator power is reflected from each element, and no power is radiated from the array. The E-plane scan range of this array is thus limited to 46° - as a matter of fact, the scan range should probably be reduced by about 10° because of the severe mismatch in the vicinity of the true blindness angle.

The variation of active element impedance (hence, reflection coefficient) with scan angle is a manifestation of mutual coupling between the radiating elements. It is worth noting that all infinite arrays (and, thus, all large arrays) have non-negligible mutual coupling, and it is not possible to eliminate this coupling. That this is true is easy to infer from the fact that an infinite array cannot radiate power away from the array face for endfire scanning, and so must have a unity reflection coefficient magnitude at this angle (in the absence of grating lobes).

Scan blindness will always occur at some scan angle for a printed array, but for thin substrates, the blind angle will be closer to endfire. Figure 2.7 for example, shows a

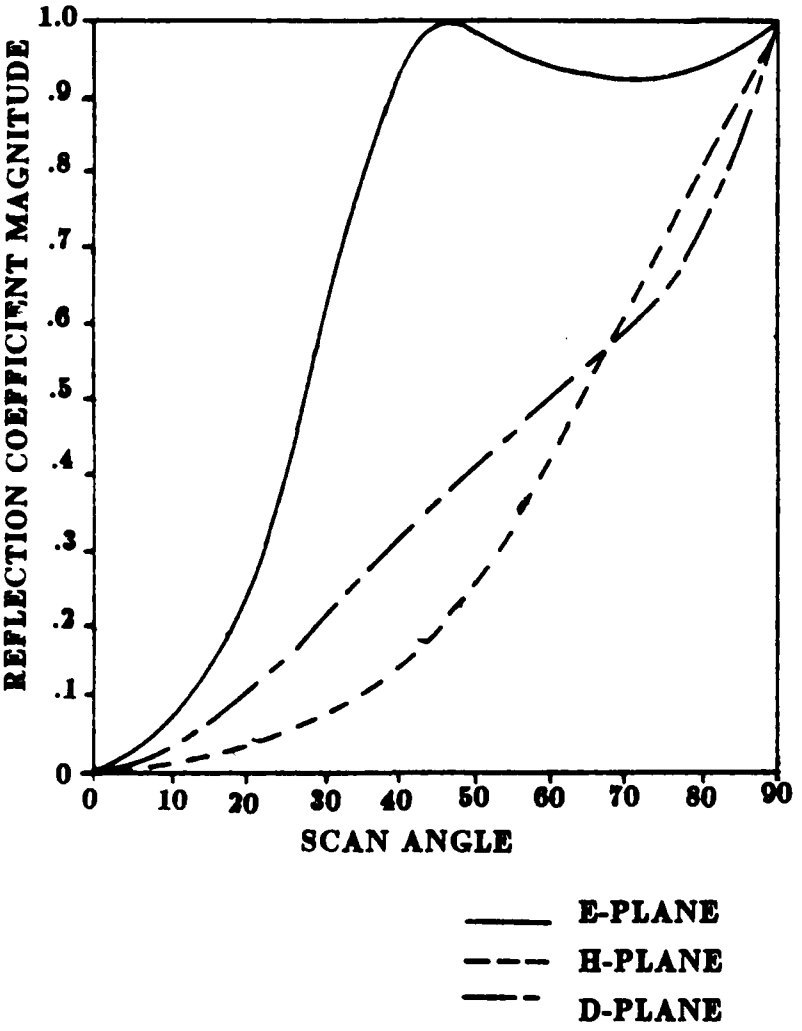

Figure 2.6 Reflection coefficient magnitude versus scan angle for an infinite array of rectangular patch antennas on a GaAs substrate $0.06\lambda_o$ thick.

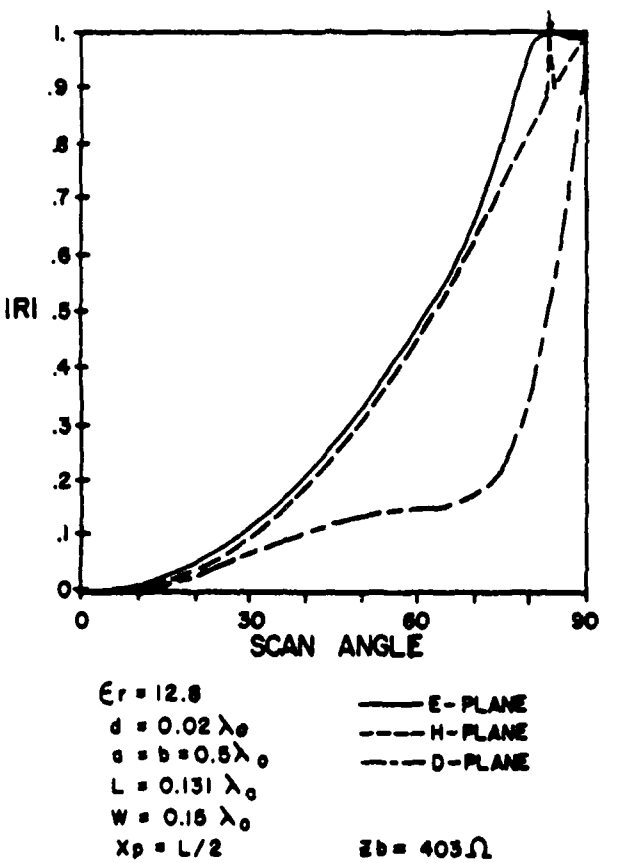

Figure 2.7 Reflection coefficient magnitude versus scan angle in three planes (E, H, and diagonal) for an infinite array of microstrip patches on a $0.02\lambda_o$ thick GaAs substrate.

calculated result from [15] for the reflection coefficient magnitude versus scan angle in the three planes, for an infinite array of microstrip patches on a $0.02\lambda_o$ thick GaAs substrate. The blindness angle is seen to occur at about 82^o in the E-plane (unity reflection coefficient magnitude), although the reflection coefficient magnitude is still about 0.5 at 60^o scan in the principal planes. If the substrate thickness is increased, because of higher frequency operation or a desire for more bandwidth, the blindness angle will move closer to broadside, as indicated in Figure 2.1.

This geometry is also susceptible to spurious radiation from the active circuitry and/or the feed network, which can degrade sidelobe levels or polarization.

A Two Layer Substrate

Figure 2.8 shows a possible two-layer design, where a grounded layer of Gallium Arsenide holds the active devices and feed network, and a superstrate or cover layer of a low dielectric constant material holds the radiating elements. Coupling from the feed to the antenna elements could be made by proximity coupling (as has already been demonstrated with dipoles [22]), or via holes.

This configuration partially corrects two of the major problems discussed above for the single layer substrate case. As can be seen from Figure 2.8, there exists essentially twice the area for radiating elements, active devices, and feed networks. In addition, the radiating elements are now mounted on a composite substrate with an effective dielectric constant which is significantly lower than that of Gallium Arsenide. This is a desirable trend for both increased bandwidth and increased scan range.

There still are problems, however. First, spurious radiation from the active device/feed layer has not been eliminated, and actually may be more harmful here because of the possibility of strong coupling to the radiating elements directly above. Second, the gains

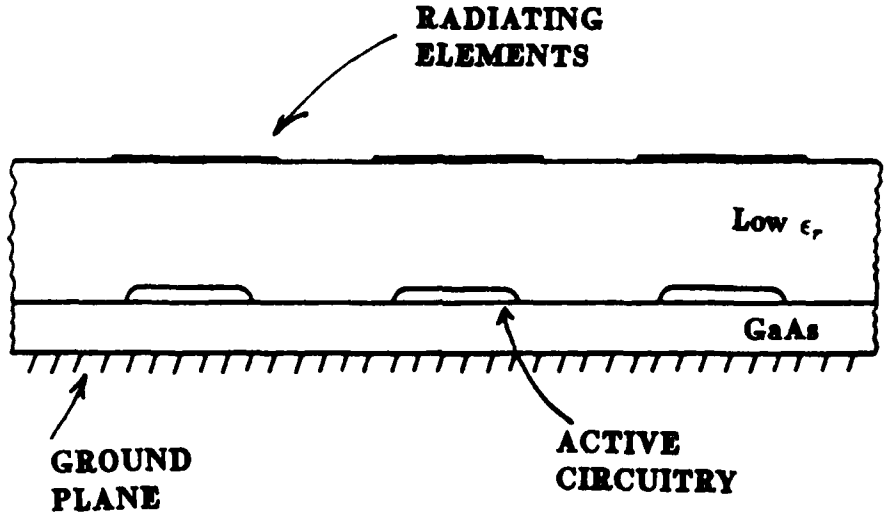

Figure 2.8 Cross-section geometry of a two-layer design for a monolithic phased array.

in bandwidth and maximum scan range are not as great as one might hope. Figure 2.9 shows the blindness angle of an array on a two-layer substrate with $\lambda_o/2$ spacing for various layer thicknesses. For 10% bandwidth and a Gallium Arsenide layer thickness of $0.02\lambda_o$, scan blindness occurs at about 68°, compared with 63° for a single layer GaAs geometry with 10% bandwidth. (Note: As discussed above, the maximum scan range should be taken to be about 10° less than the scan blindness angle, due to severe impedance mismatch near blindness.)

A Two-Sided Geometry

Figure 2.10 shows a two-sided substrate design that eliminates many of the problems encountered with the single layer case by going to the root cause of those problems, and using two separate substrates for the distinct functions of radiation and circuitry. A substrate with a low dielectric constant holds the radiating microstrip patches, while a parallel semiconductor substrate contains active circuitry and feed networks. The two substrates are separated by a ground plane, and apertures in this ground plane are used to couple RF power from the feeds to the radiating elements.

This design thus matches the substrate to the electrical function, resulting in improved blindness/bandwidth performance. For example, with an ϵ_r=2.55 antenna substrate, the thickness would have to be about $0.5\lambda_o$ for a blindness at 80°, and the situation would be even better for a lower dielectric constant substrate. Since we have two substrates, much more space is available than in the single layer case. In addition, the ground plane effectively isolates the active circuitry and feed network from the radiating elements to reduce spurious coupling and radiation.

This array configuration is dependent on the aperture coupled microstrip antenna, which has been described in detail in [14] and theoretically analyzed in [8] and [12]. Figure

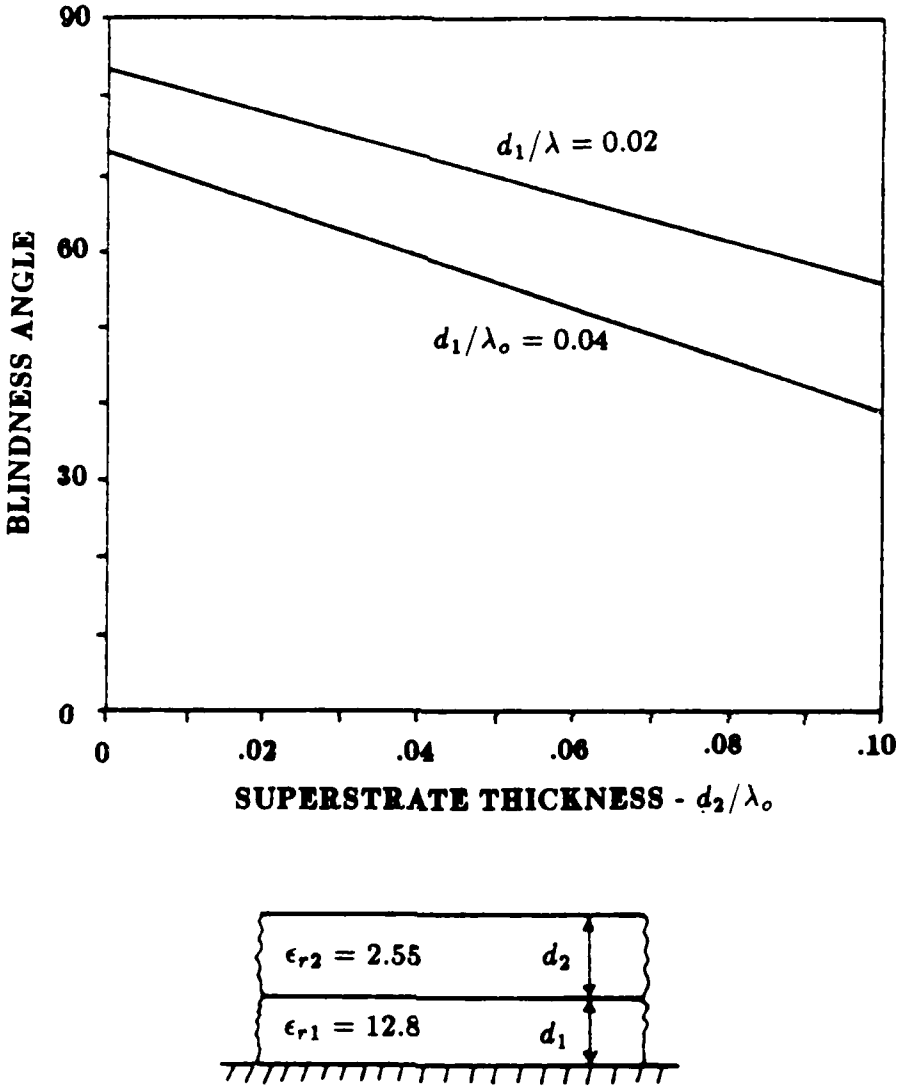

Figure 2.9 Scan blindness angle for a GaAs substrate with a PTFE cover layer.

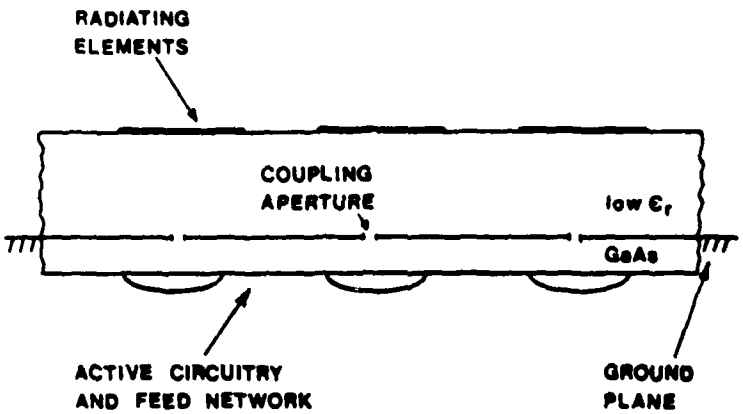

Figure 2.10 Cross-section of a two-sided integrated array geometry with aperture coupled patch radiators.

2.11 shows the geometry of a single aperture coupled patch antenna, fed by a microstripline on the feed substrate. The feedline is usually terminated in an open-circuited stub for tuning. The aperture is smaller than resonant size, so very little radiation occurs in the back region. Models have been successfully fabricated and tested at frequencies from 2 GHz to 20 GHz.

Infinite arrays of aperture coupled patches have also been analyzed, and a typical result is shown in Figure 2.12 for a feed substrate with $\epsilon_r = 12.8$ and an antenna substrate with $\epsilon_r = 2.55$. The reflection coefficient magnitude versus scan angle shows scan blindnesses at $\theta = 82°$ and 86° in the E-plane. The 86° blindness is caused by the antenna substrate, while the 82° blindness is caused by the feed substrate. Although the feed substrate does not hold the radiating patches, blindness can still be associated with this substrate because of the presence of the coupling apertures.

A final feature of the two-sided array, and the array configurations to follow, is the fact that it offers better radiation "hardening" from lightning or EMP effects compared to the single layer design, due to the shielding effect of the ground plane. The coupling of the sensitive active circuitry to the outside world must take place through the microstrip antennas and coupling apertures, which present a two-pole (or more) filter response to signals outside their bandwidth.

An Array Geometry with a Perpendicular Feed Substrate

Another design that uses separate substrates for the radiating elements and active circuitry is shown in Figure 2.13. In this case, a vertical substrate holding the radiating elements is fed by a number of parallel feed substrates. Coupling is again through apertures in the ground plane of the antenna substrate. This design also allows the use of a low dielectric constant substrate for the radiating elements and a separate semiconductor

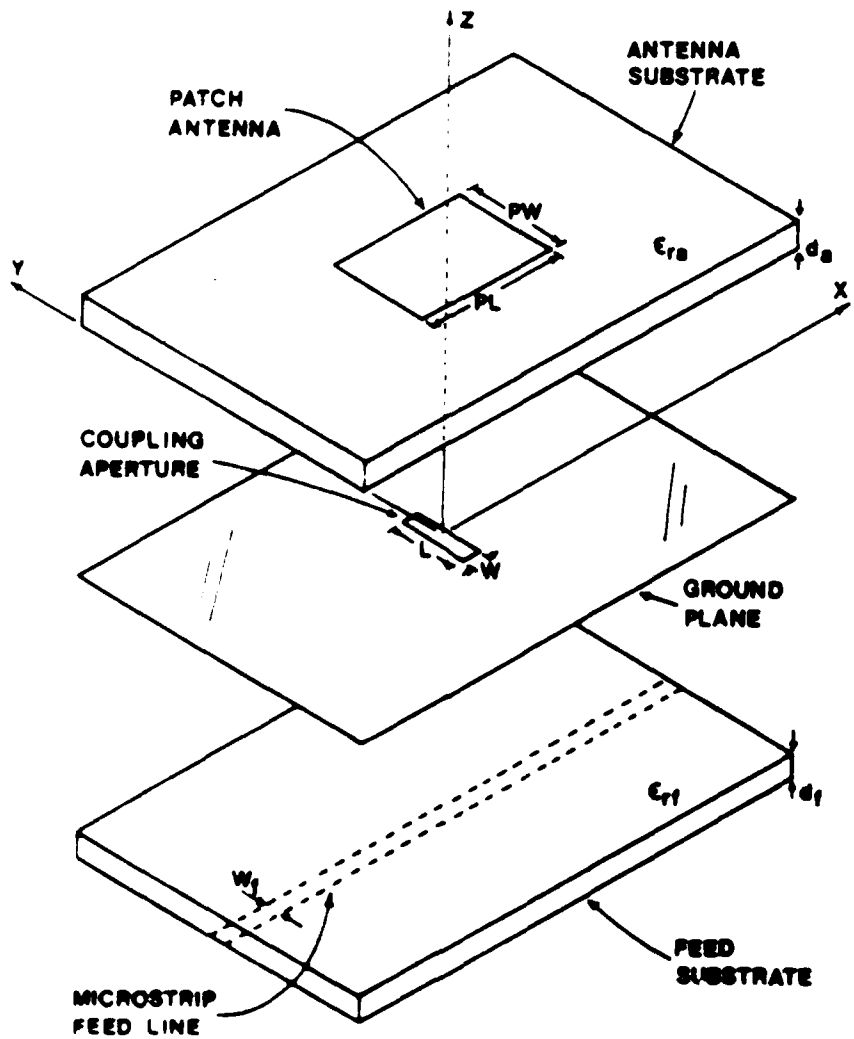

Figure 2.11 Geometry of an aperture coupled microstrip antenna.

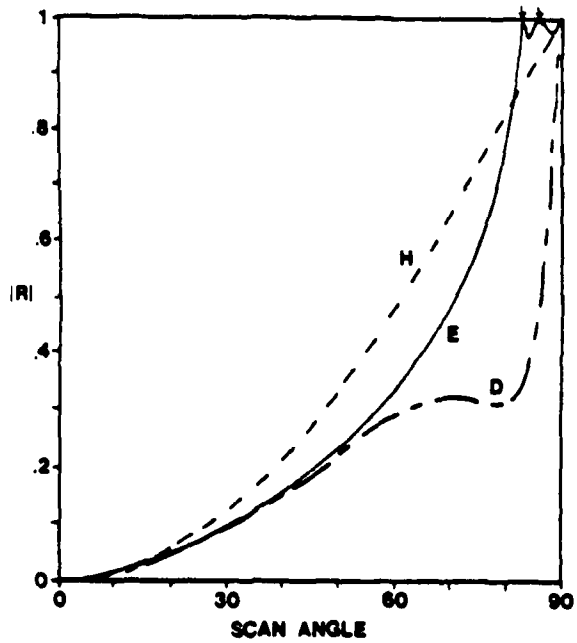

Figure 2.12 Reflection coefficient magnitude versus scan angle for an infinite array of aperture coupled patches.

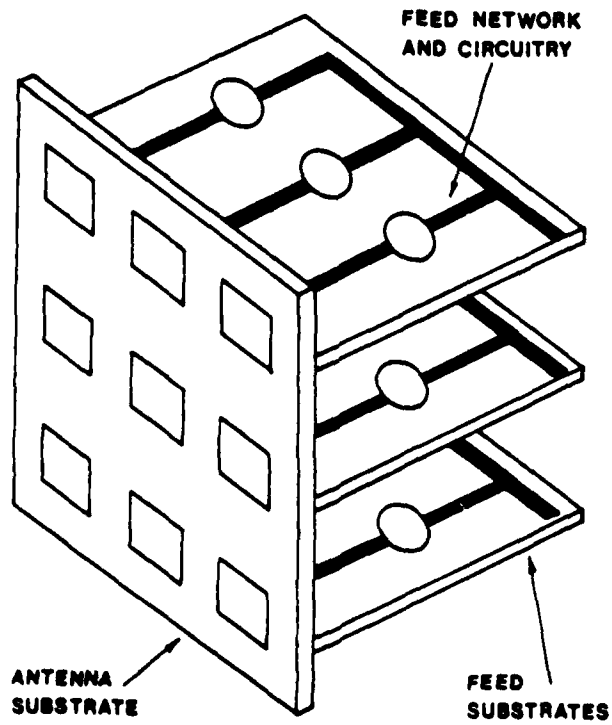

Figure 2.13 An integrated phased array configuration using a feed substrate perpendicular to the radiating element substrate.

substrate for the active circuitry, similar to the two-sided geometry, and so has the same advantages in relation to scan blindness/bandwidth performance and shielding of spurious radiation or coupling. In addition, this architecture has a number of other advantages.

First is the fact that the feed substrate can be of virtually unlimited size, since there is no immediate restriction on the "depth" dimension away from the vertical antenna substrate. Waveguide phased arrays usually used this depth dimension to a similar advantage. The geometry also permits a modular construction, where feed modules could conceivably be plugged into receptacles on the antenna substrate.

This design also allows efficient heat transfer from the ground plane of the feed substrate. At millimeter wave frequencies low device efficiency requires efficient heat transfer from active circuitry. The unobstructed ground plane of the feed substrates allows much heat removal to take place, while the embedded ground plane of the two-sided design makes heat removal more difficult.

Finally, such a geometry would lend itself well to space-fed phased array lens designs, which may be of interest for some applications. This could be implemented by having antenna substrates at both ends of the feed substrates. It does not appear, however, that this geometry would be useful if dual polarization were required.

The array with perpendicular feed substrates depends on the feasibility of feeding a single patch through an aperture with a microstrip line on a perpendicularly oriented substrate. Such a geometry is shown in Figure 2.14, and has been discussed in more detail in [10]. This design has been verified experimentally, but no theory has been developed beyond the simple arguments presented in [10].

The geometry in Figure 2.14 shows a direct connection from the feedline to the top of the aperture; the two ground planes are also in electrical contact. Another version of

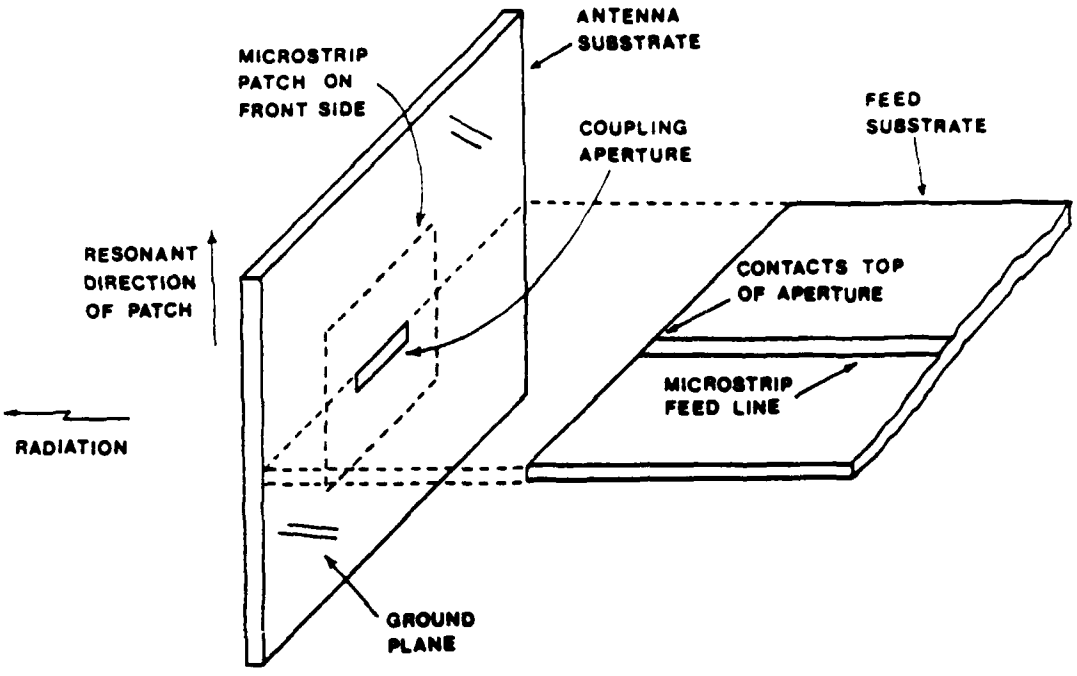

Figure 2.14 Geometry of an isolated microstrip antenna fed through an aperture with a microstrip line on a perpendicularly oriented feed substrate.

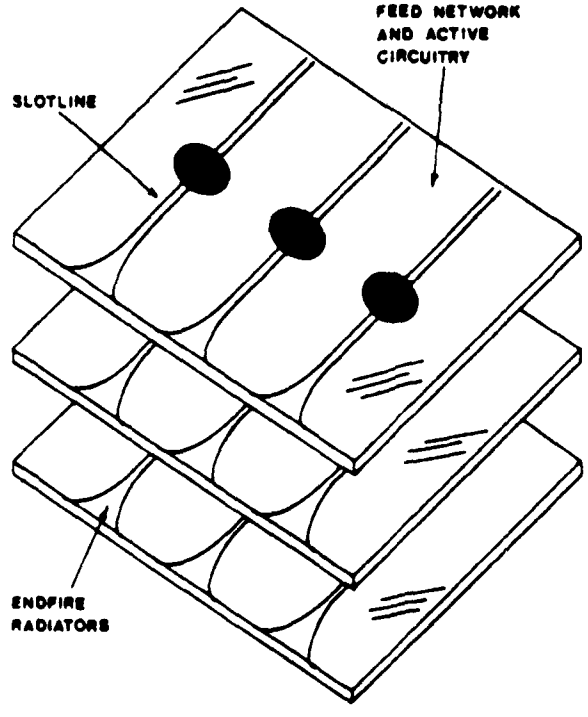

Figure 2.15 An integrated phased array geometry using tapered slot elements that radiate in the endfire direction.

the perpendicularly fed antenna excites the aperture by proximity coupling, eliminating the need for a direct connection of the feedline. Other variations, including the use of a coplanar waveguide feed, are also possible.

A Geometry Using Endfire Elements

The previously discussed integrated phased array designs all used microstrip patches or printed dipoles which radiate normal to the substrate on which they are printed. An alternative to this approach is to use elements which radiate endfire to the substrate, as shown in Figure 2.15. This example shows the use of tapered slot antennas, but other elements capable of endfire (to the substrate) radiation, such as dipoles, could be used as well.

This type of geometry then uses a single substrate for both active circuitry and radiating elements, but in a rather different way than the single layer design discussed earlier. A lot of substrate space is available for feed networks and circuitry, and the design can readily be used for space-fed lens arrays. The individual substrates can be made in modular form, and heat transfer should not be a problem.

Although surface waves can still be excited on the substrates, an additional problem is the possibility of scan blindness caused by surface waves on the protruding grid of dielectric slabs; such effects have been observed in similar arrays with protruding dielectrics [23]. In addition, this configuration would probably not be useful if circular polarization is desired.

The tapered slot element has been discussed in [24], and may be constructed with either a linear taper or a curved slot. The slot antenna can be proximity fed with a microstrip line to slotline transition, as in [24], or the slotline could be directly fed from the active circuitry. In this regard, it is interesting to note that a slotline has a number of distinct advantages over the microstrip in such millimeter wave integrated circuit applications [25].

Conclusion

This chapter has addressed the problem of designing a millimeter wave integrated phased array. Some of the constraints and performance goals of such an array have been presented, and a variety of possible array architectures have been outlined and discussed. Sample experimental and theoretical results for some new types of printed antennas that could be used in integrated phased arrays have been shown. Work is continuing in the area of analysis of canonical printed array and element geometries, and the development of novel configurations for integrated arrays.

References for Chapter 2

[1] D. M. Pozar and D. H. Schaubert, "Comparison of Architectures for Monolithic Phased Array Antennas," Microwave Journal, 29, 93-104, March 1986.

[2] D. H. Schaubert, R. W. Jackson and D. M. Pozar, "Antenna Elements for Integrated Phased Arrays," 1985 Antenna Applications Symposium, Allerton Park, IL.

[3] D. M. Pozar, "Phased Arrays of Printed Antennas," 1985 ISAP Symposium, Kyoto, Japan.

[4] D. M. Pozar, "Surface Wave Effects in Phased Arrays of Printed Antennas," 1985 Phased Arrays Symposium, Boston, MA

* [5] D. M. Pozar and D. H. Schaubert, "Comparison of Architectures for Monolithic Phased Array Antennas," 1985 Phased Arrays Symposium, Boston, MA.
RADC-TR-85-170, Aug 85. Limited to DOD & DOD contractors; Critical Technology.

[6] D. M. Pozar, "A Monolithic Phased Array Architecture Using an Aperture Coupled Microstrip Antenna," 1985 IEEE/AP-S International Symposium, Vancouver, Canada.

[7] D. H. Schaubert, D. M. Pozar, K. S. Yngvesson, and R. W. Jackson, "Considerations for Millimeter Wave Monolithic Phased Arrays," 1984 Antenna Applications Symposium, Allerton Park, IL.

[8] D. M. Pozar, "A Reciprocity Method of Analysis for Printed Slot and Slot-Coupled Microstrip Antennas," accepted for publication in IEEE Trans. Antennas and Propagation.

[9] D. M. Pozar, "Finite Phased Arrays of Rectangular Microstrip Antennas," IEEE Trans. Antennas and Propagation, AP-34, 658-665, May 1986.

[10] A. C. Buck and D. M. Pozar, "An Aperture Coupled Microstrip with Perpendicular Feed," Electronics Letters, 22, 125-126, January 30, 1986.

* NONE OF THE INFORMATION TAKEN FROM THE * LIMITED DOCUMENT (ITEM 5) WAS LIMITED INFORMATION.

[11] D. M. Pozar, "Analysis of Finite Phased Arrays of Printed Dipoles," IEEE Trans. Antennas and Propagation, AP-33, 1045-1053, Oct. 1985.

[12] P. L. Sullivan, D. H. Schaubert and D. M. Pozar, "Analysis of Aperture Coupled Patch Antenna," 1985 IEEE AP-S/URSI International Symposium, Vancouver, Canada.

[13] D. M. Pozar, "General Relations for a Phased Array of Printed Antennas Derived from Infinite Current Sheets," IEEE Trans. Antennas and Propagation, AP-33, 498-504, May 1985.

[14] D. M. Pozar, "A Microstrip Antenna Aperture Coupled to a Microstrip Line," Electronics Letters, 21, 49-50, Jan. 17, 1985.

[15] D. M. Pozar and D. H. Schaubert, "Analysis of an Infinite Array of Rectangular Microstrip Patches with Idealized Probe Feeds," IEEE Trans. Antennas and Propagation, AP-32, 1101-1107, October 1984.

[16] D. M. Pozar and D. H. Schaubert, "Scan Blindness in Infinite Phased Arrays of Printed Dipoles," IEEE Trans. Antennas and Propagation, AP-32, 602-610, June 1984.

[17] D. M. Pozar and D. H. Schaubert, "Analysis of Infinite Phased Arrays of Printed Dipoles," 1984 International IEEE AP-S/URSI Symposium on Antennas and Propagation, Boston, MA

[18] D. M. Pozar, "Considerations for Millimeter Wave Printed Antennas," IEEE Trans. Antennas and Propagation, AP-31, 740-747, Sept. 1983.

[19] D. M. Pozar, "Surface Wave Effects for Millimeter Wave Printed Antennas," 1983 International IEEE AP-S/URSI Symposium on Antennas and Propagation, Houston, TX.

[20] D. M. Pozar, M. C. Bailey and M. D. Despande, "Calculated Self and Mutual Impedance

of Rectangular Microstrip Antennas," 1982 International IEEE AP-S/URSI Symposium, Albuquerque, NM.

[21] D. M. Pozar, "Input Impedance and Mutual Coupling of Rectangular Microstrip Antennas," IEEE Trans. Antennas and Propagation, AP- 30, 1191-1196, Nov. 1982.

[22] W. G. Oltman and D. A. Huebner, "Electromagnetically Coupled Microstrip Dipoles," IEEE Trans. Antennas and Propagation, AP-29, pp. 151-157, Jan. 1981.

[23] L. R. Lewis, A. Hessel and G. H. Knittel, "Performance of a Protruding Dielectric Waveguide Element in a Phased Array," IEEE Trans. Antennas and Propagation AP-20, 712-722, Nov. 1972.

[24] I. J. Bahl and P. Bhartia, *Microstrip Antennas*, Artech House, 1980.

[25] R. W. Jackson, "Coplanar versus Microstrip for Millimeter Wave Integrated Circuits," 1986 Microwave Theory and Techniques Symposium, Baltimore, MD.

Chapter 3

ELEMENTS FOR INTEGRATED PHASED ARRAYS

Integrated phased array systems consisting of a large number of elements and operating at millimeter wavelengths have motivated many antenna developments in recent years. Reduced cost, increased reliability and performance are some of the reasons for investigating monolithic and integrated structures, and the high level of integration of active and passive components in these structures makes them different from most systems that have been developed to date. The coexistence of these components requires the use of substrates, transmission lines, and circuit designs that have not been necessary at lower frequencies in modular units. Another feature of these integrated structures is the large number of control and power supply circuits that must be included. All of these features contribute to a very dense packing of components that is difficult to achieve at best and is usually detrimental to system performance.

Elements for use in integrated phased arrays must satisfy many requirements. The electrical and mechanical considerations described in Chapter 2 define some of these requirements. Beyond these, there often are requirements for increased bandwidth and dual polarization with high isolation. The element beamwidth may need to be wide for wide-angle scanning or narrow for limited scanning with grating lobe suppression. A unidirectional pattern is usually required, so slots and dipoles cannot be used without ground planes, and these can introduce mutual coupling and blindness problems as noted in [1] for slot arrays. The element must be integrated with monolithic, active circuits so that an efficient means of "connecting" the two is required. Ease of fabrication and cost are important features that argue for the use of photolithographic fabrication procedures and

against the use of via connections. Furthermore, ruggedness and robustness of the element design are important considerations.

In this chapter, two types of antenna elements are described. These elements are integrable with monolithic circuits, but do not reside on the same substrate surface as the circuits, thus reducing component crowding. Coupling to the radiating element is via the electromagnetic fields so that no via connections (plated through holes) are needed. An added advantage of these antennas is that different substrates can be used for the active circuits and the radiators. This can help to alleviate surface wave and scan blindness effects that have been predicted for printed antenna arrays on GaAs [2-5].

The antenna elements that are described below are a microstrip patch radiator coupled to a microstripline via an aperture in their common ground plane [6, 7] and printed dipoles coupled to a slotline in the ground plane or to a coplanar waveguide. Measured impedance and radiation properties of these antennas are presented and, for the aperture coupled patch, computed parameter studies that provide useful design data are presented here and in Chapter 6.

3.1 Aperture Coupled Patch

The aperture coupled patch antenna was developed prior to this program, but it has been studied extensively during the program. The structure of the antenna is shown in Figure 3.1. The patch is resonant and radiates effectively into the upper half space, whereas the aperture is smaller than resonant dimensions and does not radiate much power into the lower half space. The operating frequency of the antenna is determined primarily by the patch dimensions and the input impedance can be controlled by the aperture size and location and the stub length.

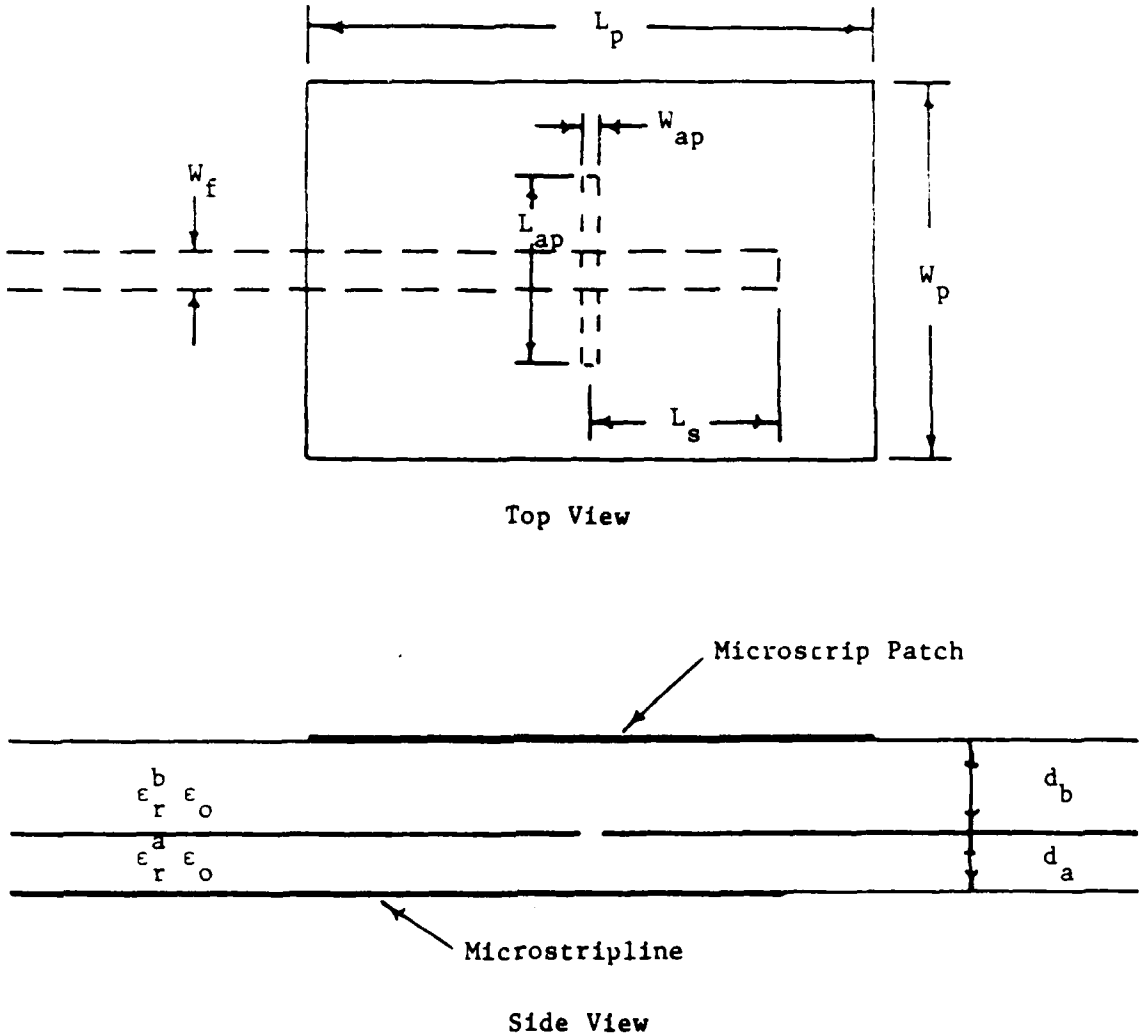

Figure 3.1. Aperture coupled patch antenna with microstripline feed.

Typical impedance data are shown in Figure 3.2 for three different stub lengths. The reference plane is located at the center of the aperture. For all impedance plots, measured results are plotted as solid lines and calculated results are plotted as dashed lines. The calculations are performed by the method outlined in Chapter 6 and described in detail in [9]. Increasing the stub length further causes the locus to rotate into the inductive part of the chart and become smaller in size, similar to the loci for shorter stub lengths. If the impedance at a single frequency is tracked for various stub lengths, it is found to follow approximately a constant resistance circle, implying that the slot and antenna appear to the feedline as an impedance in series with an open circuited stub.

The effects of aperture length are shown in Figures 3.3 and 3.4. Increasing the aperture length increases the diameter of the impedance locus and lowers the resonant frequency slightly. The combination of stub length and aperture length provides extensive control of the input impedance and allows tuning for perfect match at a single frequency or maximum bandwidth for a given VSWR. (In general, the bandwidth of aperture coupled patches is similar to that of ordinary probe fed or microstripline fed patches of similar size on the same substrate, but some results have been obtained that indicate an increased bandwidth due perhaps to double tuning.)

Increasing the relative permittivity of the feedline substrate has the effects illustrated in Figure 3.5. For these calculations, the impedance of the microstripline feed was maintained at 50 ohms and the stub length was maintained at 0.22 wavelengths of the microstripline. The specific values of the antenna parameters are listed in the figure.

Measured radiation patterns of aperture coupled patches are shown in Figures 3.6-3.8. All of these patterns were taken with a small ground plane and the coaxial transmission line that attaches to the microstripline has some effect on the E-plane patterns. The level

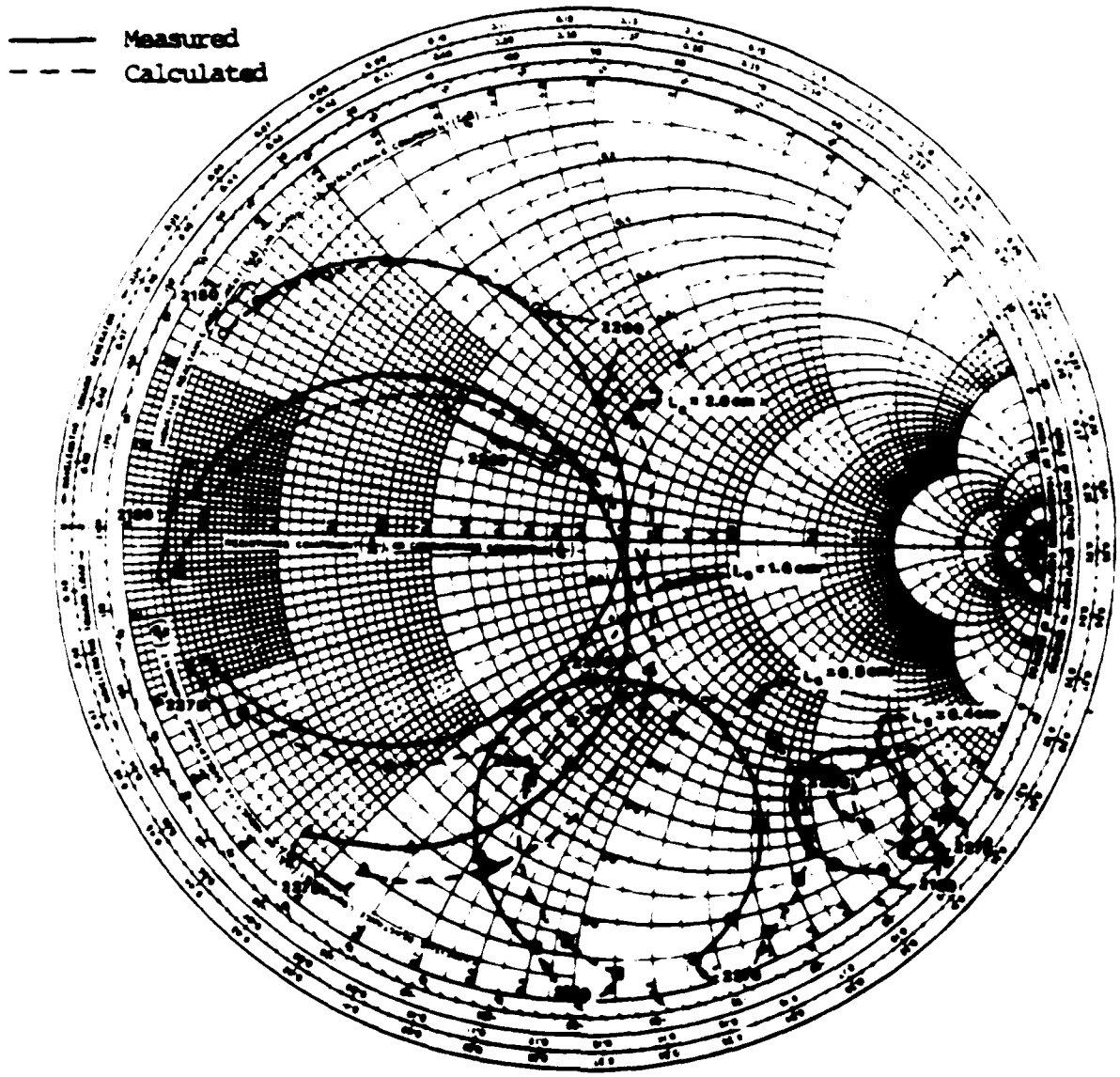

Figure 3.2. Measured versus calculated input impedance as a function of stub length. $\epsilon_r^b = 2.54, d_b = 0.16cm, L_p = 4.0cm, W_p = 3.0cm, x_{0_e} = 0.0cm, y_{0_e} = 0.0cm, L_{ap} = 1.12cm, W_{ap} = 0.155cm, \epsilon_r^a = 2.54, d_a = 0.16cm, W_f = 0.442cm.$

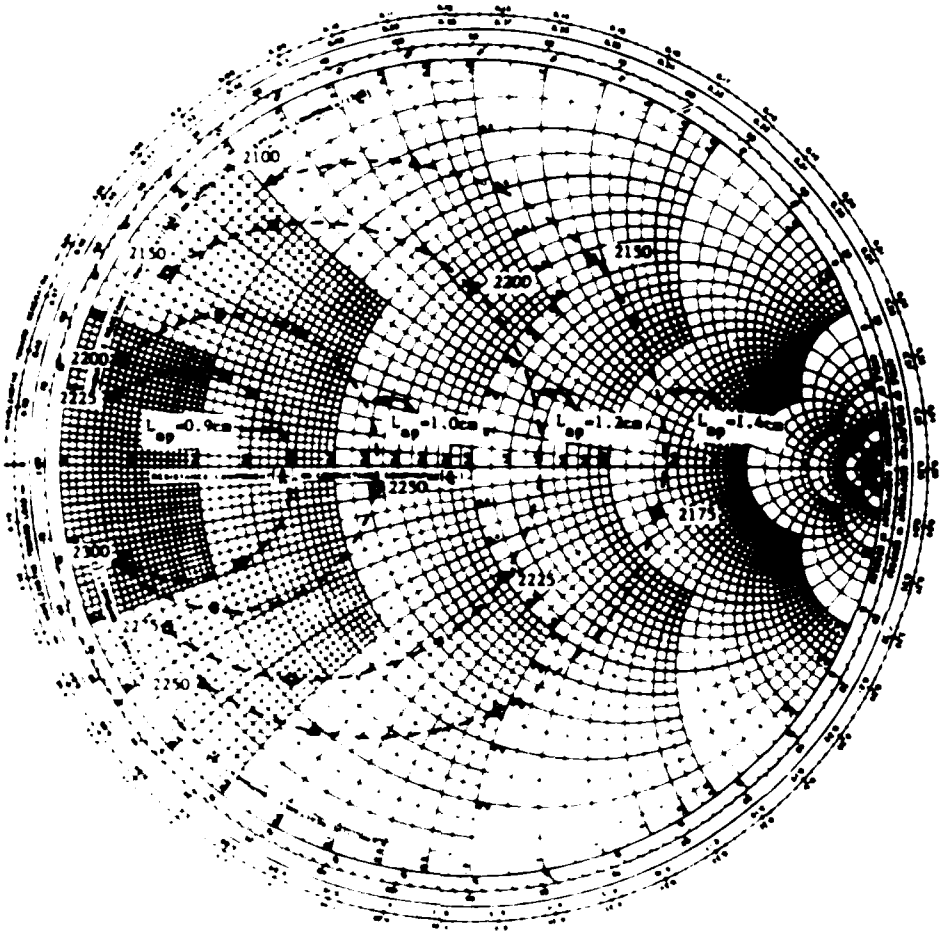

Figure 3.3. Calculated input impedance loci as a function of aperture length (long dimension). The other antenna parameters are: $\epsilon_r^b = 2.54, d_b = .16cm, L_p = 4.0cm, W_{ap} = .11cm, \epsilon_r^l = 2.54, d_a = .16cm, W_f = .495cm, L_s = 2.0cm$.

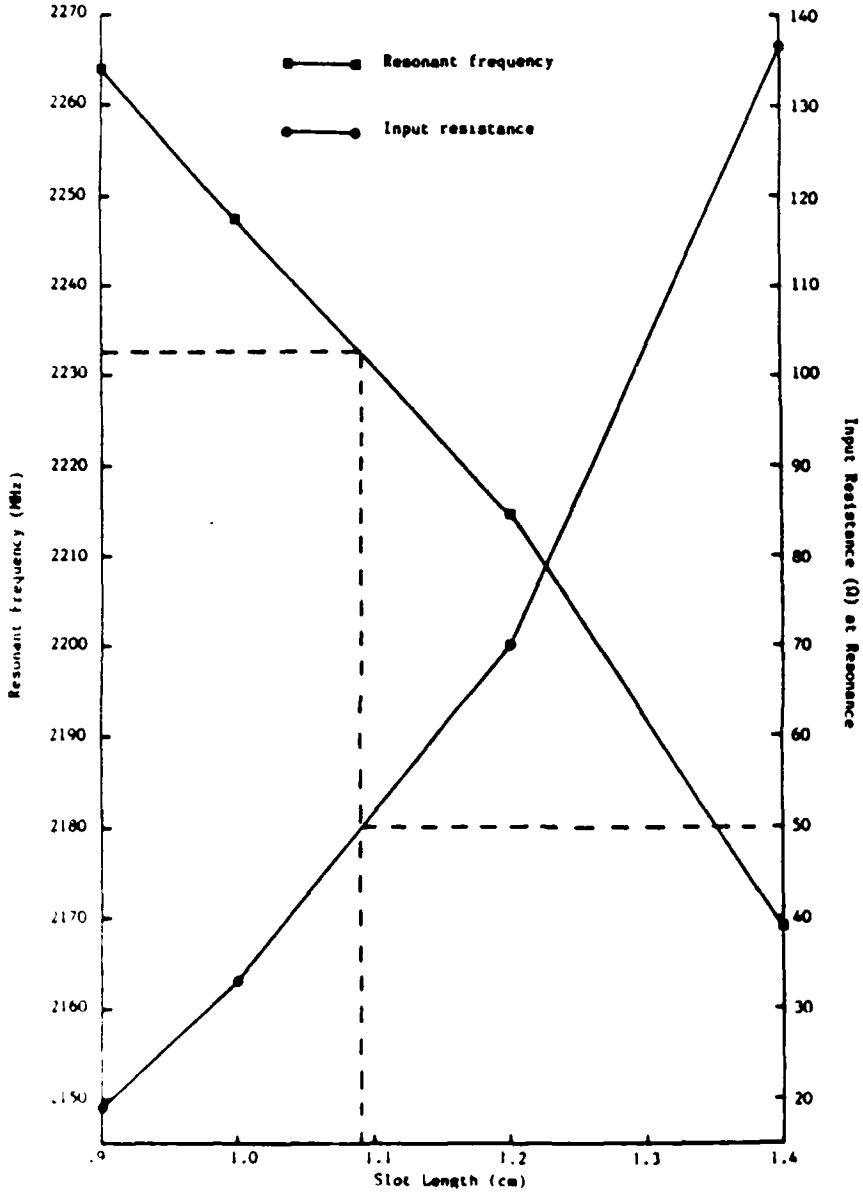

Figure 3.4. Resonant frequency and input resistance at resonance versus slot length (data from Figure 3.3).

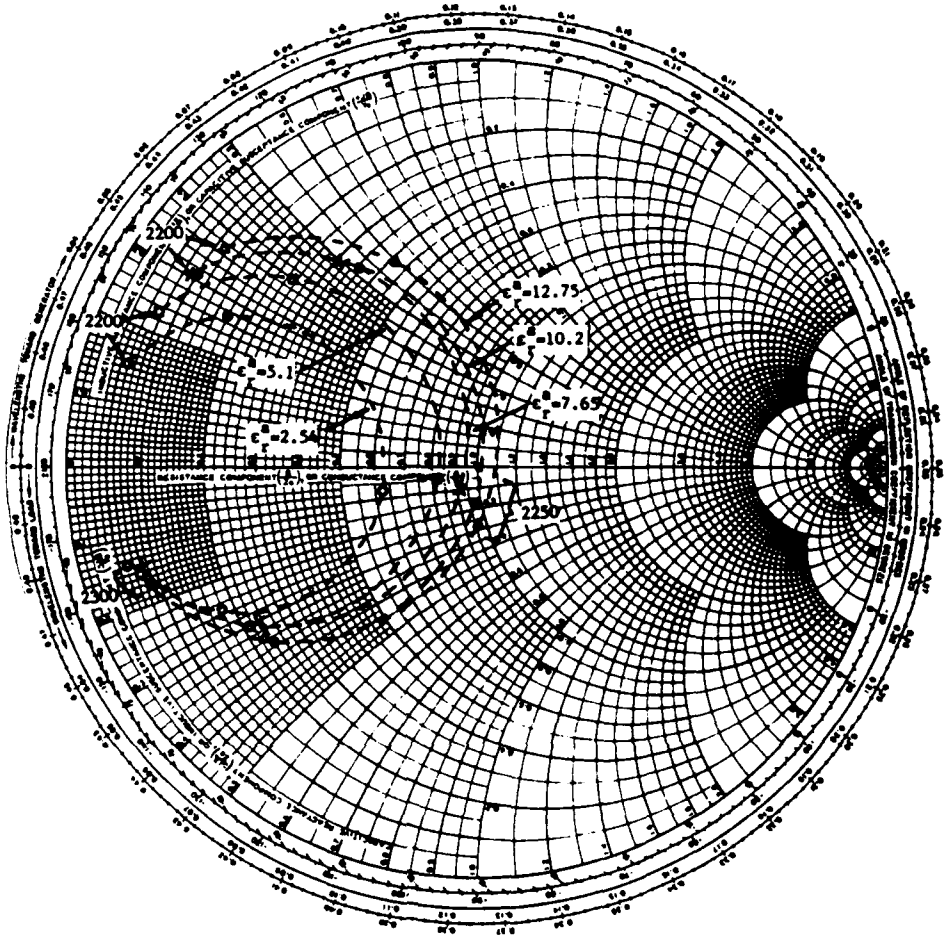

ϵ_r^a	W_f	L_s
2.54	.495 cm	2.000 cm
5.10	.310 cm	1.493 cm
7.65	.225 cm	1.255 cm
10.20	.173 cm	1.108 cm
12.75	.139 cm	1.004 cm

Figure 3.5. Calculated input impedance loci as a function of feed substrate dielectric constant. The tabular data above give the feed line width and stub length used in the analysis to maintain a 50 Ω characteristic impedance and stub length of $.22\lambda_f$ for each value of ϵ_r^a. The other antenna parameters are: $\epsilon_r^b = 2.54, d_b = .16cm, L_p = 4.0cm, W_p = 3.0cm, L_{ap} = 1.0cm, W_{ap} = .11cm, d_a = .16cm$.

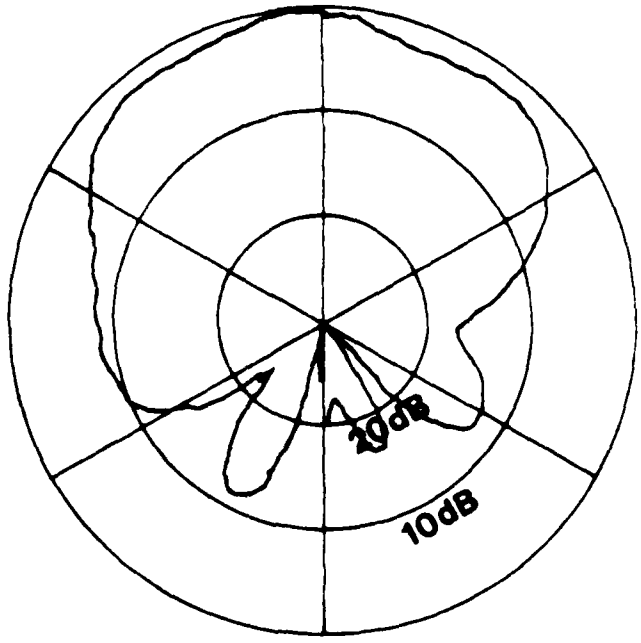

E Plane

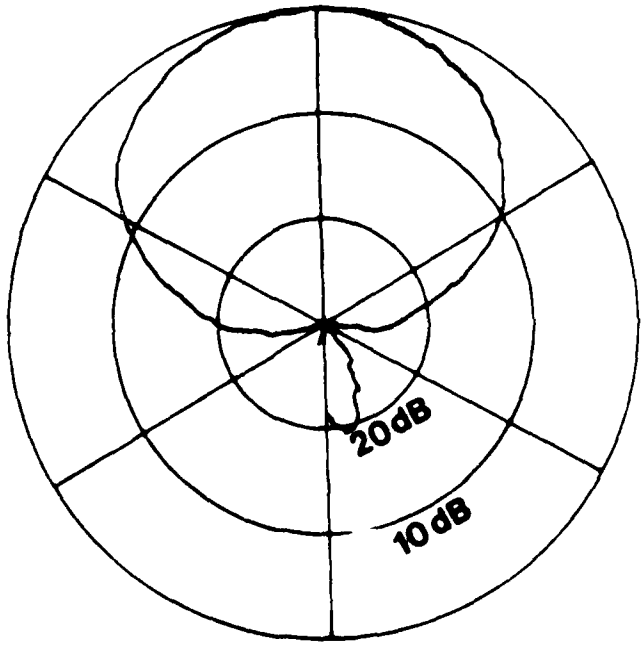

H Plane

Figure 3.6. Radiation patterns of 4.17 GHz antenna. $\epsilon_r^b = 2.2, d_b = .16cm, L_p = 2.17cm, W_p = 3.0cm, L_{ap} = 1.0cm, W_{ap} = .16cm.$

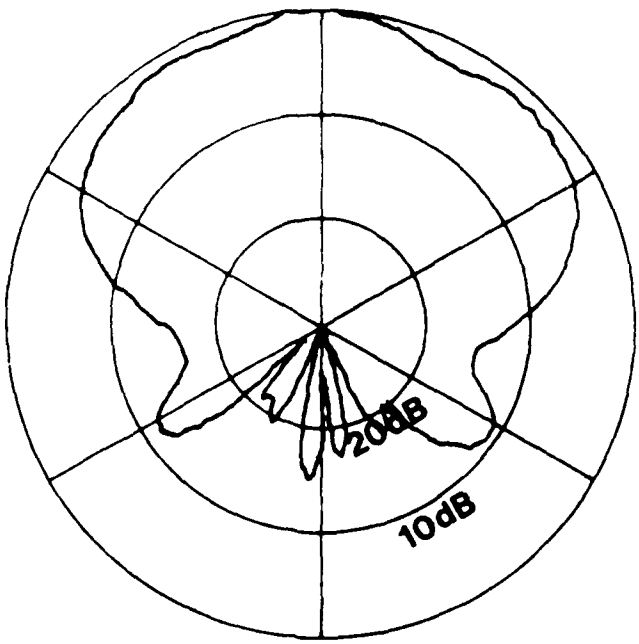

E Plane

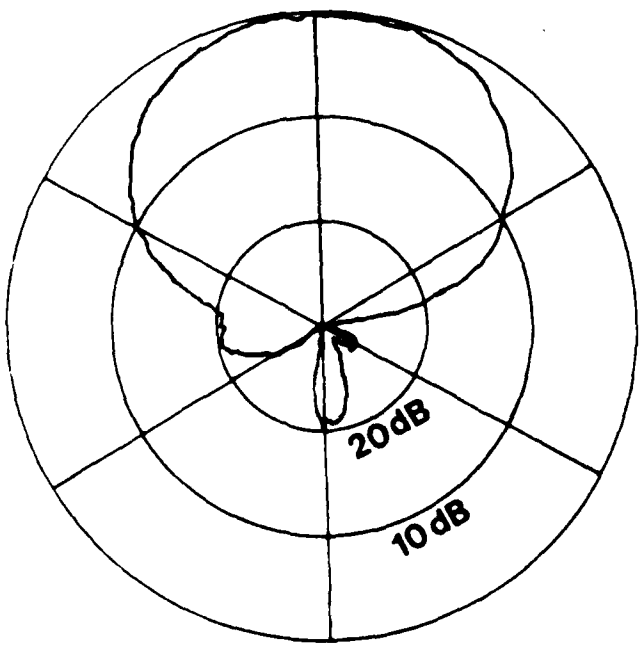

H Plane

Figure 3.7. X-band (9.65 GHz) aperture coupled patch with high permittivity feed substrate, $\epsilon_r^b = 2.2, d_b = .05cm, L_p = .94cm, W_p = 1.28cm, L_{ap} = .35cm, W_{ap} = .09cm, \epsilon_r^a = 10.2, d_a = .064cm, W_f = 0.6cm, L_s = 1.83cm.$

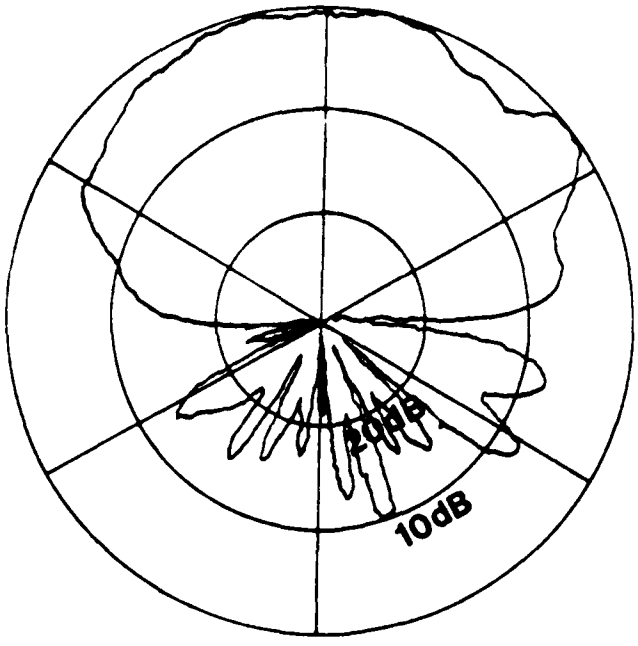

E Plane

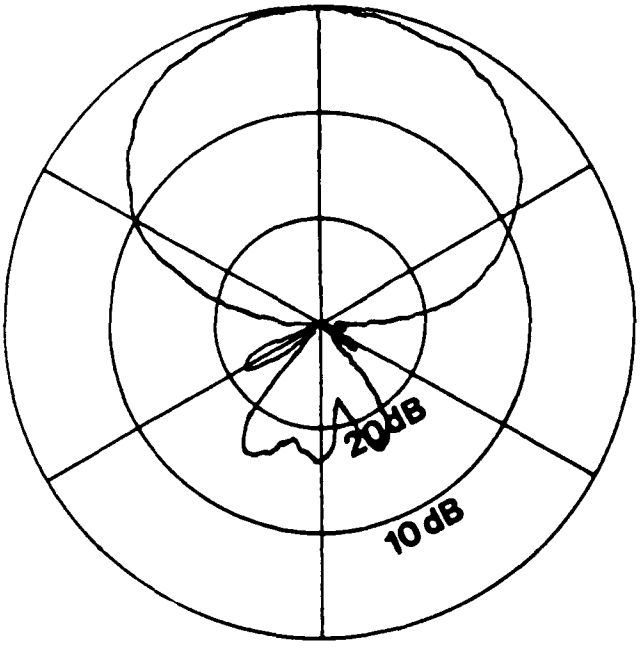

H Plane

Figure 3.8. 16.68 GHz radiation patterns. $\epsilon_r^b = 2.2, d_b = .05cm, L_p = .52cm, W_p = .7cm, L_{ap} = .115cm, W_{ap} = 0.08, \epsilon_r^a = 10.2, d_a = .64cm, W_f = 0.06cm, L_s = .44cm.$

of radiation into the back (feed) region is not indicative of what can be obtained with a large ground plane. A typical computed pattern of an aperture coupled patch on an infinite ground plane is shown in Figure 3.9. The back-lobe level of -20 to -25 dB has been confirmed by measurements using a large ground plane. Therefore, it appears that the resonant patch is providing the primary means of radiation and the feed region would be relatively free of radiated power if the ground plane were large enough.

The antennas that were used to obtain the patterns in Figure 3.7 and 3.8 were both fabricated by using 0.025-inch Duroid 6010.2 (ϵ_r=10.2) for the feedline and 0.020-inch Duroid 5880 (ϵ_r=2.22) for the antenna. The other antenna parameters are given in the figures. The feed substrate in Figure 3.8 is twice as thick electrically as that in Figure 3.7, and this may contribute to the increased radiation in the backward region. Nonetheless, relatively little power is radiated to the feed side of the ground plane and placing absorber in this region should help to control stray coupling effects without significant loss of gain or adverse effects on the upper half space radiation pattern.

3.2 Printed Dipoles Fed by Slotline and Coplanar Waveguide

Three configurations have been studied which involve slots feeding printed dipoles; (a) a single slot feeding a single dipole (Figure 3.10), (b) coplanar waveguide feeding two dipoles (Figure 3.11a) and (c) coplanar waveguide feeding crossed dipoles for circular polarization (Figure 3.11b). All three structures are based upon the slot fed dipole shown in Figure 3.10. As in the aperture coupled patch two substrates are used: one enhances antenna operation by having a low relative permittivity, and the other simulates the semiconducting material used for active devices. Interest in coplanar waveguide feeds is due to the superior R.F. grounding it offers to active devices at millimeter wave frequencies. This grounding advantage can be critical for the design of high gain millimeter wave amplifiers.

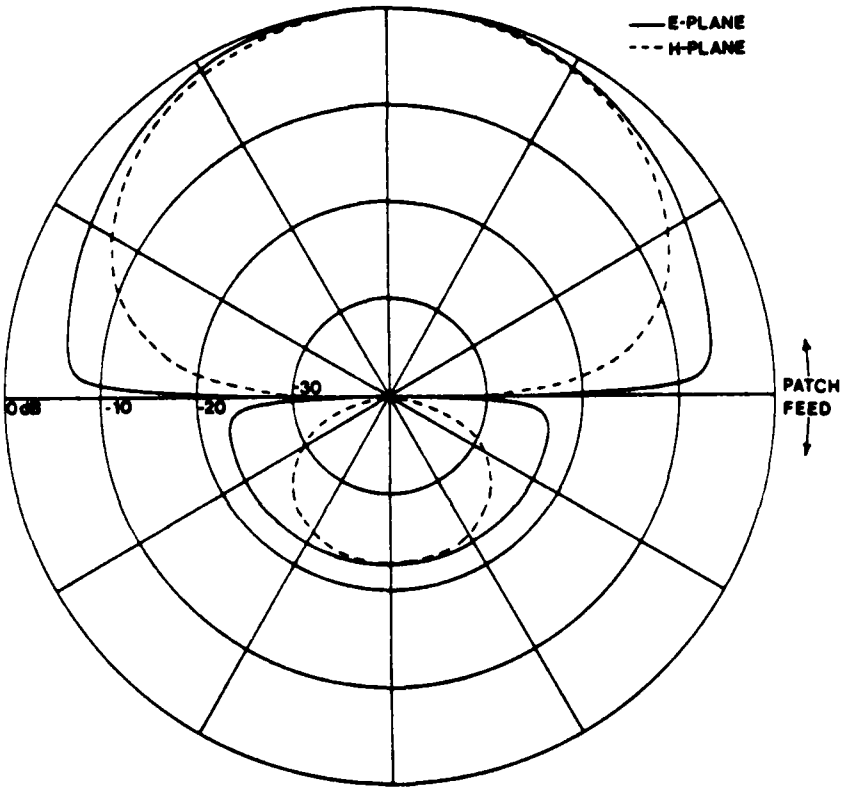

Figure 3.9. Calculated principal plane patterns of an aperture coupled patch antenna.

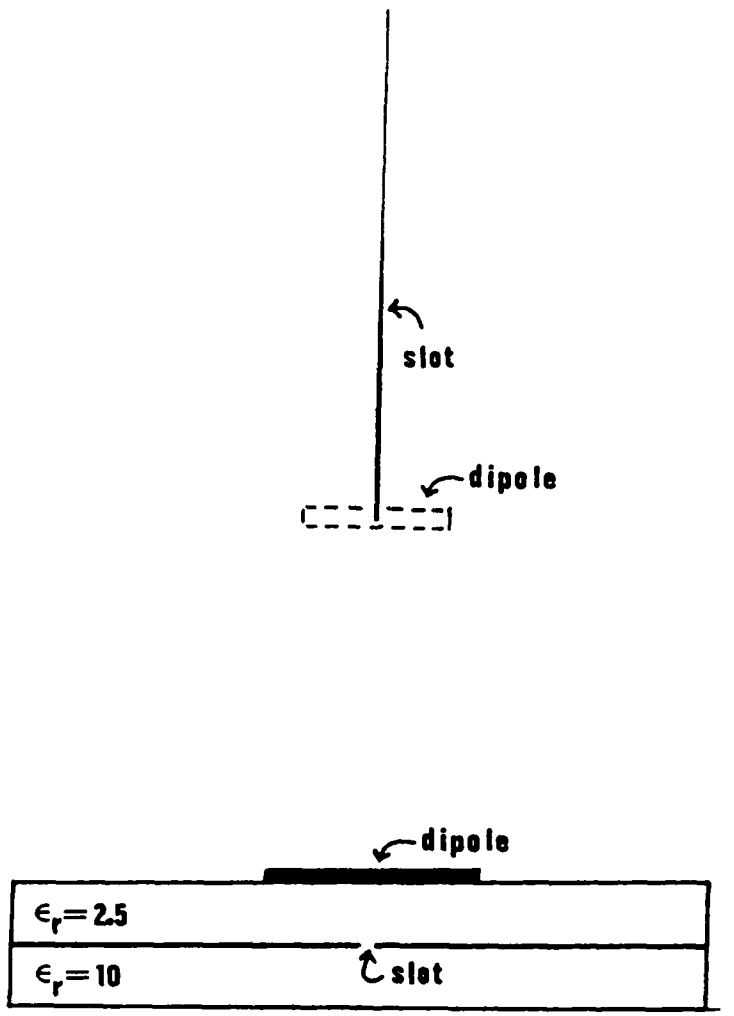

Figure 3.10. Single slot-fed dipole.

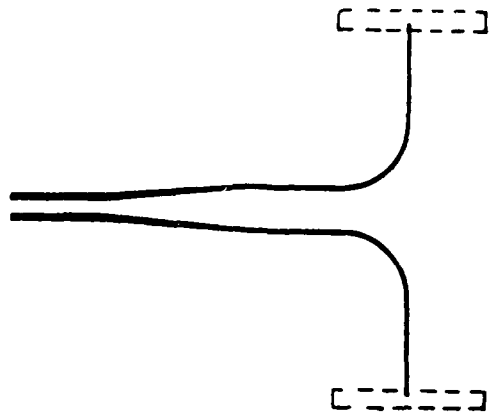

a.

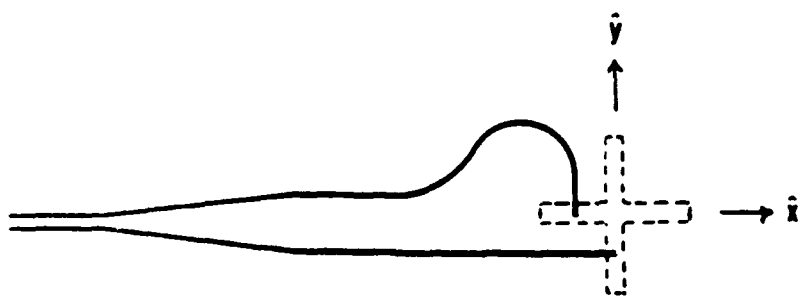

b.

Figure 3.11. Coplanar-waveguide fed dipoles. (a) Linearly polarized pair. (b) Circularly polarized crossed dipoles.

A possible disadvantage in comparison with the aperture coupled patch is the disruption of the antenna's ground plane caused by the presence of the slots or coplanar waveguide.

The slot fed dipole structure is motivated by the well known slotline-to-microstripline transition [10]. In that application, the slot and microstrip lines cross and then extend beyond each other by about one quarter wavelength. For the slot fed dipole case, it was found that placing the slot end almost directly under the dipole gave the best results. Coupling is tightest when the slot is located at nearly the center of the dipole's long dimension, lessening as it is moved closer to an end. The interaction can be considered as inductive coupling between the current flowing around the slot end and the current on the dipole.

The structure shown in Figure 3.10 was constructed with the antenna supported on a substrate (ϵ_r=2.5) with a thickness of .060" and the slot supported on a substrate (ϵ_r=10.2) with a thickness of .050". A slot of width .010" was excited by a semirigid coaxial line and then tapered to a width of .030" under a dipole which is .820" long and .100" wide. (The dimensions of the dipole, the substrate and the slot under the dipole are the same for the configurations shown in Figure 3.11a and 3.11b.) The measured antenna patterns are shown in Figure 3.12. Impedance plots show a well behaved resonance with roughly a 1% bandwidth (VSWR<2) and greater than 20 dB return loss at 4.72 GHz. The patterns show some significant back radiation which is attributed to radiation from the slot feed and from the coax-to-slot transition.

Figure 3.11a illustrates the second configuration, a coplanar waveguide feeding two dipoles. At the board edge, the coplanar waveguide dimensions are chosen for a 50Ω impedance. The coupled slots are then gradually thinned to a width of .030", separated by several slot widths (to decouple one from the other) and then routed to each dipole. By

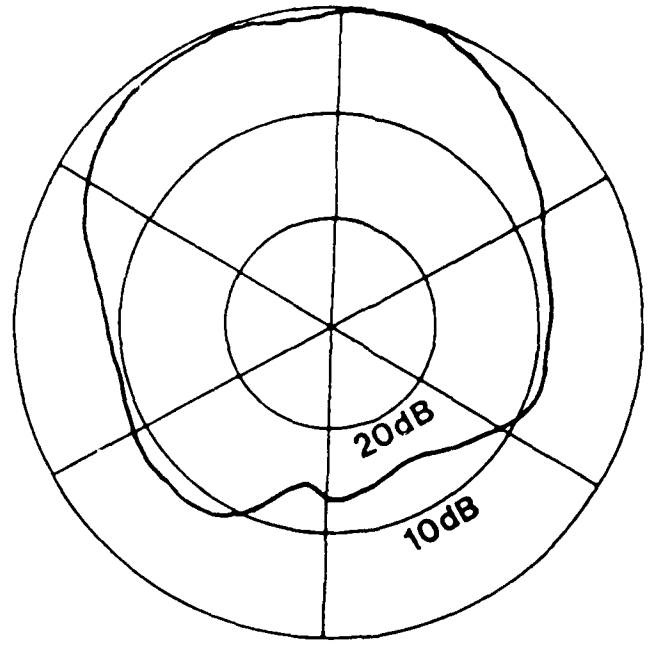

E Plane

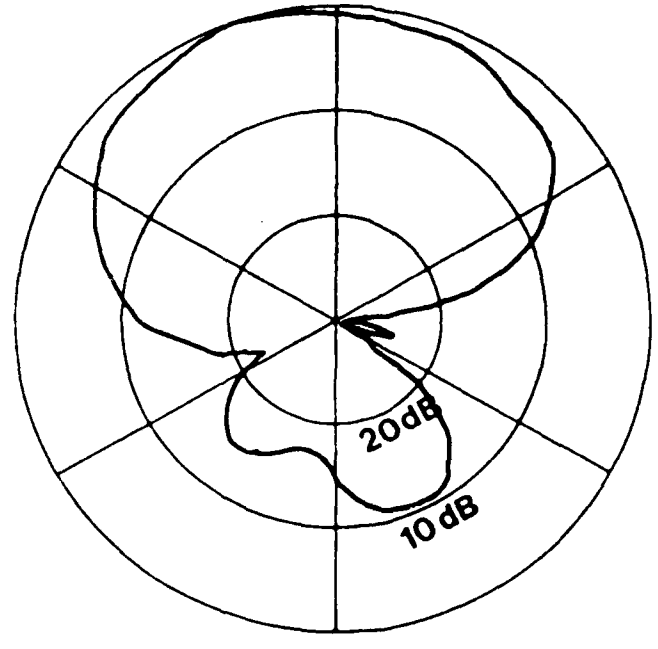

H Plane

Figure 3.12. Pattern of single slot-fed dipole.

adjusting the placement of the dipoles relative to the slots, a return loss greater than 20 dB is achieved at the resonant frequency (see Figure 3.13a). Bandwidth and slot location were, as expected, nearly the same as for the single slot/dipole structure. Patterns for the coplanar waveguide fed dipoles are shown in Figure 3.13b. Dipole separation was such that H-plane nulls should exist at $\pm 39°$ from broadside. Since no nulls are evident, it appears that the feed slots are participating in the radiation such that the effective radiating centers of the dipole/slot combination are closer to each other than the physical distance between the dipoles. As a check of this hypothesis, the feed locations were shifted so that the slots pass under the dipoles one quarter dipole length from the dipoles' ends. This reduces the coupling from slot to dipole and pattern nulls appear at the proper angles. For dipoles offset fed in this manner the return loss is 10 dB.

Finally, in Figure 3.11b, we show crossed dipoles fed by coplanar waveguide for circular polarization. As in the second structure, the slots are gradually decoupled from each other, the slot path to one dipole is then made one quarter wavelength longer than the path to the other. Each slot feeds its dipole roughly one quarter dipole length from the dipole end. A return loss of greater than 15 dB is observed at an operating frequency of 4.81 GHz (see Figure 3.14a). In Figure 3.14b, pattern plots of $E_\theta(\phi = 0°, \theta)$, $E_\phi(\phi = 90°, \theta)$, $E_\phi(\phi = 0°, \theta)$, and $E_\phi(\phi = 90°, \theta)$ are presented. The coordinates ϕ and θ are defined in the usual way with respect to the x and y axes in Figure 3.11b. From relative gain measurements at ϕ=0, 45° and 90° an axial ratio of 2.8 dB is estimated.

Spurious slot radiation seems to play a role in each of the three structures tested. It is likely that this effect could be further minimized by adjusting slot width and location.

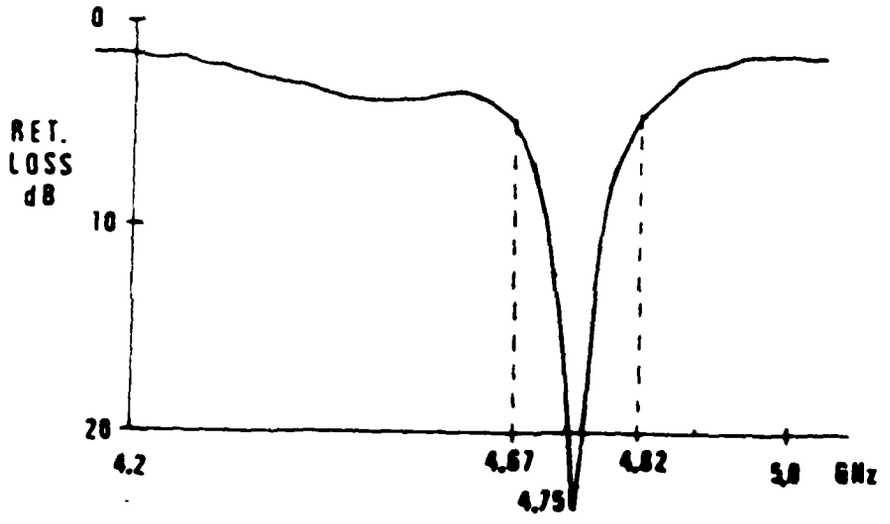

Figure 3.13a Return loss of dipoles center-fed by coplanar waveguide.

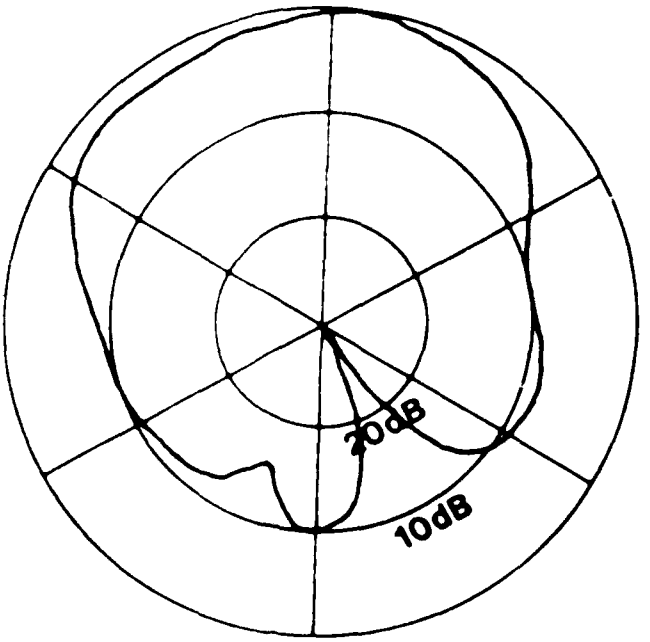

E Plane

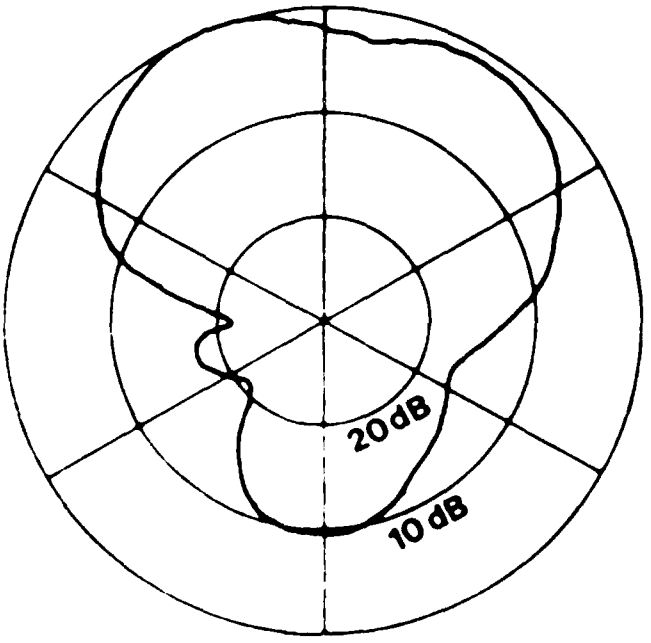

H Plane

Figure 3.13b Pattern of two dipoles fed by coplanar waveguide.

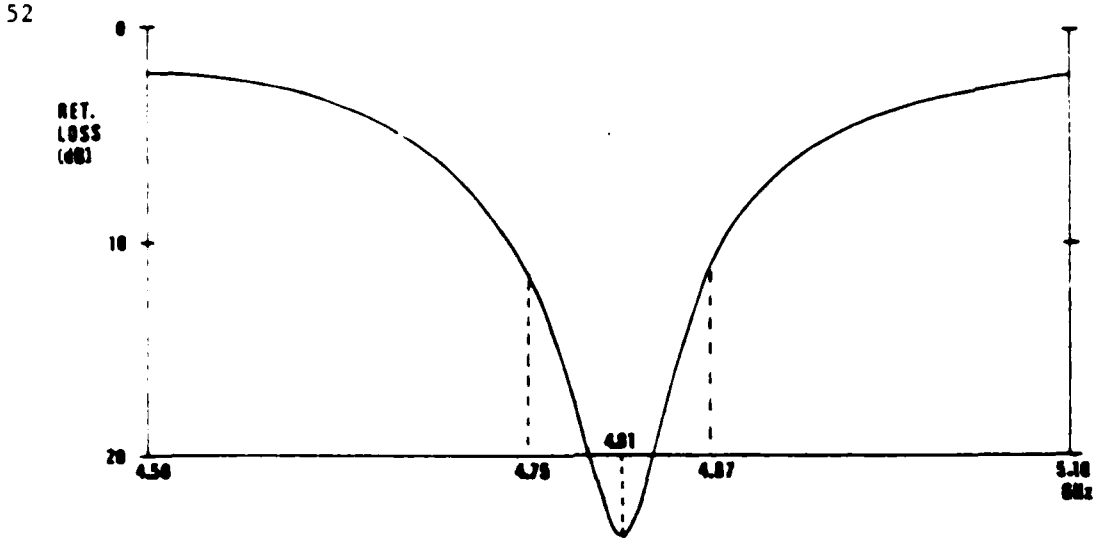

a.

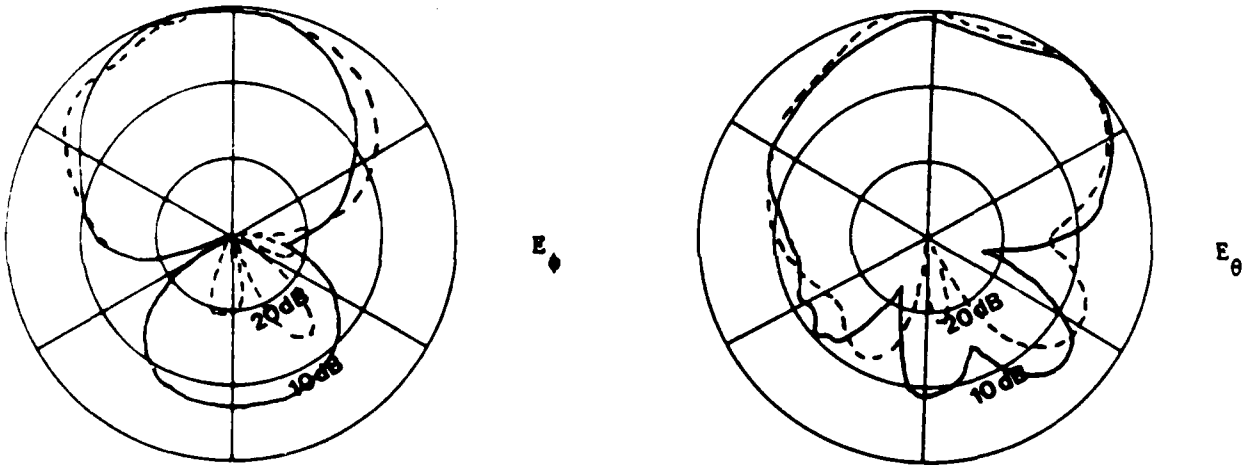

b.

Figure 3.14. Measured performance of crossed dipoles. (a) Return loss. (b) E_θ and E_ϕ patterns,— —$\phi = 0^0$,- - - - -$\phi = 90^o$.

3.3 Summary

Two types of antenna elements for use in integrated phased arrays have been investigated. Both allow the use of two substrates, a low permittivity substrate to optimize antenna performance and a high permittivity substrate (such as GaAs) on which active devices can be fabricated. The aperture coupled patch radiates well, can be impedance matched by simple adjustment of the antenna parameters, and is compatible with microstripline circuit techniques. The slot-fed dipoles can be used singly with slotline feeds or in pairs with coplanar waveguide feeds, which offer good grounding for millimeter wave FET devices. A circularly polarized version of the antenna has been obtained by using crossed dipoles and a coplanar waveguide feed.

References for Chapter 3

1. R. J. Mailloux, "Phased Array Architecture for mm-Wave Active Arrays," Microwave Journal, Vol. 29, No. 7, 117-124, July 1986.

2. D. M. Pozar, "Considerations for Millimeter Wave Printed Antennas," IEEE Trans. Antennas and Propagat., Vol. AP-31, 740-747, September 1983.

3. D. M. Pozar and D. H. Schaubert, "Scan Blindness in Infinite Phased Arrays of Printed Dipoles, IEEE Trans. Antennas and Propagat., Vol. AP-32, 602-610, June 1984.

4. D. M. Pozar and D. H. Schaubert, "Analysis of an Infinite Array of Rectangular Patches with Idealized Probe Feeds," IEEE Trans. Antennas and Propagat., Vol. AP-32, 1101-1107, October 1984.

5. D. H. Schaubert, D. M. Pozar, K. S. Yngvesson, and R. W. Jackson, "Considerations for Millimeter Wave Monolithic Phased Arrays," Proc. 1984 Antenna Applications Symposium, University of Illinois.

6. D. M. Pozar, "Microstrip Antenna Aperture Coupled to a Microstripline," Electronics Letters, Vol. 21, 49-50, January 17, 1985.

7. P. L. Sullivan and D. H. Schaubert, "Analysis of an Aperture Coupled Microstrip Antenna," IEEE Trans. Antennas Propagat., Vol. AP-34, 977-984, August 1986.

8. D. H. Schaubert, R. W. Jackson and D. M. Pozar, "Antenna Elements for Integrated Phased Arrays," Proc 1985 Antenna Applications Symposium, University of Illinois.

9. P. L. Sullivan and D. H. Schaubert, "Analysis of an Aperture Coupled Microstrip Antenna," RADC-TR-85-274, Rome Air Development Center, February 1986.

10. J. B. Knorr, "Slot-line Transitions," IEEE Trans. on Microwave Theory and Techniques, Vol. MTT-22, 548-554, May 1974.

Chapter 4

ACTIVE CIRCUITS FOR MONOLITHIC PHASED ARRAYS

In this chapter, circuit issues and novel circuit techniques are discussed. A brief investigation of the effects of scan impedance variation on current gain is reported. The use of injection locked oscillators as compact high gain phase shifters is discussed in some depth. A review of a high gain amplifier, constructed under this program, is reported. Its novelty is due to the fact that it was built using the coplanar waveguide circuit medium.

Coplanar waveguide (CPW) has received some emphasis in this work due to its possible advantages when compared to microstrip for some applications [1]. Since CPW has its R.F. grounds and active circuitry on the same surface, via holes are eliminated and construction is greatly simplified. CPW also lends itself to integration with field effect transistors. The inductance introduced in FET circuits due to microstrip via holes can significantly reduce circuit performance, especially at millimeter wave frequencies. CPW eliminates this problem. On the other hand, CPW circuits can be difficult to design since air bridges are often necessary, the addition of ground planes on the active surface reduces circuit flexibility, and circuit components in CPW are not as well known as those for microstrip. Also, high power circuits may have some problems with heat removal. A more detailed comparison of microstrip and CPW can be found in [1].

4.1 Coplanar Waveguide Amplifier

Figure 4.1 shows a single stage high gain amplifier which was built in coplanar wave guide. A detailed description of the design and fabrication of this amplifier can be found in [2]. A summary is presented herein.

Two amplifiers were constructed, one intended for operation at 10 GHz and one for operation at 20 GHz. A Mitsubishi chip FET #1403 was used for the first and a #1404 for

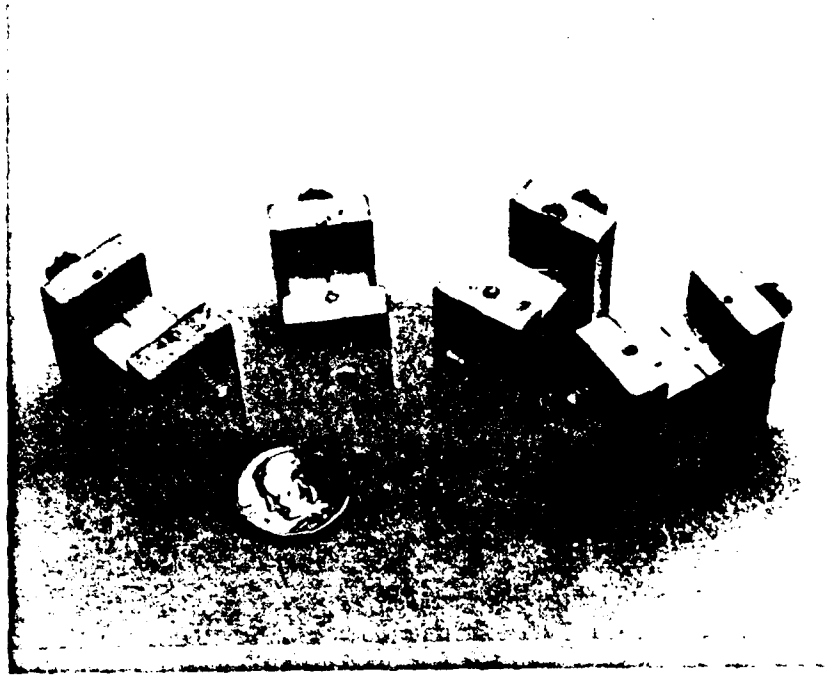

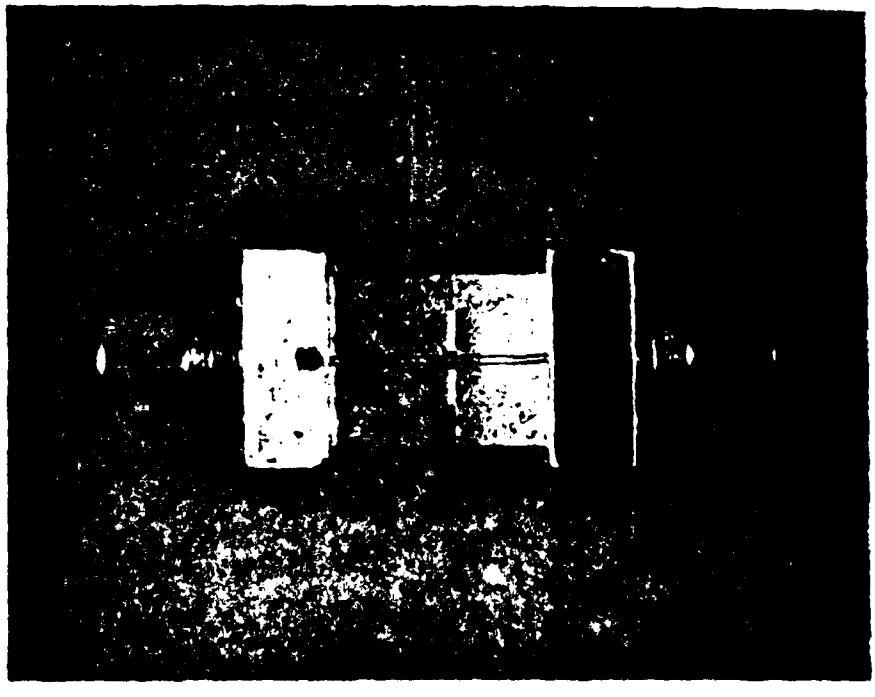

Figure 4.1 CPW K connector test fixtures and amplifier.

the second. In both cases considerable care was used to insure that the circuits looked as monolithic as possible. Ceramic substrates with permittivities of 13 were used to simulate GaAs and chips were carefully mounted in a groove so that the active FET surface was on the same plane as the circuitry. This minimized bond wire length. Figure 4.2a shows the FET mounting arrangement. Each substrate was 0.025" thick and was not metalized on the lower side. An air space separated the lower side from the ground plane of the fixture by about 0.15". Wiltron K connectors were used and the entire fixture was found to perform well up to 26 GHz.

The scattering parameters for the FET mounted in the groove were de-embedded from the fixture using the Δl de-embedding method described in [2] and an HP-8510 measurement system. Matching networks were designed using these measurements and modeled on SUPERCOMPACT. An enlargement of the mask used for the 10 GHz circuit is shown in Figure 4.2b. Figure 4.3 plots the measured results for two duplicate versions of the 10 GHz amplifier. The output match (not shown) was not as good as the input match at the operating frequency. It was measured to have roughly 10 dB of return loss. In addition, the center frequency was roughly 9.5 GHz, 5% below the design frequency. Computer modeling indicates that much of this discrepancy can be attributed to discontinuity effects.

A 20 GHz amplifier was designed using de-embedded measurements of the 1404 FET. The resulting amplifier did not operate at all correctly and it was found that an erroneous measurement of the FET had occurred. Subsequently, the FET was remeasured. The new scattering parameters were used in a computer model of the amplifier which included the matching network designed from the incorrect FET measurements. Using the new FET characteristics, the computer model gave excellent agreement with the measured amplifier results. It should be noted that discontinuity effects were included, approximately, in

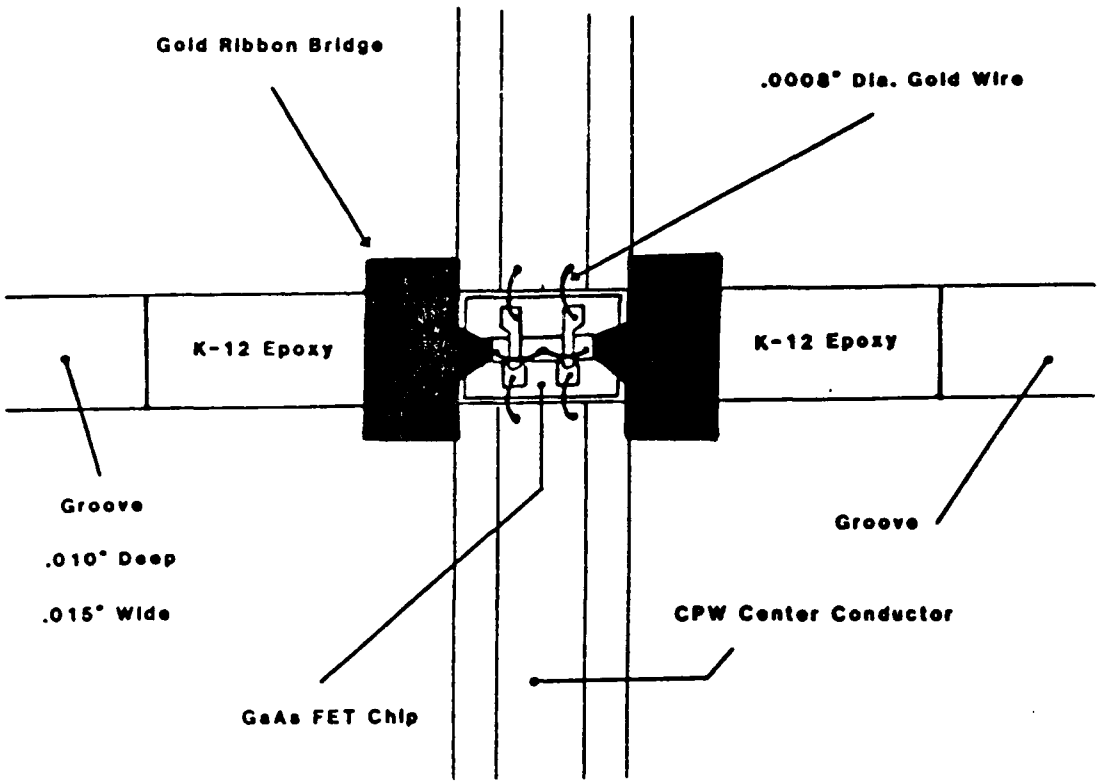

a.

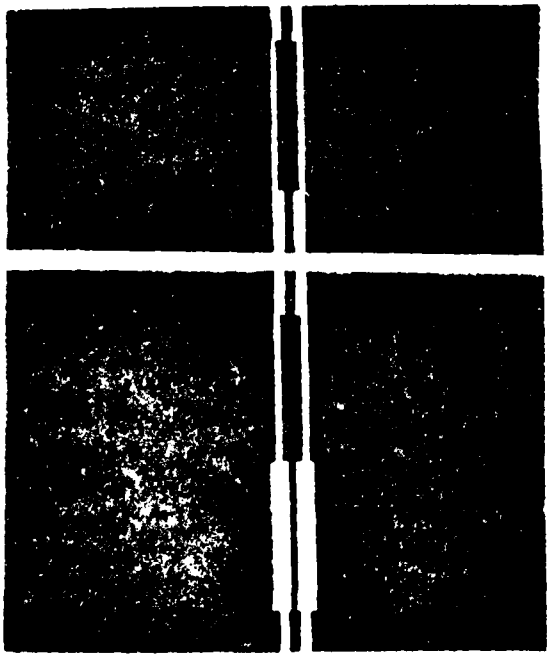

b.

Figure 4.2 (a) GaAs FET mounting arrangement (b) Enlargement of 10 GHz amplifier matching circuit photomask.

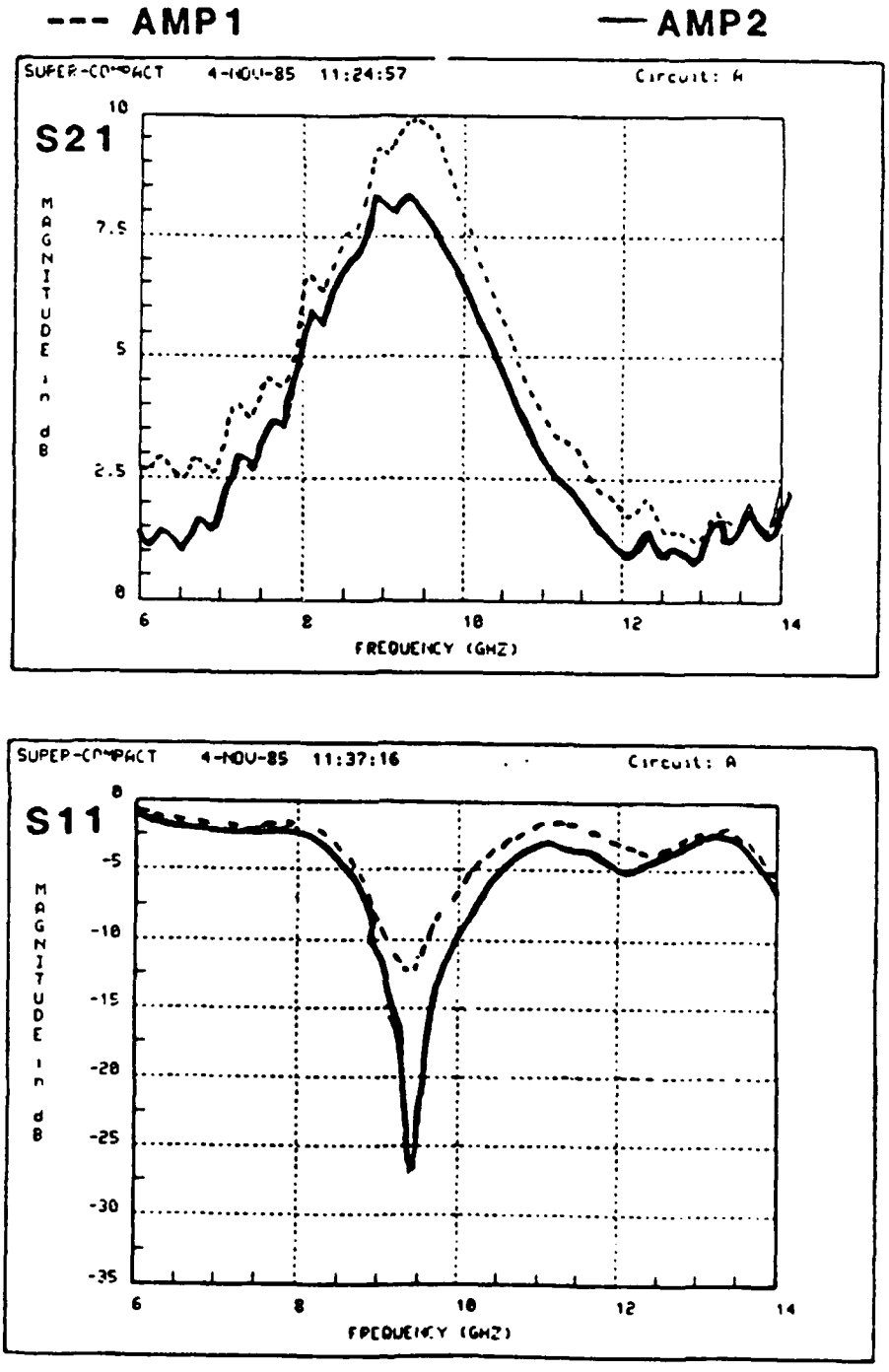

Figure 4.3 S_{21} and S_{11} of assembled 10 GHz CPW amplifier.

the 20 GHz design and it seems that this made some improvement in the match between measured and predicted results. The good agreement which was observed indicates that a redesigned matching network would have produced a satisfactory amplifier.

As a final note, FET bias was applied through the input and output ports for this device and no bias networks were constructed. In the study of injection locked oscillators reported in a later section, two schemes for biasing were used successfully with CPW.

4.2 Variation of Amplifier Gain with Scan Angle

The scan angle variation of the input impedance of an antenna element in a large array has been calculated and discussed in a number of previous sections. This scan impedance is of interest due to the difficulties it causes in matching to the amplifier driving the antenna. To investigate this question, antenna impedance has been calculated versus scan angle for a patch antenna embedded in an infinite array of patch antennas (L=0.13 λ_o, w=0.15λ_o) on a fairly thick substrate (ϵ_r=12.8, d=0.025λ_o). These impedance values are listed in Table 4.1. When an antenna presents these impedances to the output of an amplifier, the following gain (power delivered to antenna/power available to amplifier) and amplifier input return loss expressions result.

$$G_T = 10\ log\ (|S_{21}|^2(1 - |\Gamma_A|^2))$$

$$Ret.Loss = -20\ log\ (|S_{21}||S_{12}||\Gamma_A|)$$

Γ_A is the reflection coefficient presented to the amplifier (normaled to $\theta = 0°$ impedance) and S_{21} and S_{12} are the S parameters for the total amplifier (matching circuit and transistors) which we assume to be matched for maximum available gain. Using the impedances

Table 4.1 Scan Impedance for Infinite Phased Array of Patches with $\lambda_o/2$ Separation

$\epsilon_r = 12.8$ $\quad d = 0.025\lambda_o$ $\quad W = 0.15\lambda_o$ $\quad L = 0.128\lambda_o$

	E plane	H plane
θ	Z_{in}	Z_{in}
0	386	386
10	383–j8	393–j4
20	369–j33	412–j23
30	339–j68	442–j63
40	288–j101	471–j141
50	220–j118	466–j264
60	142–j113	381–j370
70	60–j81	230–j463
80	.4–j1	87–j442
90	.2+j43	.7–j383

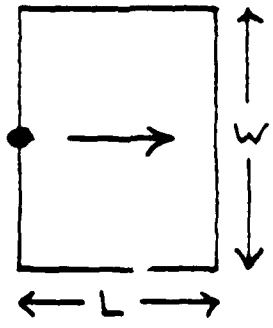

in the table we see that the gain has degraded by 1 dB at a scan angle of 60° in the E plane.

The degradation of match seen at the amplifier input depends upon the amplifier S parameters. If the amplifier were unilateral ($|S_{12}| = 0$), no degradation would occur. For an amplifier designed around a lower power FET (NE71000) at 18 GHz, the relevant amplifier S parameters are ($|S_{21}| = 2.68$ and $|S_{12}| = .215$. The input return loss to this amplifier drops to 10 dB (from infinity) when $|\Gamma_A| = .51$. This occurs at a scan angle of 60° in the E-plane. H-plane values are similar.

For an amplifier whose input is fed by a scanning antenna, the expressions for gain and output match (of the amplifier) would be the same as the ones given above.

4.3 Phase Shifting Injection Locked Oscillators

Injection locked oscillators (ILO) have been used for a number of years primarily to quiet a noisy high power source by locking it to a quiet low power source. The principle is also used for combining the power from several sources either in a cavity or in free space with a phased antenna array. This last application is one of the motivations for the discussion which follows.

Integrated circuits for use with scanned arrays must be small in order to keep wafer yields high, or, if integrated with an antenna element, to minimize the use of scarce surface area. Phase shifting injection locked oscillators are potentially very space efficient since the phase shifting and gain/power stages are combined. The concept of an ILO phase shifter was used by Cohen [3] who constructed a one-port Gunn diode oscillator which was tuned with a varactor diode. He achieved 160° phase shift at microwave and millimeter wave frequencies with a very small power deviation over the phase shift range.

In the following work, Cohen's results are extended by the creation of two different circuits which are amenable to integration. Both of these circuits are two-ports, use general purpose field effect transistors, and are phase shifted using varactor diodes. The first circuit consists of two reflection type oscillators which are combined with a quadrature hybrid to create a two-port. Coplanar waveguide is the circuit medium. The second circuit combines phase shifting and frequency doubling in one circuit which was designed in the microstrip transmission medium.

Bandwidth Considerations in Phase Shifting I.L.O.'s. Figure 4.4 illustrates the use of injection locking for scanning a phased array. Both oscillators are locked to the same injection frequency, ω_i, but oscillator 1 has a different unlocked, free running frequency, ω_{fr1}, while oscillator 2 has a free running frequency ω_{fr2}. The reader is reminded that the free running frequency does not appear at the output of the circuit after it is locked. Using an analysis which is similar to Kurokawa's [4], one can show that

$$\sin(\phi_1) = \frac{\omega_i - \omega_{fr1}}{\Delta\omega_m}$$

$$\Delta\omega_m = \frac{1}{Q_{ext}\sqrt{\frac{P_i}{P}}}$$

where ϕ_1 is the phase of the output signal of the first oscillator relative to the injection signal, $\Delta\omega_m$ is one half the locking range of the oscillator, P_i is the injection power, P is the output power, and Q_{ext} is the external Q. A similar equation is obtained for oscillator 2. Relative phase shift between the two oscillator assemblies in Figure 4.4 is accomplished if ω_{fr1} is made to be different to ω_{fr2} by, in this case, adjusting a varactor bias voltage.

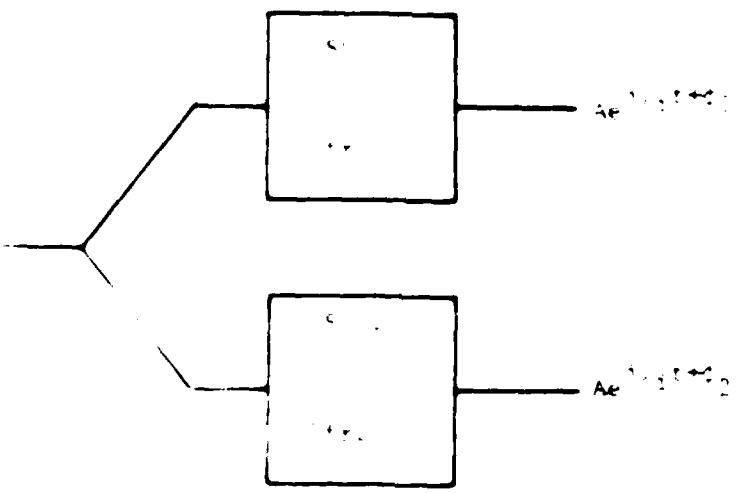

Figure 4.4 Block diagram of two injection locked oscillators which produce relative phase shift due to their different free running frequencies

As the preceding equations show, the largest theoretically achievable phase shift between the two oscillators is 180 degrees. This occurs when $\omega_i - \omega_{fr1} = \Delta\omega_m$ and $\omega_i - \omega_{fr2} = -\Delta\omega_m$. In order to achieve a full 360 degrees of phase shift, an additional phase shifter must be added to give the extra 180 degrees (this could be a switched line phase shifter, for example). Or, as in the microstrip oscillator to be described shortly, the second harmonic may be used.

In practice, one can almost achieve the maximum theoretical phase shift if the injection frequency remains constant and if the oscillators are not switched (and thus required to unlock and relock at the edge of their locking range). If, however, the injection frequency varies over a band due to phase or frequency modulation, then this maximum phase shift cannot be achieved. At maximum phase shift slight changes in ω_i will cause either one or the other oscillator to come unlocked. In fact, even if the phase shift were reduced from the maximum one would not operate at the band edge where unlocking is nearly ready to occur since the relative phase shift becomes very frequency dependent at that point. This is especially evident if one examines Figure 4.5 where relative phase shift versus normalized frequency is plotted using the previously described equation (only half the band is shown). Note the weak frequency dependence near the center of the band for low phase shifts. This particular plot assumes that each oscillator taken by itself will have a locking range $2\Delta\omega_m / \omega_i$ of 20%. As an example, suppose a maximum phase shift of 90° were needed, Figure 4.5 indicates roughly a 4% bandwidth is possible. All that is needed to plot Figure 4.5 is the locking bandwidth of the typical oscillator. Thus the system aspects of a set of these oscillators can be estimated from the measured characteristics of one oscillator. Of course mutual coupling other than through the feed network is neglected.

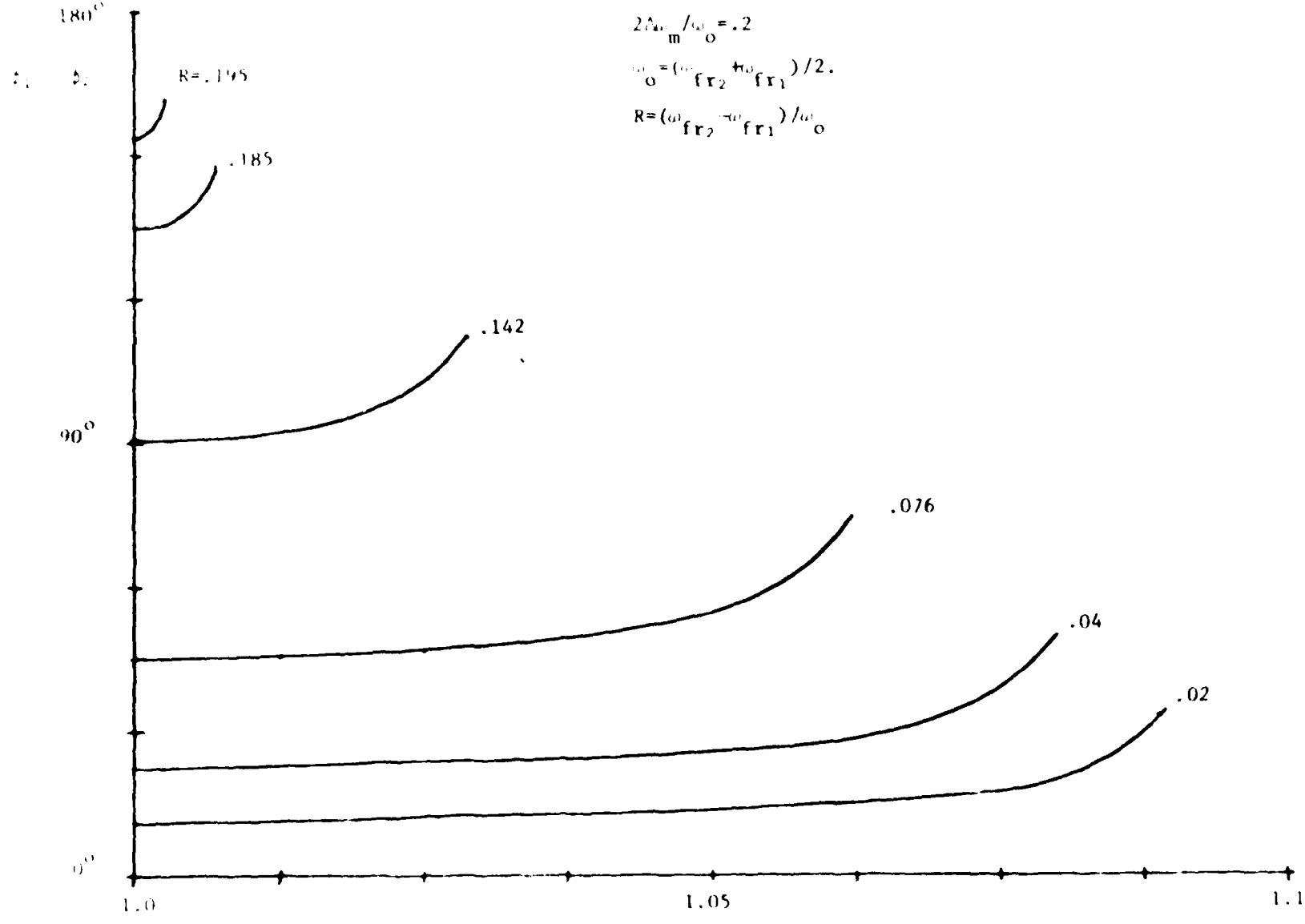

Figure 4.5 Theoretical frequency response of a phase shifting injection locked oscillator

Finally, we note that the bandwidth discussion presented above applies to only modulation bandwidth in one channel. If one wanted to operate around a different center frequency, a new set of varactor control voltages would be used which causes $\Delta\phi_{12}$ and $\Delta\phi_{23}$ to straddle a new frequency. This changing of the center frequency of a channel can be done over a much broader band than the modulation bandwidth. We also note that this method is not a true time delay and thus will cause the antenna pattern to squint if a large bandwidth signal is used in one channel.

Oscillator Phase Shifter in Coplanar Waveguide. Figure 4.6 shows a drawing of a voltage controlled oscillator built in coplanar waveguide (CPW). The device used was a general purpose GaAs FET type Ne71083. Instability was introduced using short circuit stubs in the source circuit. Another stub on the gate served as a resonator and the effective length of this stub was varied using a chip varactor diode bonded at the stub's end. Gate, drain and varactor bias was applied using microstrip quarterwave and radial stubs which were mounted on top of the ground plane of the CPW. Only the gate bias is shown in the figure. The operating frequency was 5 GHz and could be varied over a 20% band. Output power was measured to be 15 dBm with no output matching network.

One further note on the biasing network, measurements of this decoupling network on a test through line which was separate from the oscillator showed that it was indeed transparent at this operating frequency. Use of this type of circuit in an integrated monolithic circuit would require a multilayer structure similar to what is common in digital integrated circuits. The process needed for multilayers on GaAs is not yet clear. Another bias technique which we have tried uses short circuit quarterwave CPW stubs. It was found that these also work very well if sufficient airbridges are used where the CPW stub meets the CPW main line. These airbridges serve to short out the unwanted even CPW

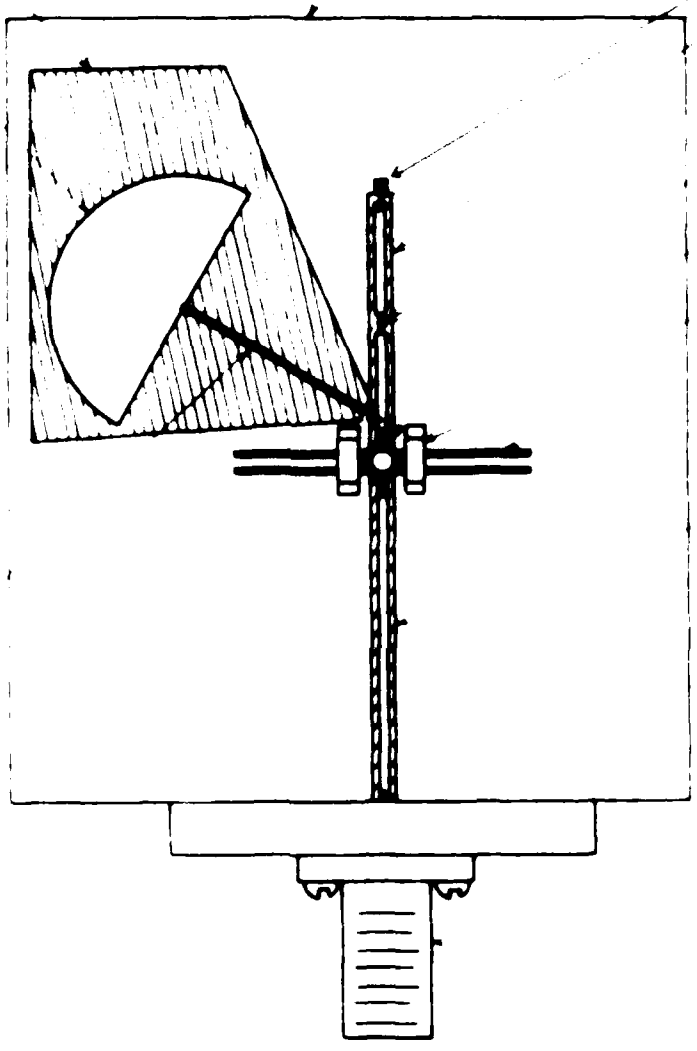

Figure 4.6 Drawing of a coplanar waveguide varactor tuned oscillator. Drain bias and varactor bias not shown

mode which is introduced at asymmetries. Two were used across the main line and one across the stub itself.

Two of these oscillators were used in the reflection type injection locking system shown in figure 4.7. A quadrature hybrid is used to create a two port. Each oscillator ideally has the same free running frequency for the same varactor control voltage. When both are injection locked to the signal entering port 1, their outputs combine and exit port 4. This entire assembly (two oscillators and a hybrid) makes up one block in figure 4.4. With reference to figure 4.7, phase shift relative to the injection signal is produced by varying the varactor control voltage and thus changing the free running frequencies of the oscillators. In a monolithic circuit, the oscillators would have nearly equal free running oscillation frequencies for a given control voltage. The discrete circuits which are reported herein each require a different varactor voltage to achieve matched free running frequencies. To achieve various phase shifts control voltage pairs were applied to the oscillator system. Except for control voltage, the oscillators were fairly well matched in terms of output power and operating frequencies. Figure 4.8a shows measured phase shift relative to one of the control voltages for three different injection frequencies. Over 150° of phase shift was measured at 5 GHz for each injected power. As expected, the phase shift becomes more sensitive to control voltage when injected power is reduced. Figure 4.8b shows measured output power deviation over the phase shift range for the three injection frequencies. The output power varies by less than ±0.5 dB over the phase shift range.

One of the advantages of this type of phase shifting scheme is its high locking gain. Gains of 20 dB or more have been measured. This gain must be reduced (by increasing injection power) to achieve more bandwidth as was discussed in the first section. Gain is further degraded if the hybrid has poor directivity (real and effective).

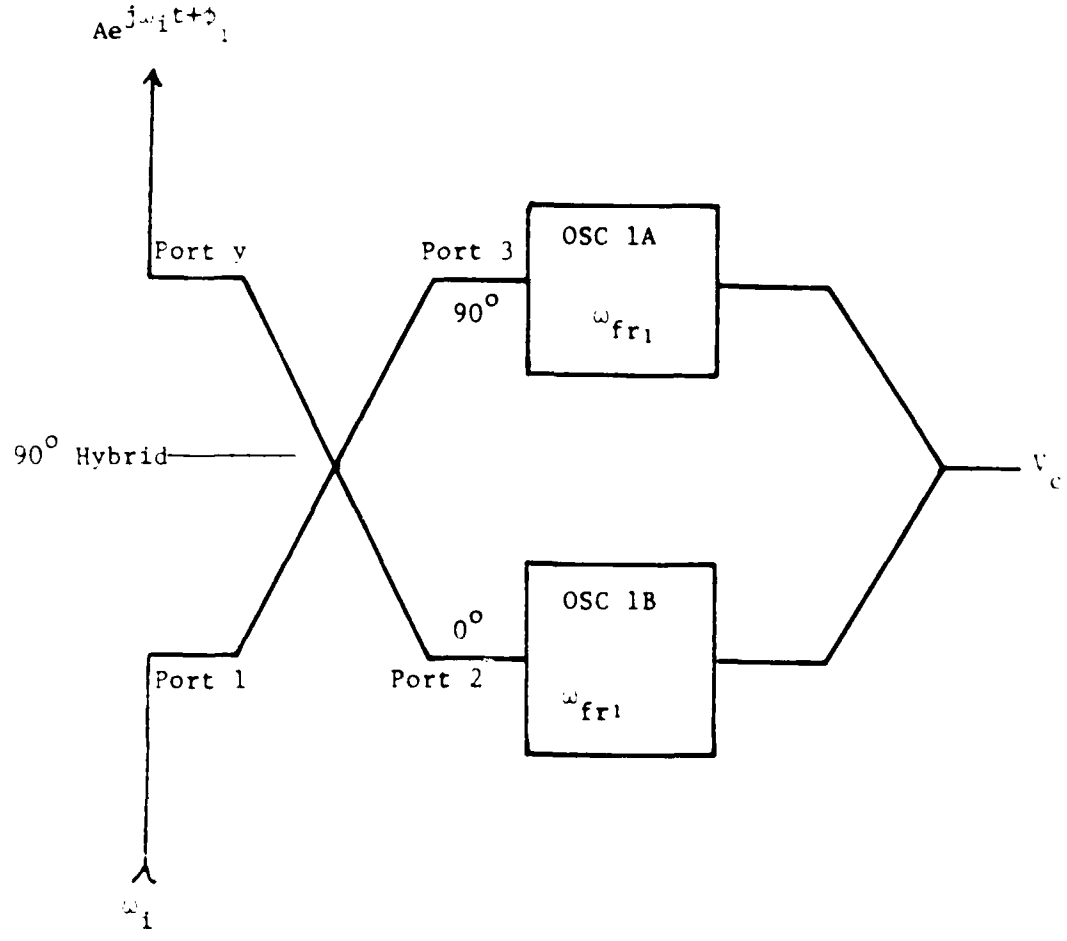

Figure 4.7 Schematic of two-port phase shifting oscillator using two one-port oscillators.

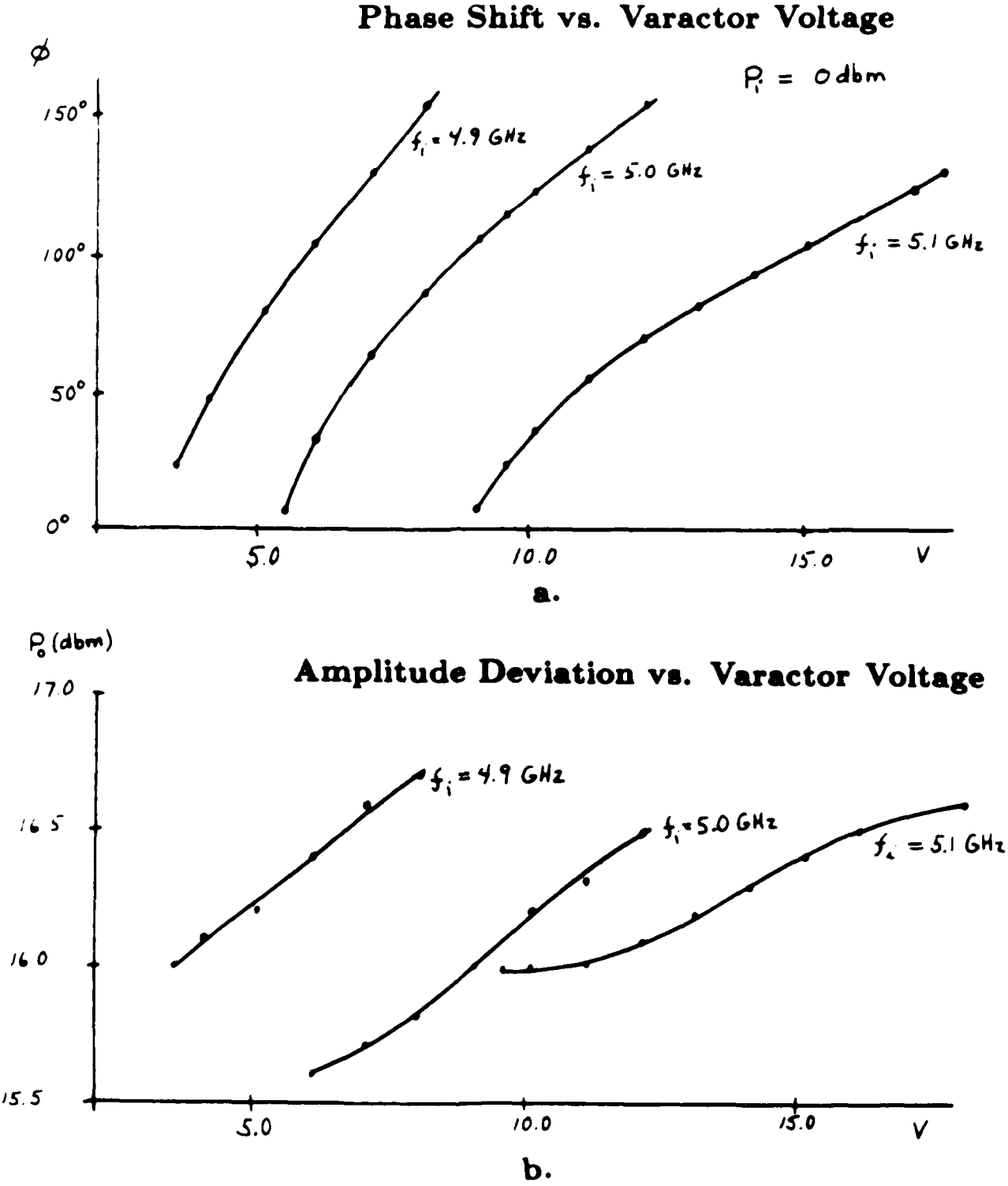

Figure 4.8 (a) Measured phase shift relative to injection signal (b) measured amplititude variation.

Oscillator, Phase Shifter/Doubler. Figure 4.9 is a diagram of a phase shifting oscillator doubler which was constructed in microstrip on low permittivity teflon circuit board. The circuit operates with a fundamental frequency of 4.65 GHz and is varactor tuneable over a small band. The quarter wave open circuit stub shown in the diagram on the left passes the second harmonic to the output port and blocks the fundamental. The injection signal comes in on the right. The FET is the same as was used on the CPW oscillator and is used in a common gate configuration which is made unstable with a short circuit stub in the gate circuit. A small resistance has been added to lower the circuit Q. The fundamental oscillation frequency is determined by the location of the larger stub and by the varactor. Second harmonic is blocked from leaving the input port by two open circuit stubs which are a quarter wavelength at 9.3 GHz.

The output power at the second harmonic has been measured to be about -1dBm. As little as -15 dbm injection power at the fundamental has been sufficient to lock. So the fundamental to second harmonic gain is as much as 15dB. The D.C. to R.F. efficiency is only a few percent. No attempt has yet been made to match the 10 GHz output so that this efficiency could improve. At present the oscillator is operated at a class A bias point. Operation at a class B point may also improve efficiency.

Two of these oscillators were constructed and locked to an injection signal of 4.65 GHz via a two-way power divider. The block diagram is similar to Figure 4.4 except that the output frequency and phase are twice as large as the non-doubling oscillator. Figure 4.10 shows a plot of measured 9.3 GHz phase of one oscillator relative to the phase of the other over the control voltage range. In this case, one oscillator's free running fundamental frequency remained fixed at the injection frequency and the other was varied from above to below the injection signal. A phase shift of nearly 360° is observed at the

Transmission Type Doubling I.L.O.

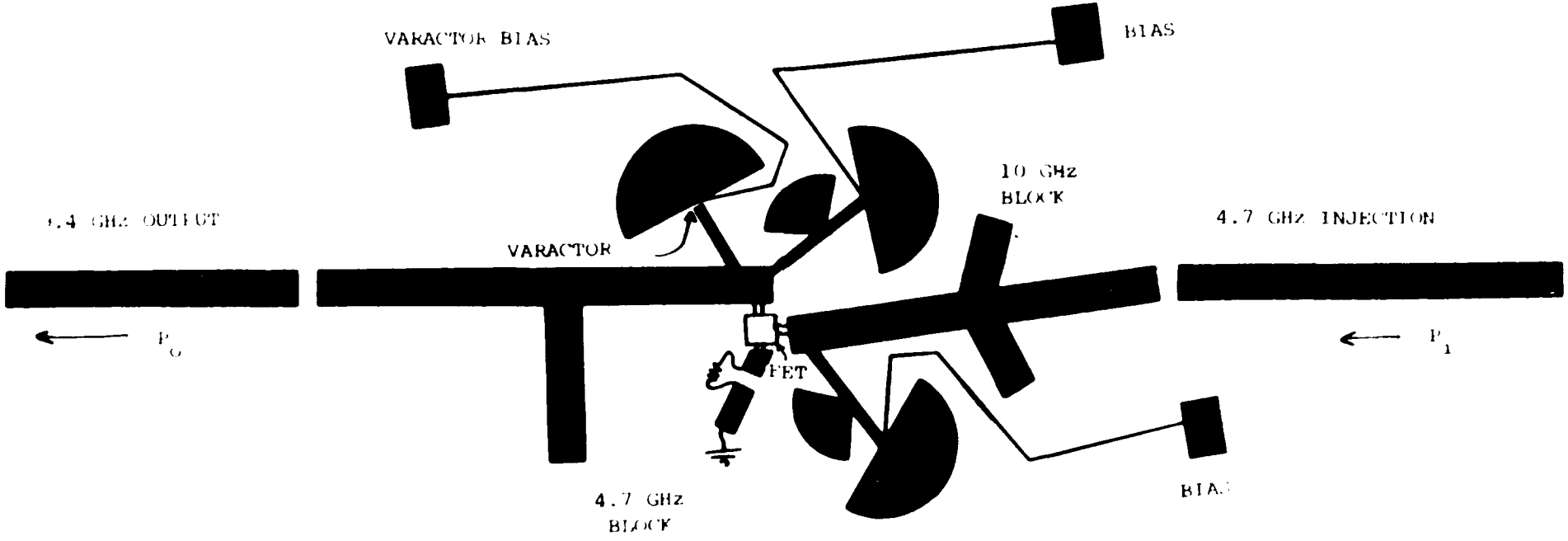

Figure 4.9 Layout of phase shifting/doubling injection locked oscillator.

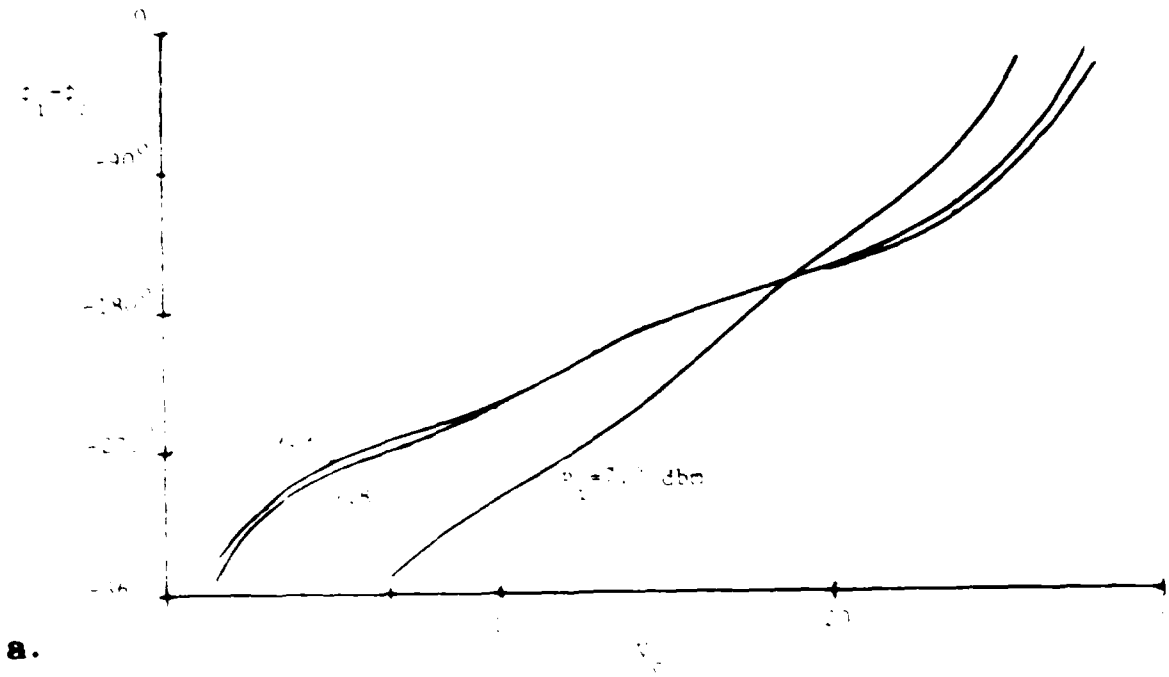

a.

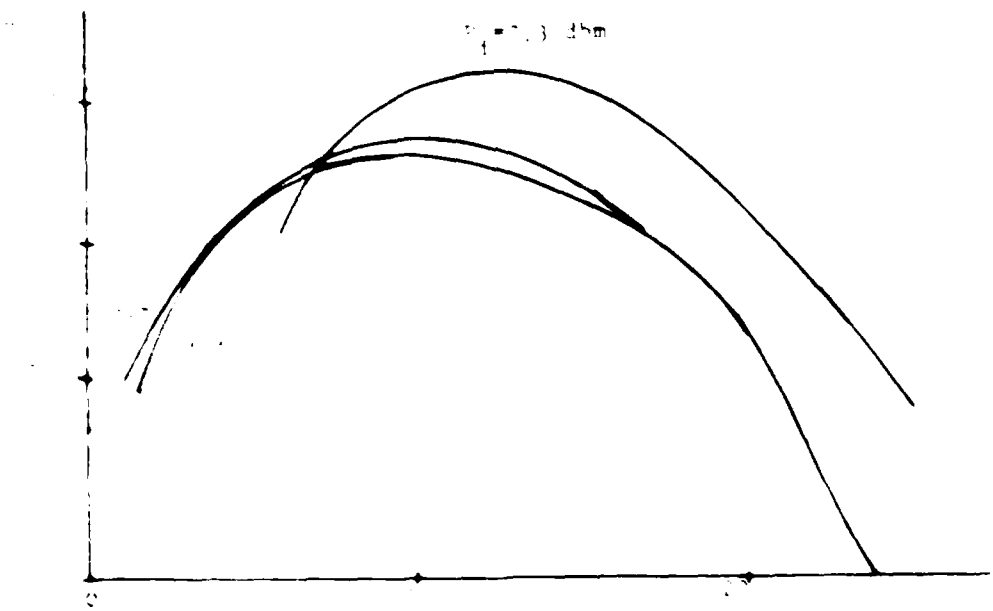

b.

Figure 4.10 a. Relative phase shift between two injection locked doubling oscillators b. Relative output power

high injection powers shown. At 0.0 dbm roughly 240° of phase shift has been observed probably due to noise in the system causing the oscillators to unlock. It is expected that further modifications will lower the injected power necessary for complete 360° phase shift..

References for Chapter 4

1 R. W. Jackson, "Considerations in the Use of Coplanar Waveguide for Millimeter Wave Integrated Circuits," IEEE Trans. on Microwave Theory and Tech., Vol. 34, December 1986.

2 P. Rainville, "Investigations of SHF FET Amplifiers in Coplanar Waveguide," M.S. Thesis, University of Massachusetts, 1986.

3 L. D. Cohen, "Active Phase Shifters of the Millimeter and Microwave Bands," IEEE Microwave Theory and Tech. Symposium Digest, 1984.

Chapter 5

PROTOTYPE ARRAYS

During this project, several small arrays were fabricated and tested. In this chapter, the results of those tests are presented. The arrays described below are: an 8-element, C-band, linear array of microstripline-fed slots; an 8-element, 20-GHz, linear array of microstrip patches; a 2x2, 20-GHz array of microstrip patches; and an 8-element, C-band, linear array of aperture coupled patches. Attempts to fabricate hybrid integrated PIN phase shifters on Duroid 6010.2 substrate for the aperture coupled array are described also.

5.1 Microstripline-Fed Slot Array

An 8-element, linear array of microstripline-fed slot antennas was built and tested. This work provided a basis for comparison and evaluation of some of our earlier ideas for array architecture. The array geometry is depicted in Figure 5.1 where a corporate feed network in microstripline is etched on one side of a 0.062" circuit board, $\epsilon_r = 2.5$. Open-ended sections of the microstripline extend across the center of the slots that are etched in the ground plane on the other side of the circuit board. The input impedance of the array is shown in Figure 5.2 and the E-plane radiation pattern is shown in Figure 5.3. In order to produce a unidirectional pattern, a reflector was placed one quarter wavelength from the feed network side of the array. The input impedance and radiation patterns are shown in Figures 5.4-5.6.

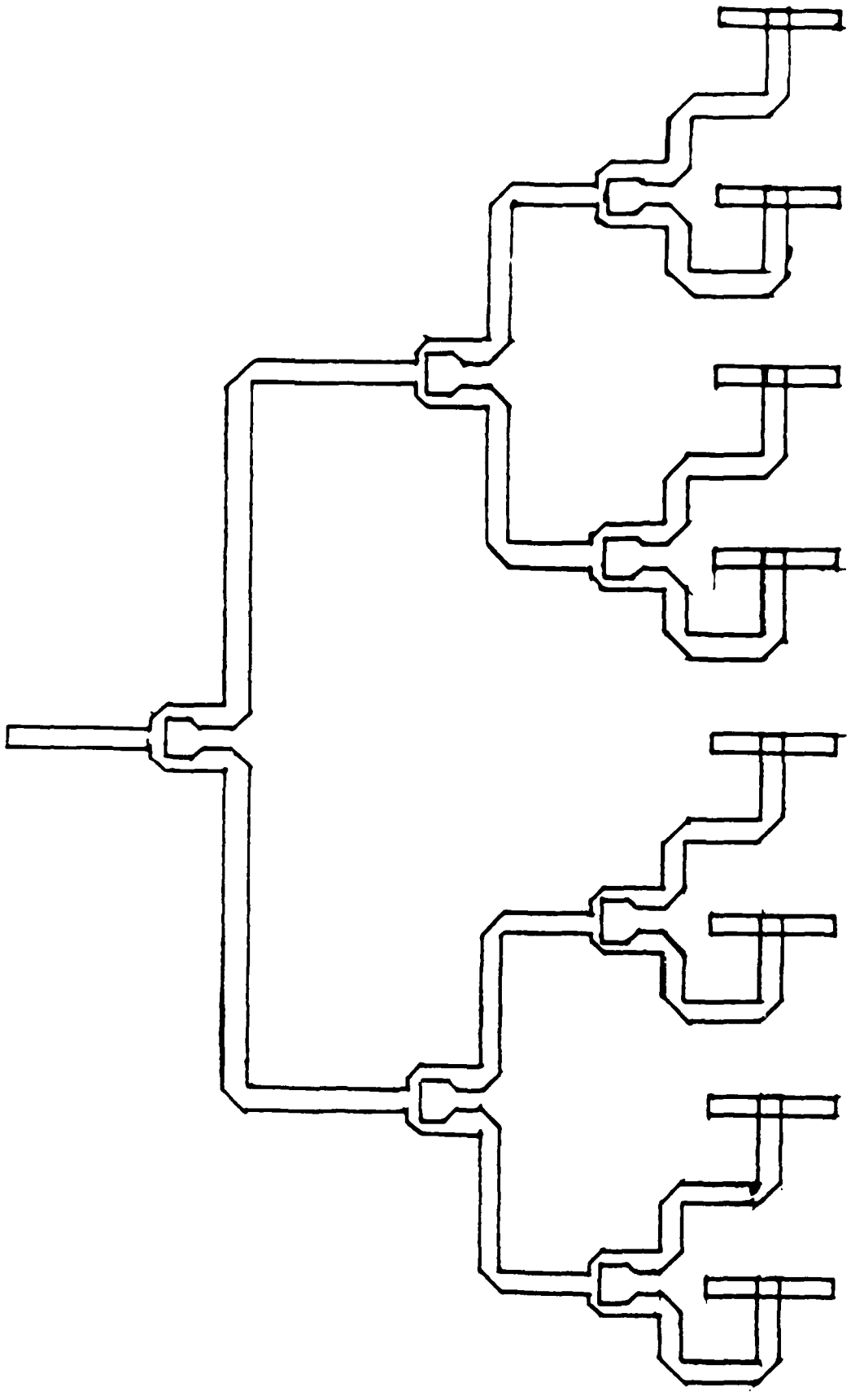

Figure 5.1 Geometry of slot array with microstripline corporate feed network.

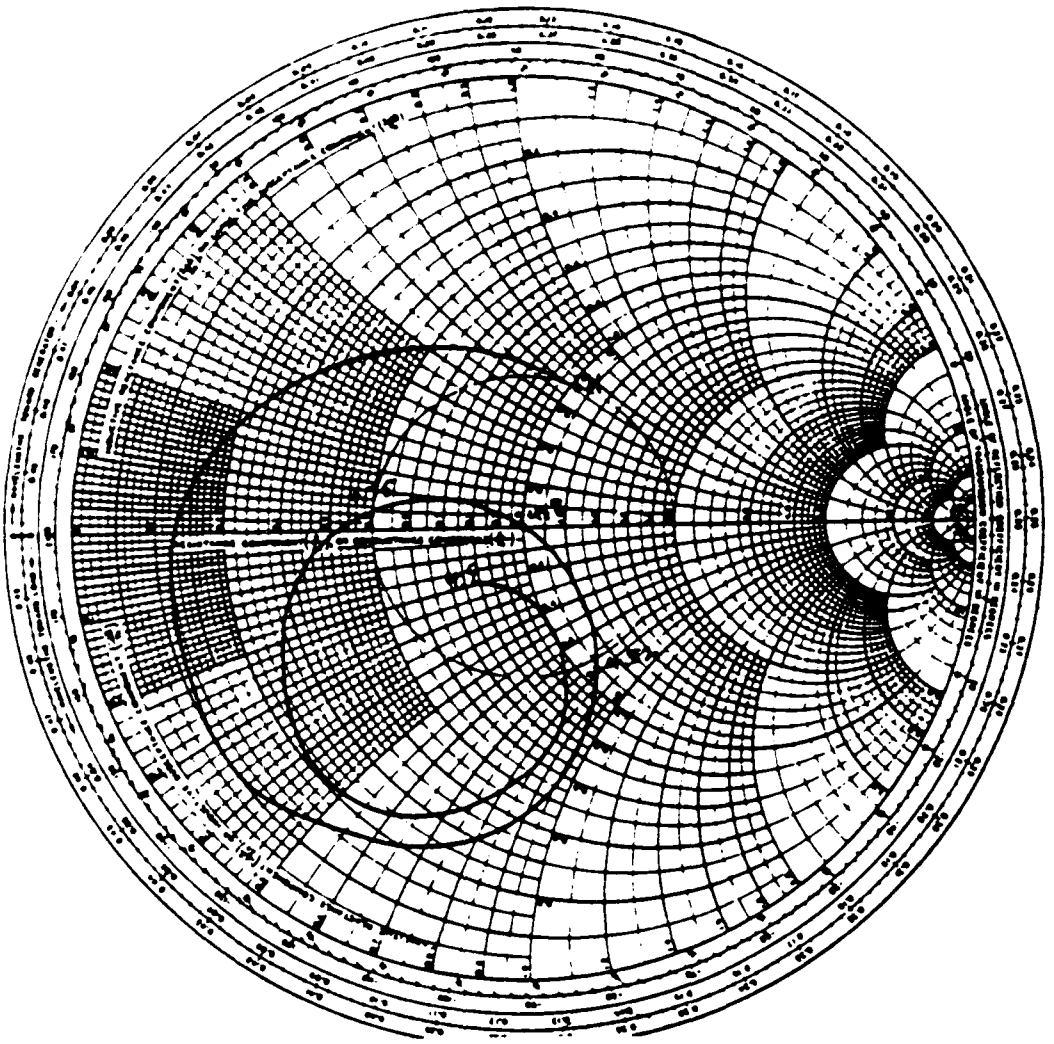

Figure 5.2 Input impedance of slot array.

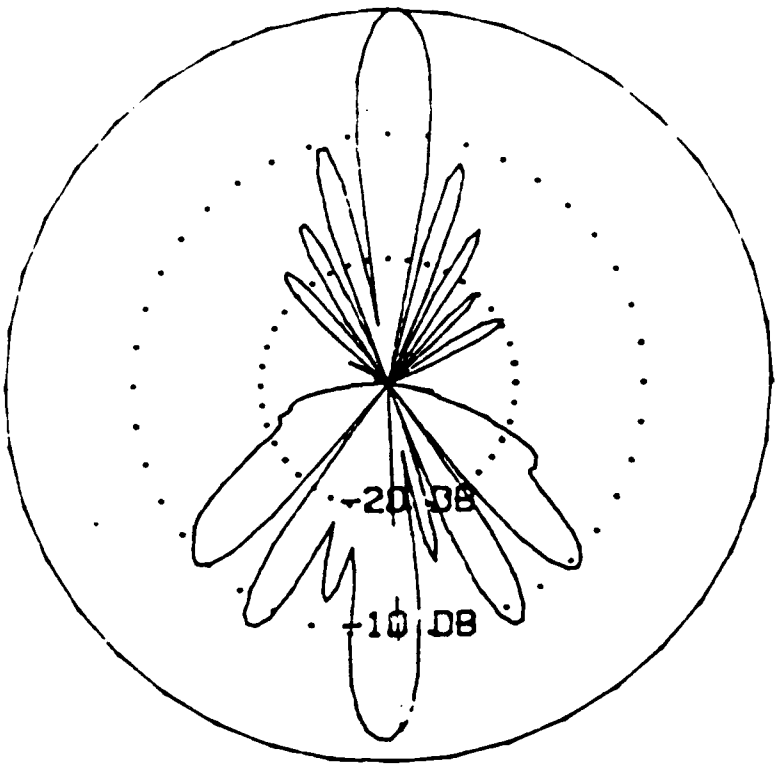

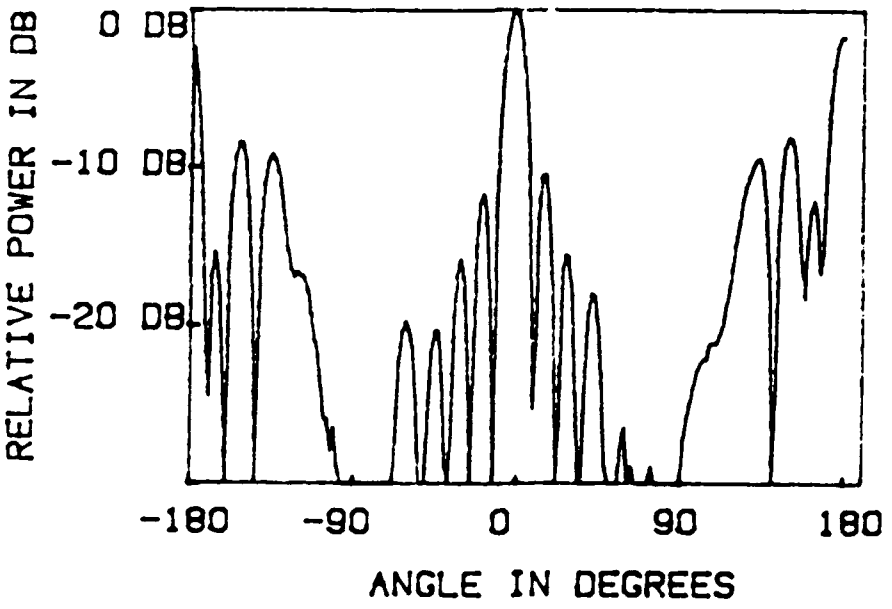

Figure 5.3 E-plane radiation pattern of slot array.

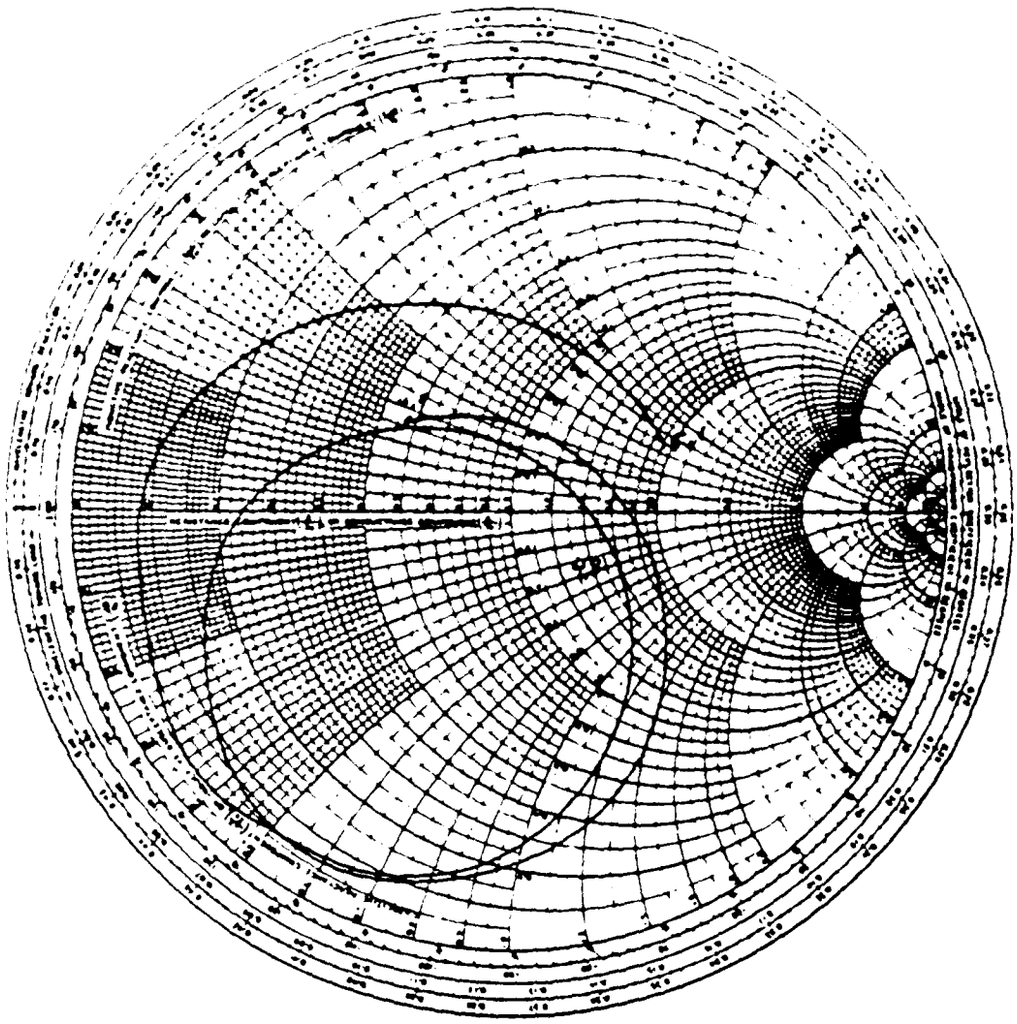

Figure 5.4 Input impedance of slot array with reflector.

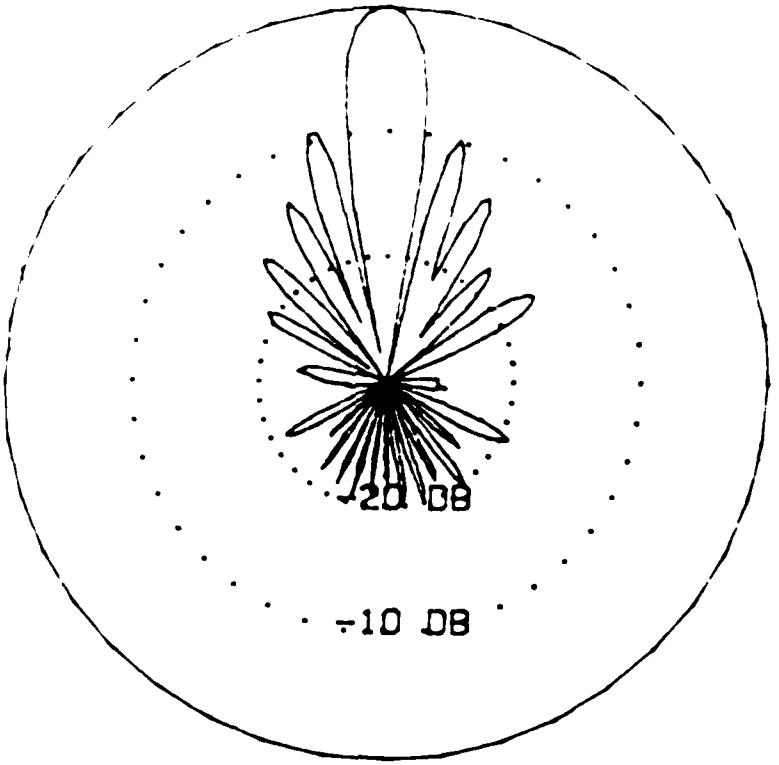

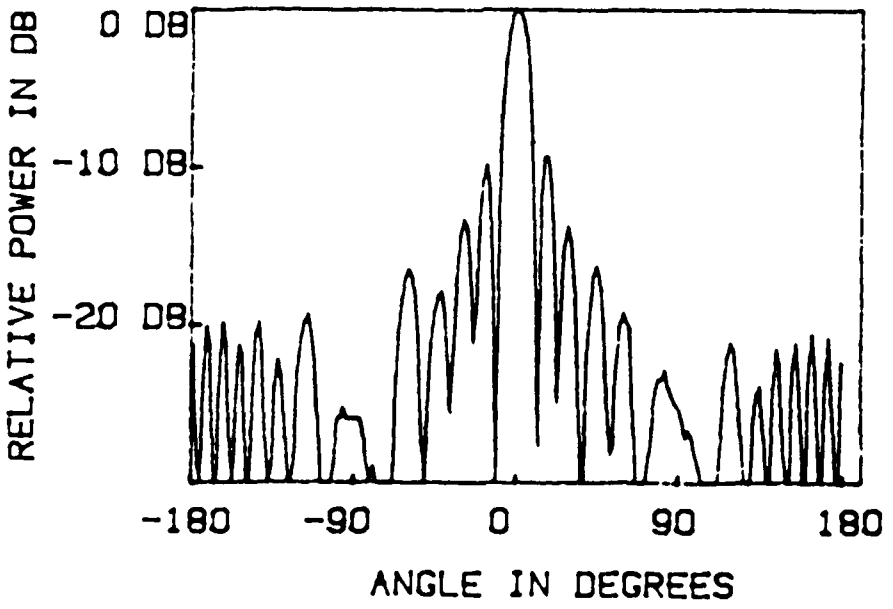

Figure 5.5 E-plane pattern of slot array with reflection.

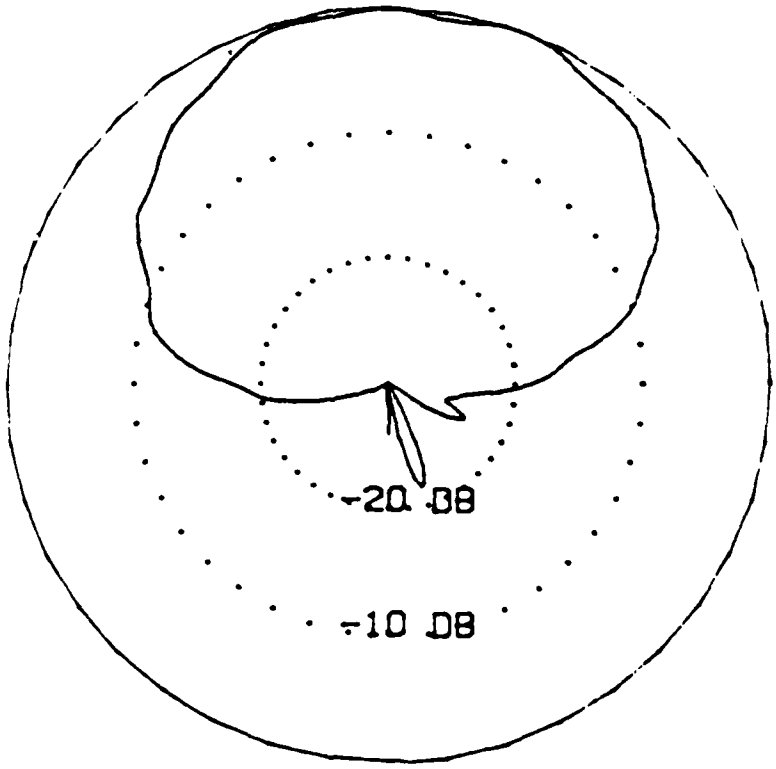

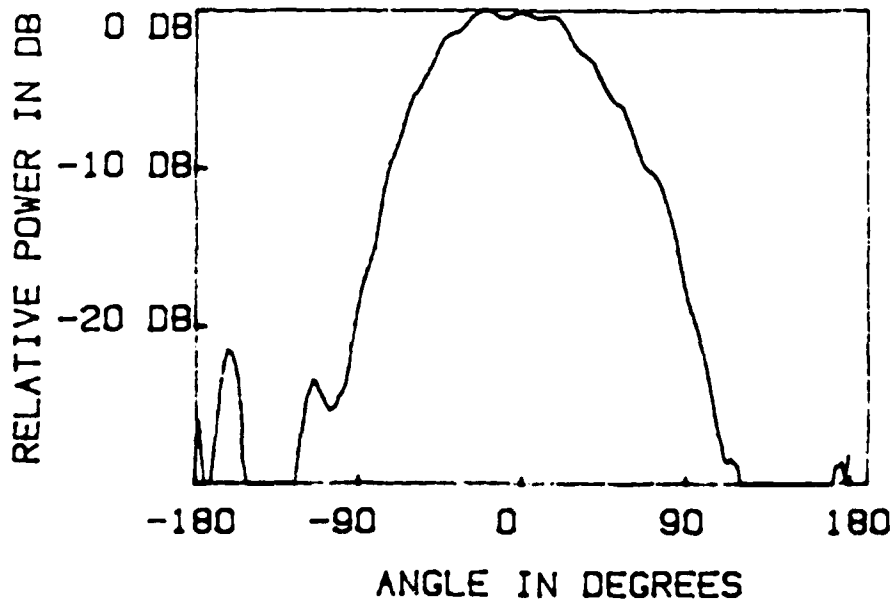

Figure 5.6 H-plane pattern of slot array with reflector.

5.2 20-GHz Linear Array

An 8-element, E-plane array of microstrip patches was fabricated on 20-mil Duroid 5880 (ϵ_r = 2.2) and tested. The mask for the array and corporate feed are shown in Figure 5.7. The operating frequency of the array was 20.23 GHz, and the main purpose in building this array was to improve our capabilities for fabricating millimeter wave arrays. The radiation patterns of the array are shown in Figures 5.8 and 5.9. The cross-polarized maximum is approximately 15dB below the copolarized maximum in the mainbeam direction. The measured return loss of the array is plotted in Figure 5.10, where a very good match is observed at 20.23 GHz.

5.3 2x2 Microstrip Patch Array

A 2x2 planar array of microstrip patches has been constructed and tested at 20.9 GHz. A four-way corporate feed network was also made on the same substrate, which was 20 mil Duroid 5880 (ϵ_r=2.2). The patches were fed with 100 Ω microstrip lines at the center of the radiating edges.

The performance was quite good. The return loss was measured to be about 13 dB, and the main beam in the principal planes was well-formed, with low side lobes (see Figure 5.11). The apparent beam squint is caused by the alignment chosen for the tests. The E-plane sidelobe region was unsymmetric, probably as a result of the feedline proximity to one row of patches. Cross-pol levels were -20 dB or lower.

5.4 Aperture Coupled Prototype Array

One of the objectives of this work was to fabricate and test a prototype array demonstrating some of the proposed concepts of integrated phased arrays. The aperture coupled patch was chosen as the candidate element because it provides one surface and substrate

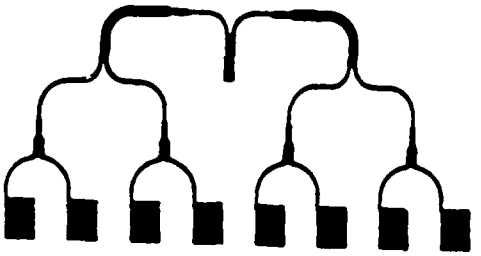

Figure 5.7 Mask for 20 GHz array.

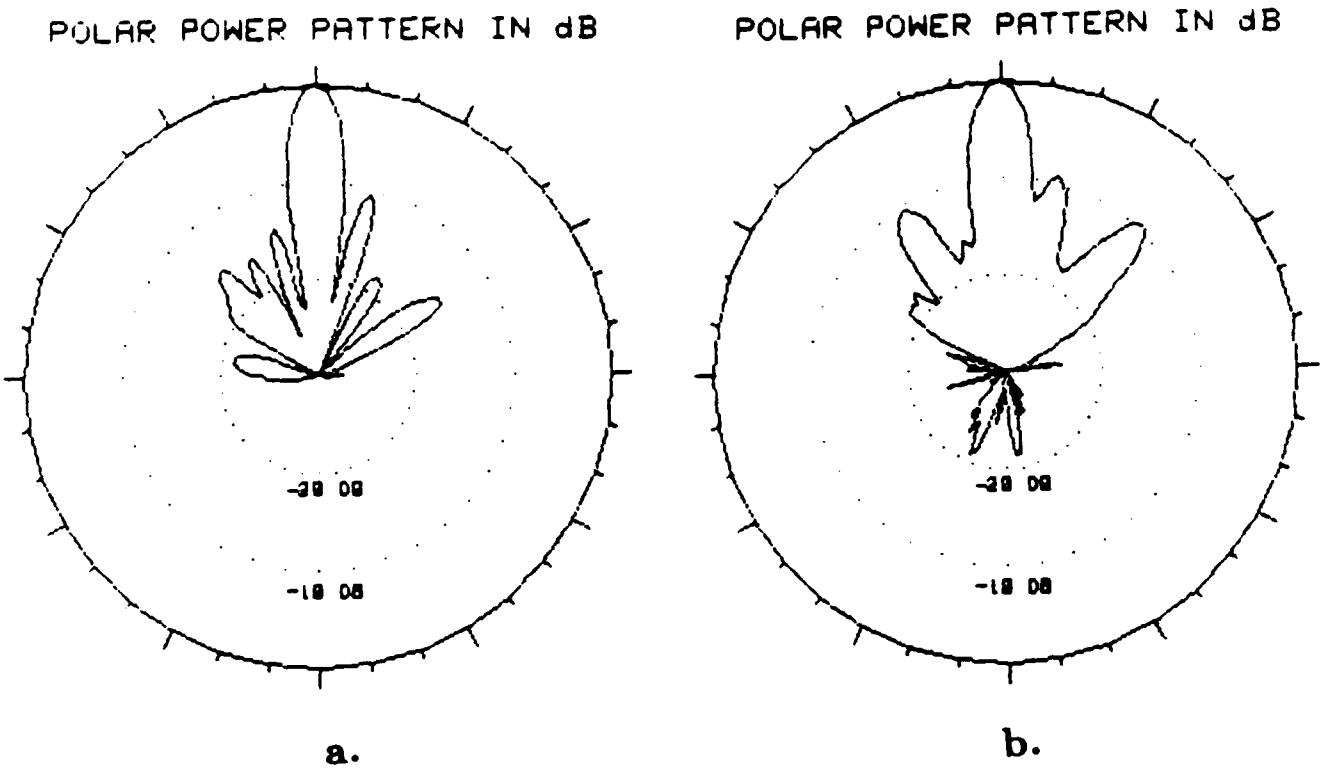

Figure 5.8 E-plane radiation patterns of array at 20.23 GHz. (a) Co-polarized. (b) Cross-polarized with maximum gain 15 dB below co-polarized.

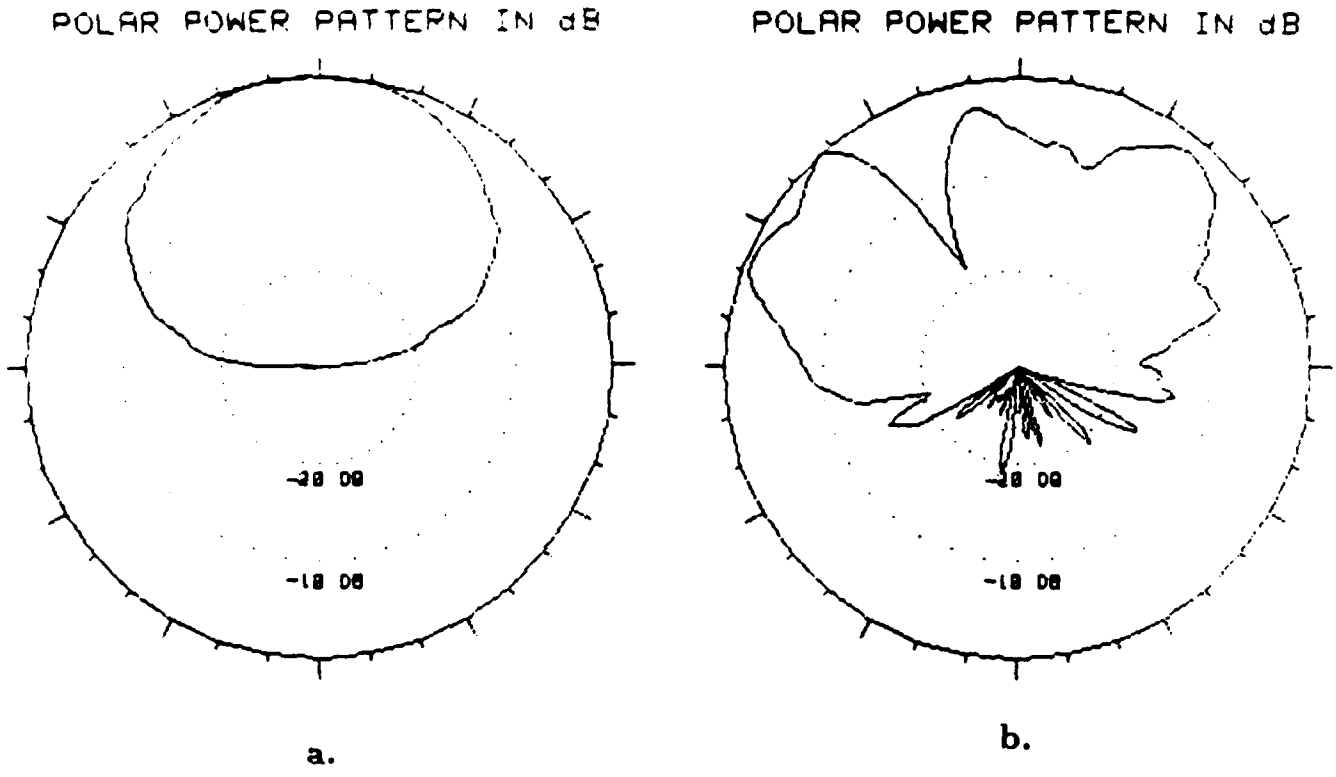

Figure 5.9 H-plane radiation patterns of array at 20.23 GHz. (a) Co-polarized. (b) Cross-polarized.

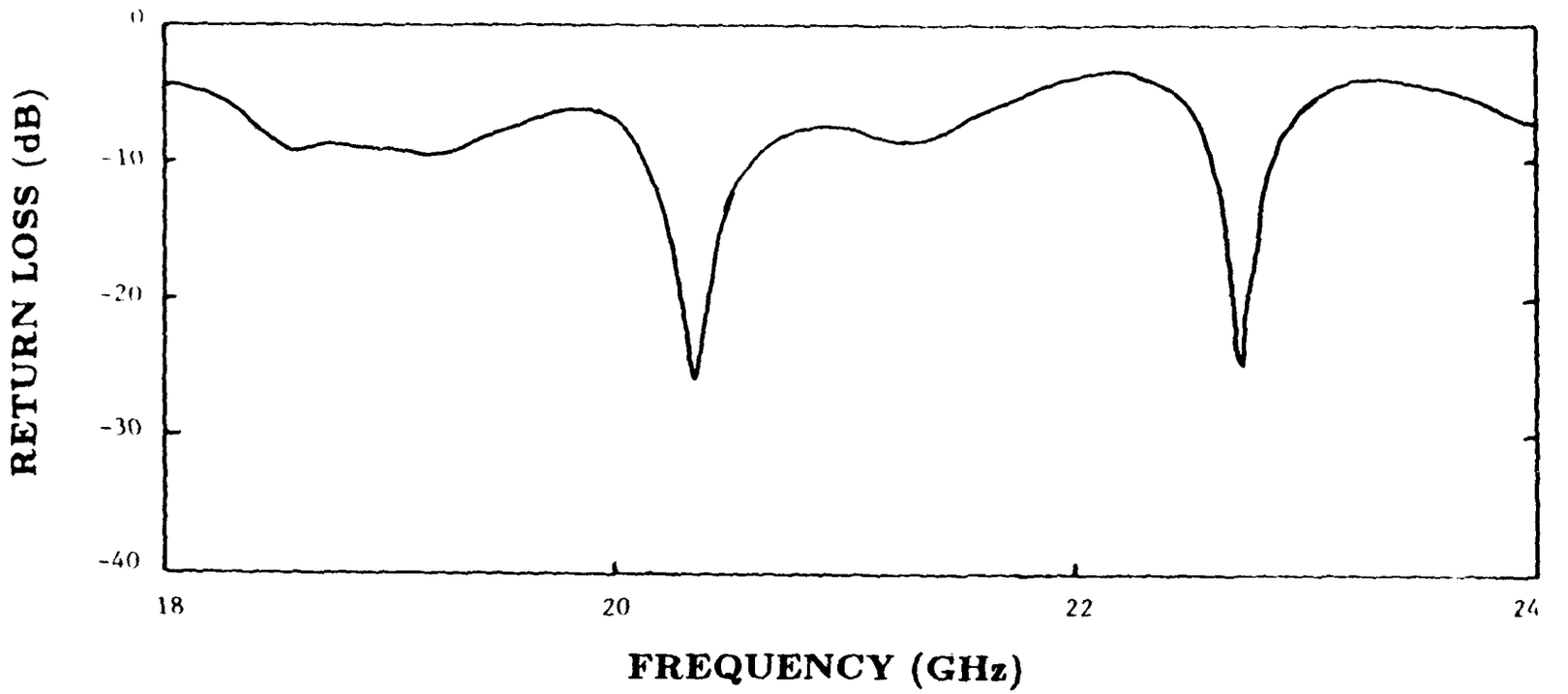

Figure 5.10 Return loss of array.

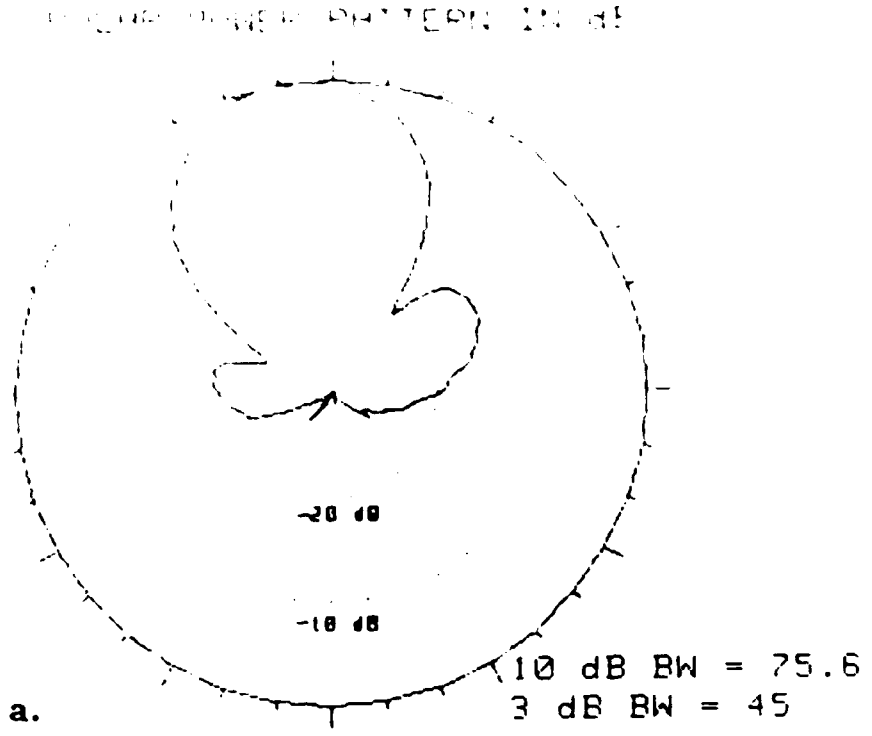

a.

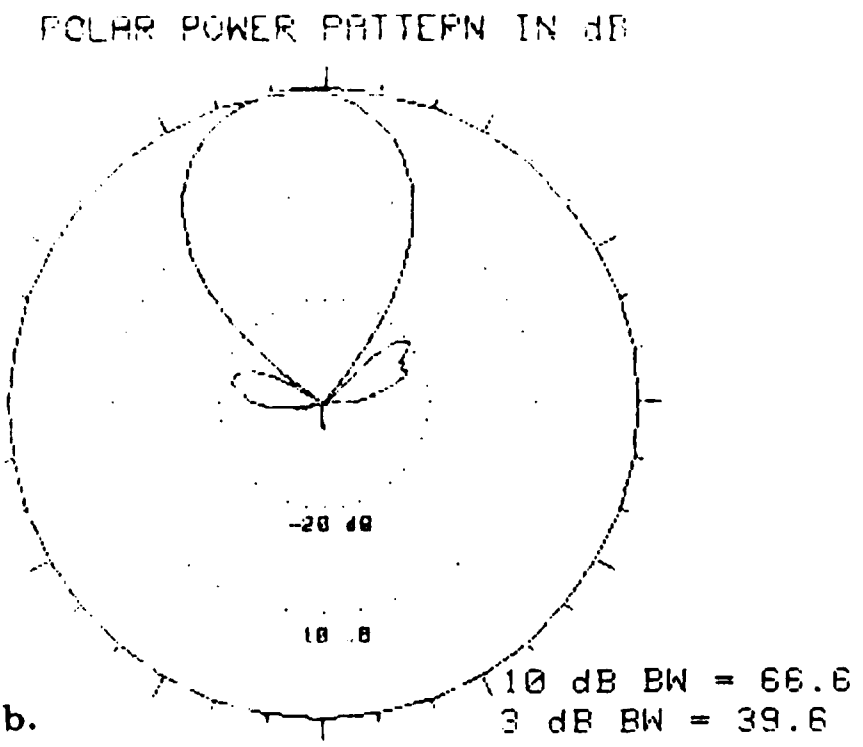

b.

Figure 5.11 Radiation patterns of 2x2 array at 20.91 GHz. (a) E-plane. (b) H-plane.

dedicated to the radiating elements and a second surface and substrate dedicated to the feed network. This permits use of the optimum substrate for each function, provides a surface area of $\lambda_o/2 \times \lambda_o/2$ for the phase shifters and amplifiers of each element, and the ground plane prevents spurious radiation from the feed network.

The primary objective of the prototype array is to demonstrate that an array of aperture coupled patches with PTFE substrate for the antennas and high permittivity substrate (ϵ_r=10.2 to simulate approximately GaAs) for the feed network can be used as an integrated, phase-steered array at EHF. Rather than to operate at EHF where measurements and phase shifting are difficult, a scaled model was built at 5 GHz. Tolerance studies have shown that misalignment of the feed network on the order of 10% of the patch length has minimal effect on the performance of the antenna elements, so that the scale model should be representative of the results that can be achieved at 20 or 25 GHz. The use of 25 mil Duroid 6010.2 for the feed substrate simulates approximately 5-mil GaAs at 25 GHz, and the 60-mil Duroid 5880 antenna substrate is $0.025\lambda_o$ thick at the operating frequency. The dimensions of the array are given in Figure 5.12. In a monolithic feed version, phase shifters would be fabricated on GaAs, but the antenna tested here has microstriplines (approximately λ_o long) that connect to the coaxial corporate feed network through coax-to-microstripline transitions.

5.4.1 Element Characteristics

The input impedance, referenced to the center of the coupling slot, of an isolated element is shown in Figure 5.13. The element is well matched at 5 GHz. The input impedance of a typical element in the array (measured with the other elements terminated in 50 ohms) is shown in Figure 5.14. The return loss plots of some of the elements (referenced to the coaxial input connector) are shown in Figure 5.15, where the worst case return loss at 5

AD-A182 608 TECHNOLOGY DEVELOPMENT FOR MILLIMETER WAVE PHASED ARRAYS(U) MASSACHUSETTSUUNIV AMHERST DEPT OF ELECTRICAL AND COMPUTER EN D H SCHAUBERT ET AL MAY 87 2/2

UNCLASSIFIED RADC-RR-87-42 F19628-84-K-0022 F/G 9/1 NL

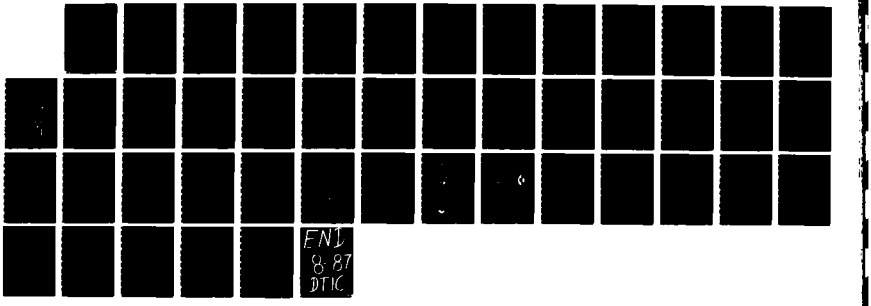

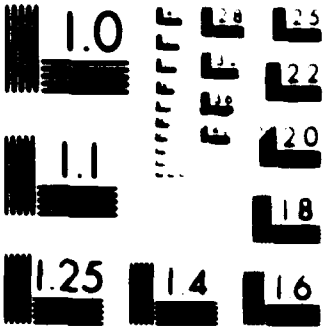
1.0
1.1
1.25
1.4
1.6
2.2
2.0
1.8

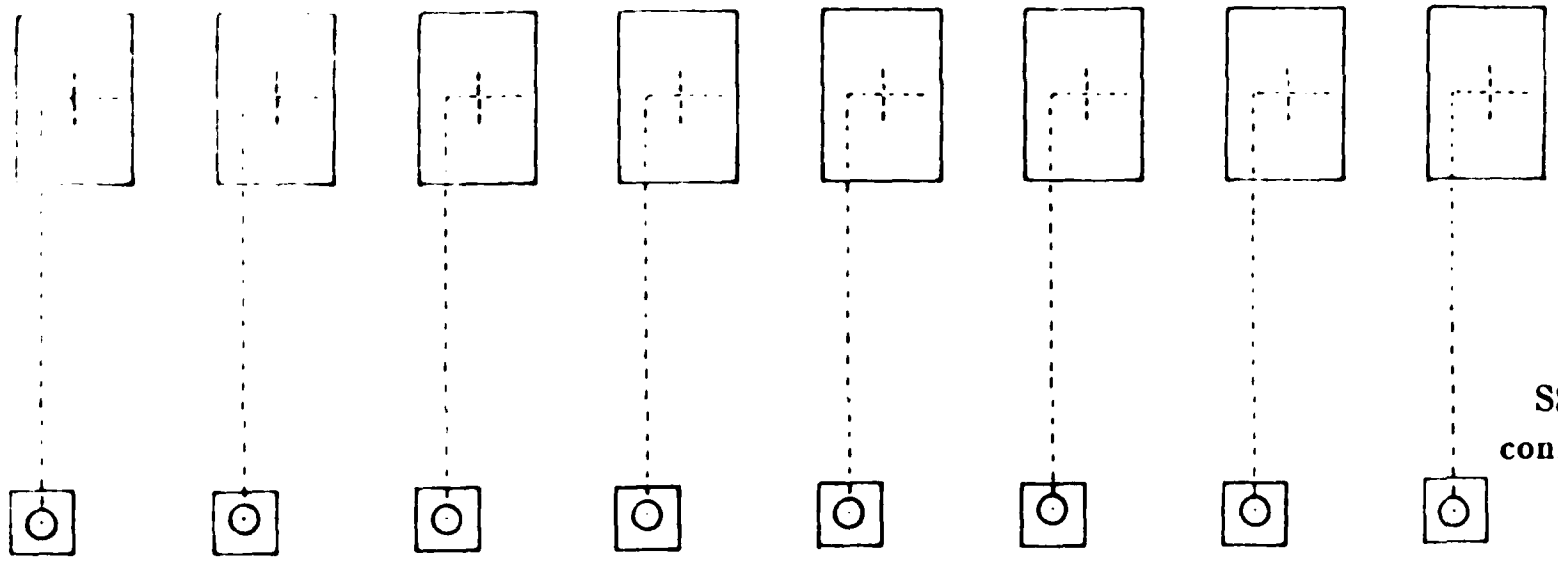

Patch Length = 1.78 cm
Patch Width = 2.54 cm
Slot Length = 0.83 cm
$\epsilon_r^{ant} = 2.22$
$d^{ant} = 0.159$ cm

Element Spacing = 3.0 cm
Stub Length = 0.42 cm
Slot Width = 0.056 cm
$\epsilon_r^{feed} = 10.2$
$d^{feed} = 0.064$ cm

Figure 5.12 8-element, E-plane array.

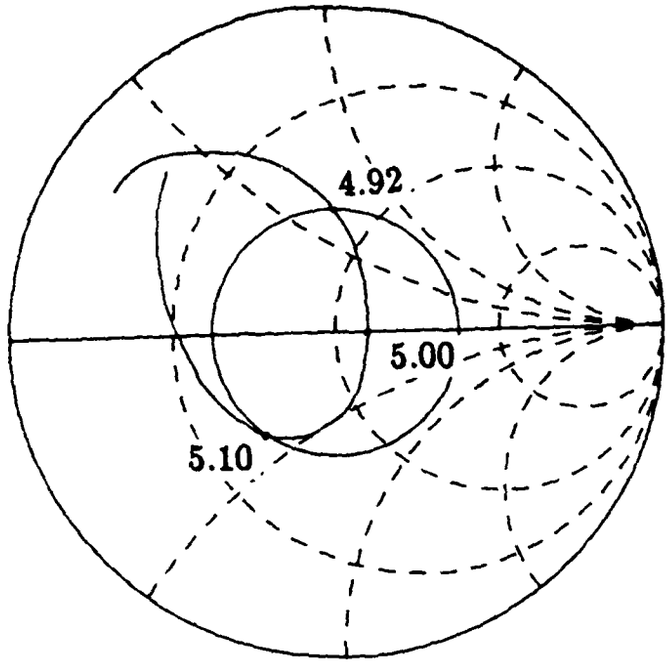

Figure 5.13 Input impedance of isolated element, 4.5-5.5 GHz. Circle indicates VSWR=2.

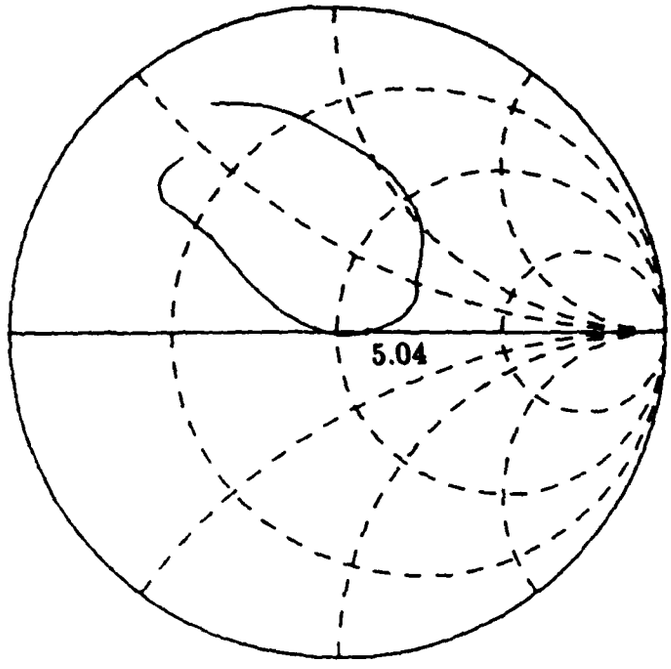

Figure 5.14 Input impedance of element 6 in the array. Other elements terminated in 50 ohms.

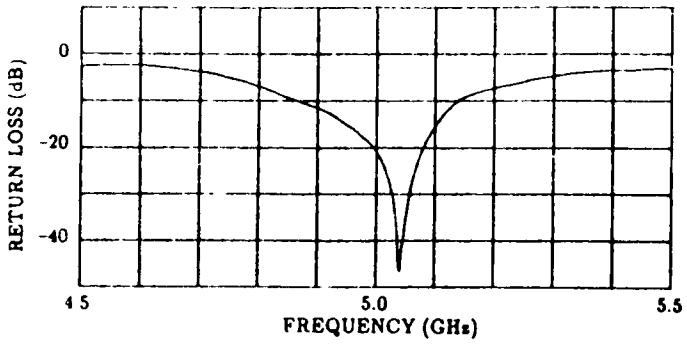

ELEMENT 1

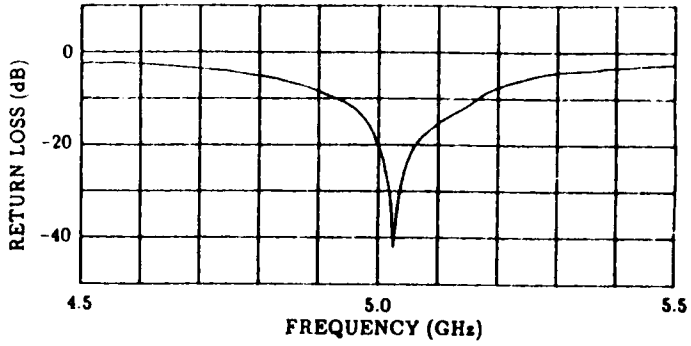

ELEMENT 2

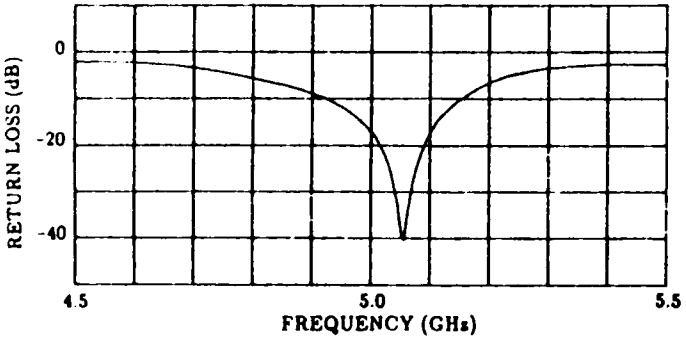

ELEMENT 3

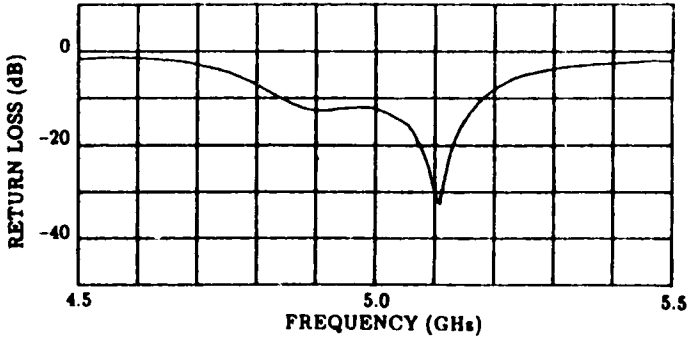

ELEMENT 4

Figure 5.15 Return loss of elements 1, 2, 3, and 4 measured at the coaxial connectors.

GHz is about 12 dB. Mutual coupling is approximately -20 dB between adjacent elements of the array and drops to -30 dB for center-to-end element coupling (see Table 5.1).

E-plane radiation patterns of several elements are shown in Figures 5.16 and 5.17. The unused elements are terminated in 50 ohms. The expected mirror symmetries are evident, otherwise the patterns exhibit the broad beamwidth and endfire levels of approximately -10 dB that are typical of patch radiators. Some pattern irregularities and scattering behind the ground plane, which was approximately $4\lambda_o x 2\lambda_o$, are seen, but the patterns are generally good and should result in useful array patterns over a fairly wide range of scan angles.

Table 5.1 MUTUAL COUPLING IN ARRAY

$$P_L = 1.78cm \quad P_W = 2.54cm \quad s = 3.0cm$$

$$\epsilon_r^{ant} = 2.22 \quad d^{ant} = 0.159cm$$

$$\epsilon_r^{feed} = 10.2 \quad d^{feed} = 0.064cm$$

	$\lvert S_{ij}\rvert$(dB)	$\angle S_{ij}$(deg)
S_{41}	-30.7	-79
S_{42}	-24.8	102
S_{43}	-21.6	-46
S_{45}	-22.1	-52
S_{46}	-27.0	103
S_{47}	-30.3	-110
S_{48}	-31.8	70

5.4.2 Array Characteristics

Radiation patterns of the array were obtained by feeding the elements with equal-amplitude, in-phase signals. This was accomplished by using a commercially available coaxial 8-way power divider connected to the array by equal lengths of semi-rigid coaxial cable. The return loss of the array measured at the input to power divider is shown in

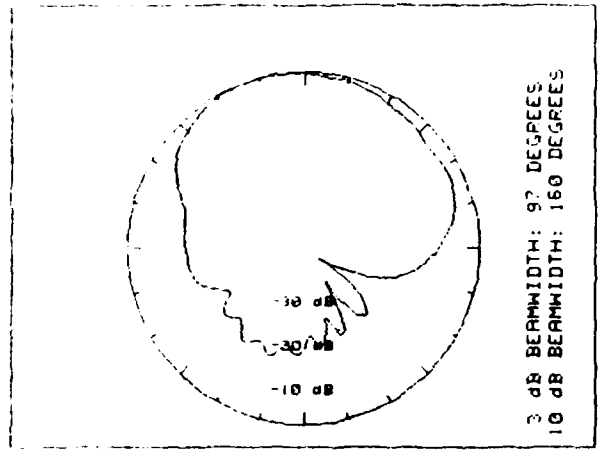

ELEMENT 1

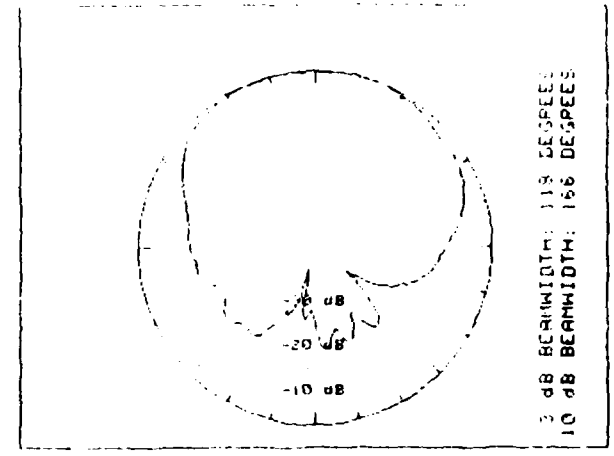

ELEMENT 2

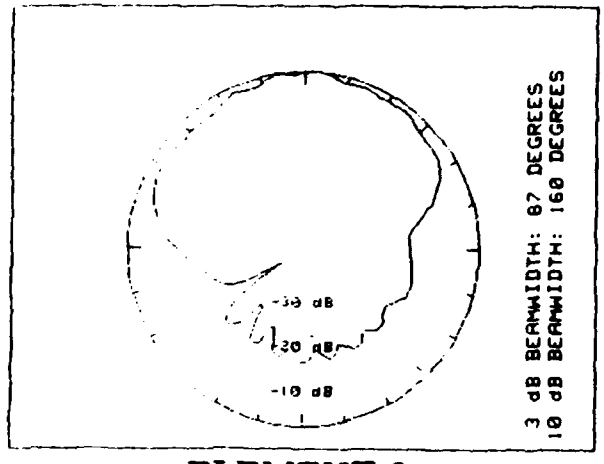

ELEMENT 8

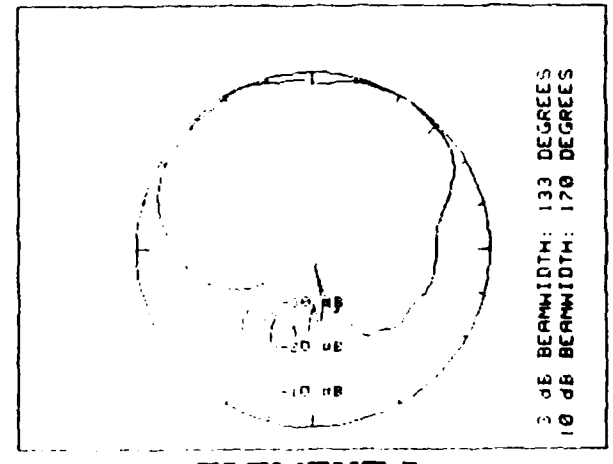

ELEMENT 7

Figure 5.16 E-plane patterns of end elements in array at 5.0 GHz. Unused elements terminated in 50 ohms.

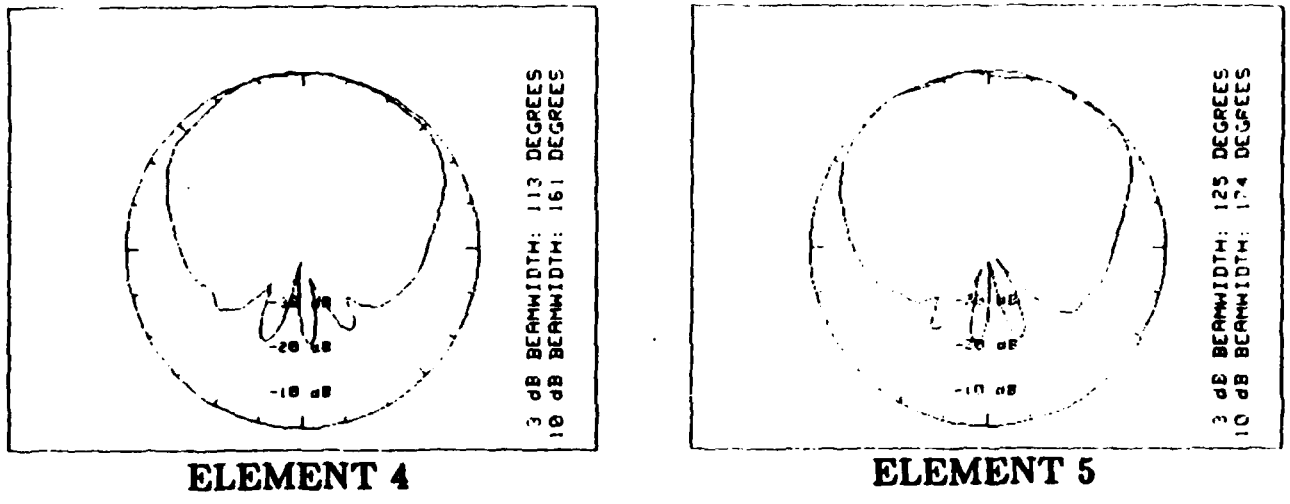

Figure 5.17 E-plane patterns of central elements in array at 5.0 GHz. Unused elements terminated in 50 ohms.

Figure 5.18. The VSWR is less than 2:1 over the frequency range 4.9-5.2 GHz. E-plane radiation patterns at four frequencies are shown in Figure 5.19. The 20 dB front-to-back ratio implies that the slot apertures in the ground plane do not radiate significantly on the feed side. The sidelobes are a little higher than one would expect for a uniform distribution and they exhibit some asymmetries, but the patterns are generally good. It appears that the performance of the aperture coupled patch in small arrays will be about the same as that of the probe-fed patch, but the fabrication may be simpler since no via connection is required.

A second array was fabricated by using the same masks, but the coax-to-microstripline transitions were reinforced by soldering a 0.062-inch brass strong back to the ground plane of the feed lines in the vicinity of the connectors. This technique has been found to improve the performance and reliability of the transition. The patterns of the second array are shown in Figure 5.20 at the design frequency of 5.0 GHz and at scan angles of broadside, -26° and -52°. The predicted patterns are shown below the measured patterns. The beam steering was accomplished by the use of appropriate lengths of coaxial line between the power divider on the array. The return loss measured at the input of the power divider for scan angles of broadside, ±2 beamwidths and ±4 beamwidths are shown in Figure 5.21.

The efficiency of the array has been estimated by comparing the measured gain to the directivity computed for an ideal array (the calculated broadside pattern in Figure 5.20). The results are summarized in Table 5.2. The estimated uncertainty in the measured gain is due to measurement errors and a lack of calibrated gain standards at our facility. This uncertainty places the efficiency in the range 54% to 85%. Nevertheless, the results indicate that the efficiency of the aperture coupled array can probably be as good as that of a patch array fed by other means.

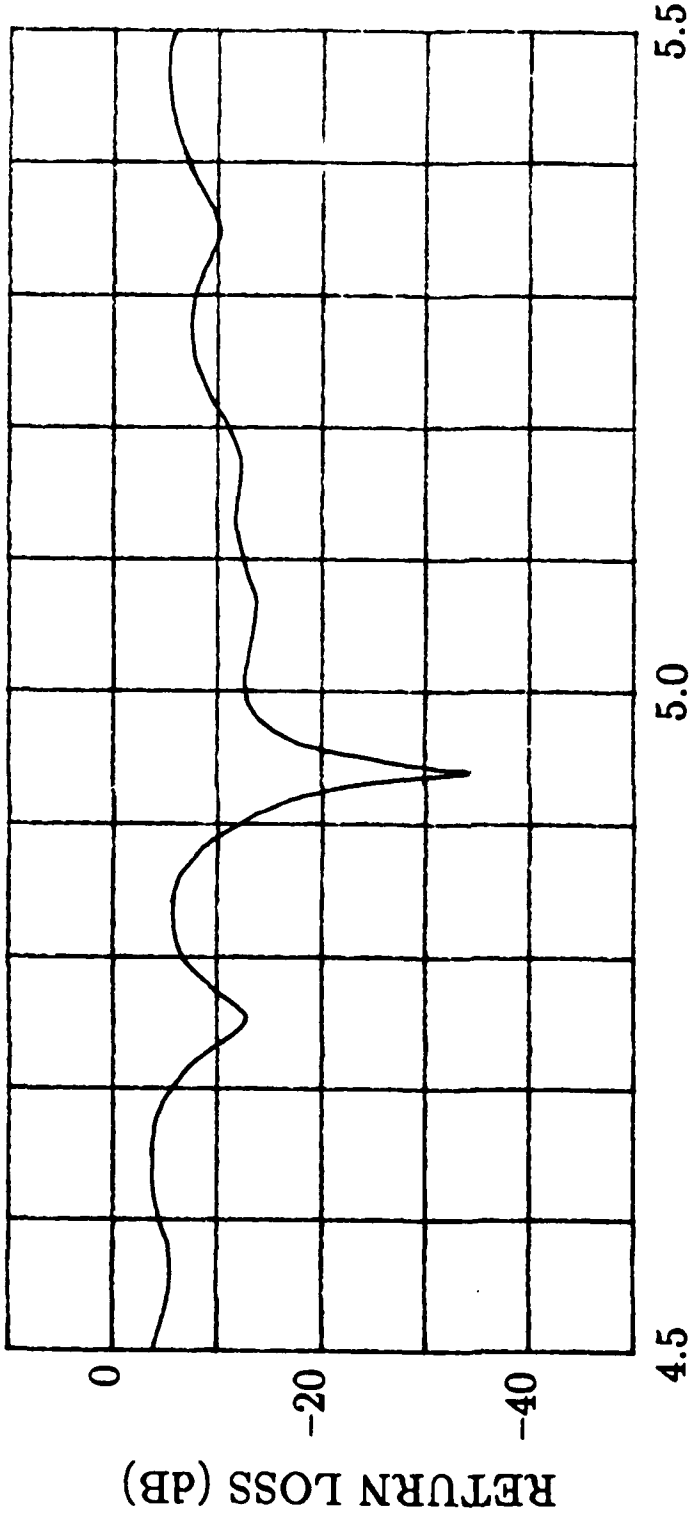

Figure 5.18 Return loss of 8-element array at input to coaxial power divider.

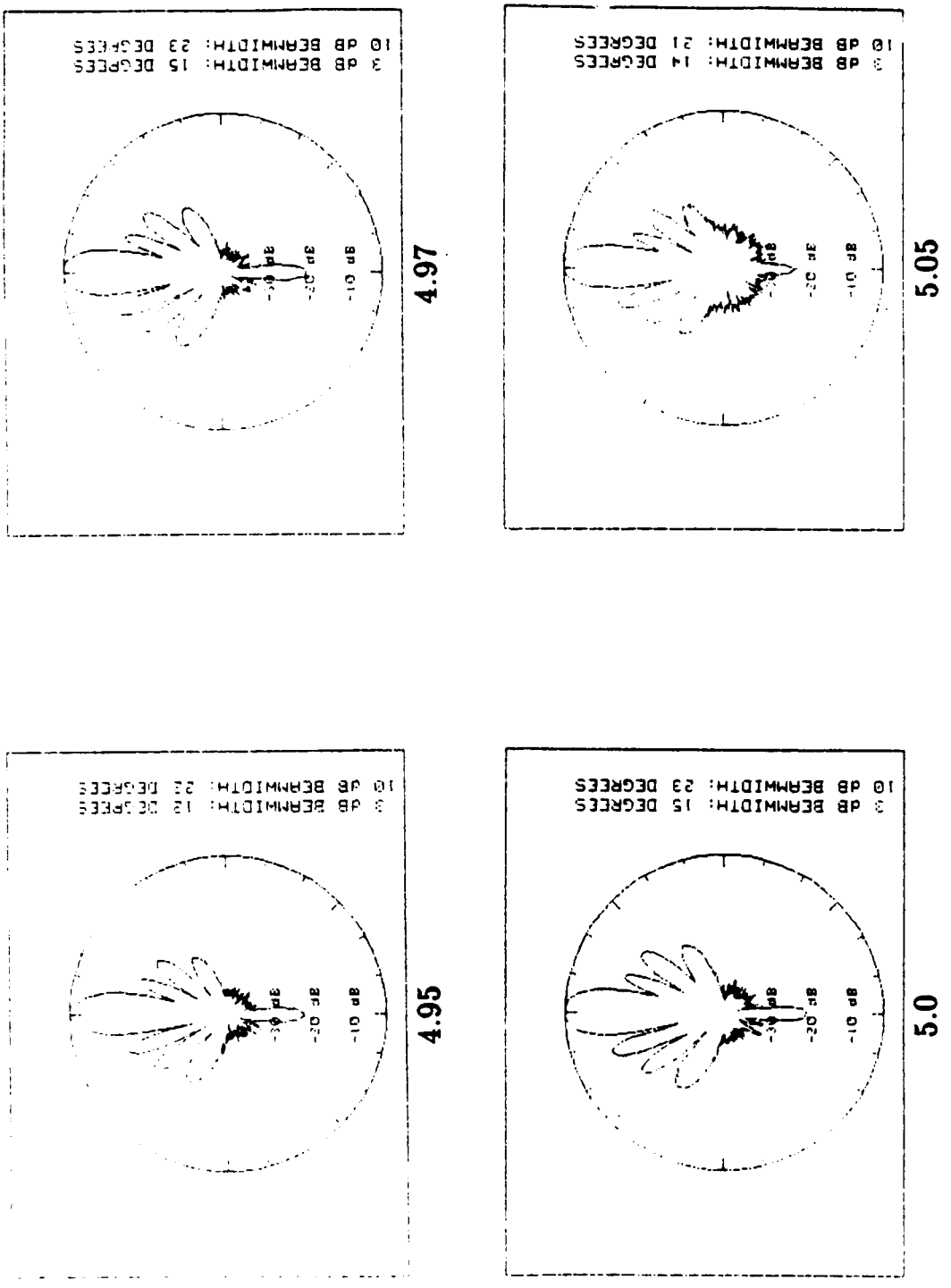

Figure 5.19 E-plane radiation patterns of 8-element array.

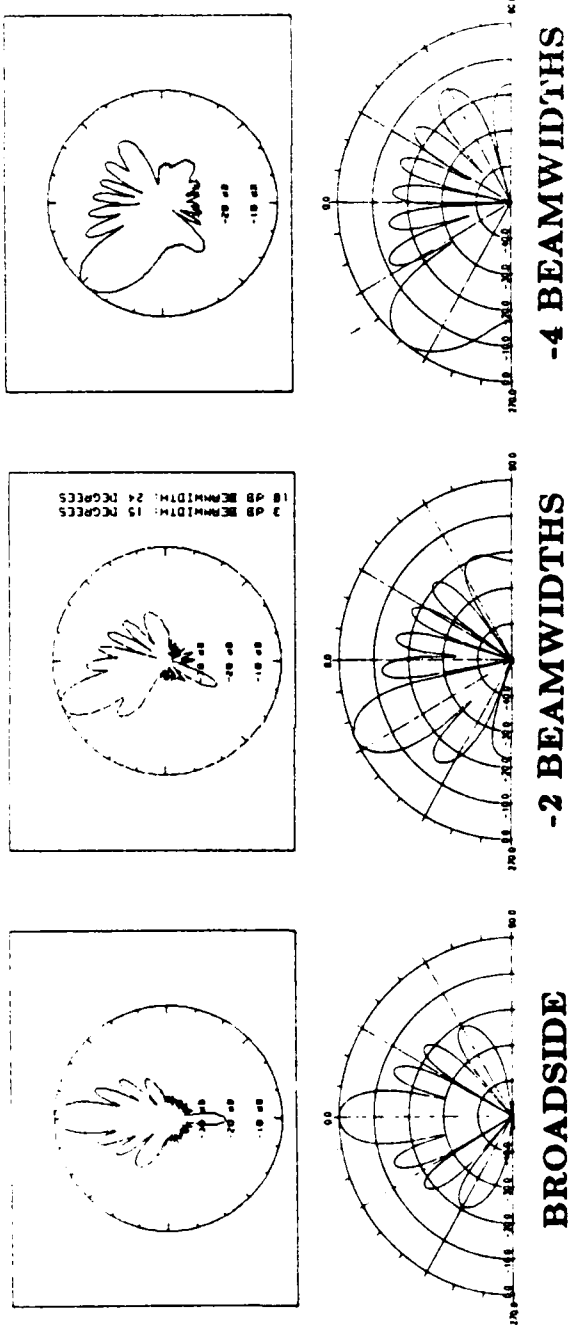

Figure 5.20 Measured and predicted E-plane patterns of second array at 5 GHz.

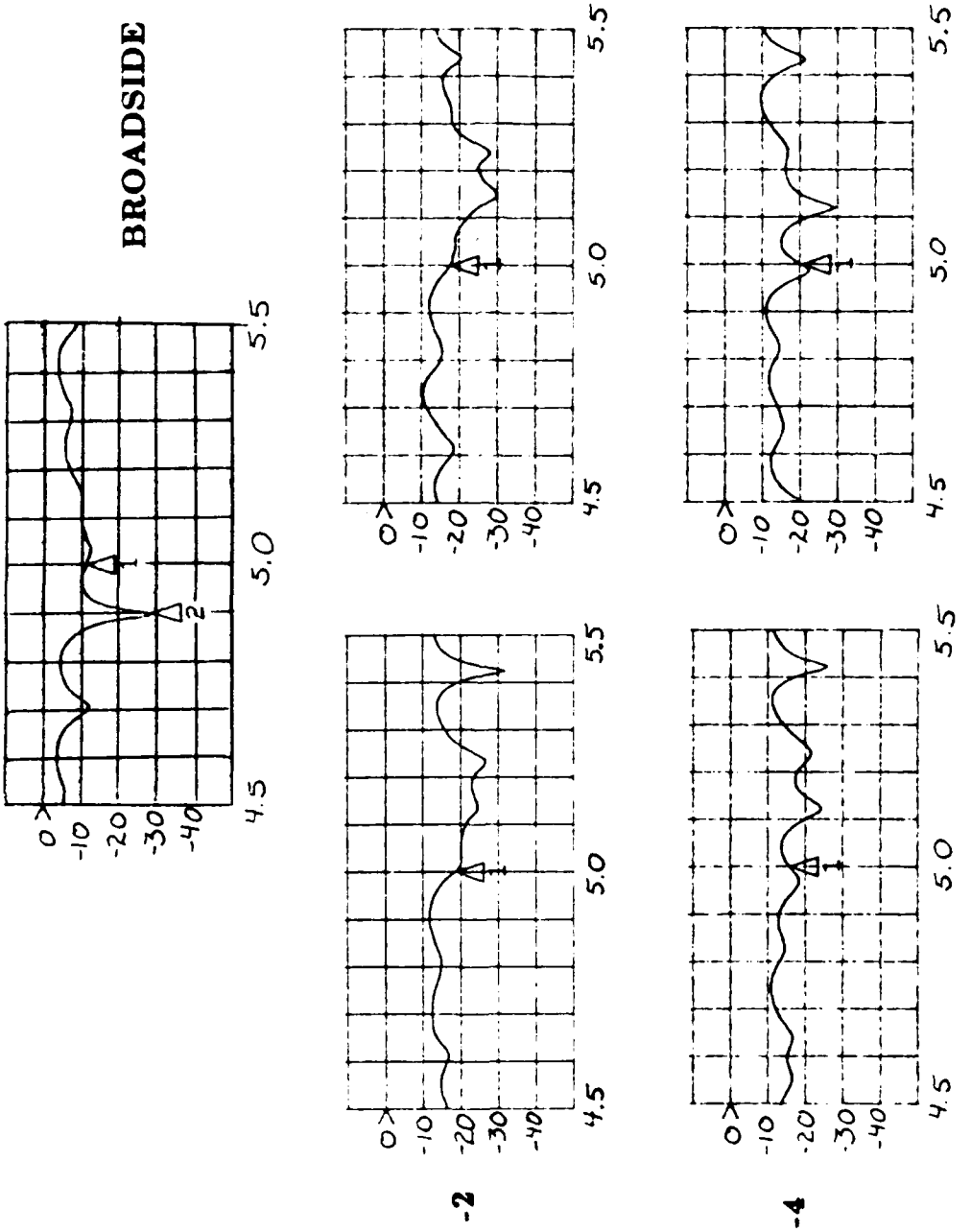

Figure 5.21 Return loss at power divider of array.

A scan blindness can occur in aperture coupled arrays due to the surface wave on either the antenna substrate or the feed substrate. However, the blindness caused by the low permittivity antenna substrate is very near to endfire. Also, the blindness caused by GaAs feed substrate occurs at scan angles greater than 80° for thicknesses up to $0.02\lambda_o$ and element spacings of $0.5\lambda_o$. Therefore, scan blindness induced by the GaAs substrate should not limit the scan range of practical antennas at frequencies below 50-60 GHz.

TABLE 5.2 LOSS BUDGET OF 8-ELEMENT ARRAY

Computed Directivity of Ideal Array	16.3 dB
Measured Gain (±1 dB estimated)	12.7 dB
Measured Feed Losses (to the aperture)	1.9 dB
Array Efficiency	67%

5.5 Phase Shifter for Prototype Array

An attempt was made to fabricate 3-bit phase shifters on Duroid 6010.2 so that they could be integrated with the prototype array described in section 5.4. The attempt was unsuccessful, and we believe that much of the difficulty was caused by our inability to repeatably attach the PIN chip diodes to the microstripline circuit. The phase shifter circuit utilizes a branch line hybrid with the two coupled ports terminated in identical, switchable, low-loss impedances (Figure 5.22). This design requires only two diodes and one bias supply voltage per bit, which is desirable for our prototype design but may not

PHASE SHIFTER BITS @ 5 GHz

Desired Δ d	Meas. Δ d	On/Off	IL (dB)	Δ IL (dB)	R.L. (dB)
45°	44.6°	On	-1.23		-10.9
		Off	-.56	.67	-19.2
90°	84.2°	On	-1.41		-14.8
		Off	-1.13	.28	-18.0
180°	186.2°	On	-2.03		-14.6
		Off	-.94	1.09	-19.4

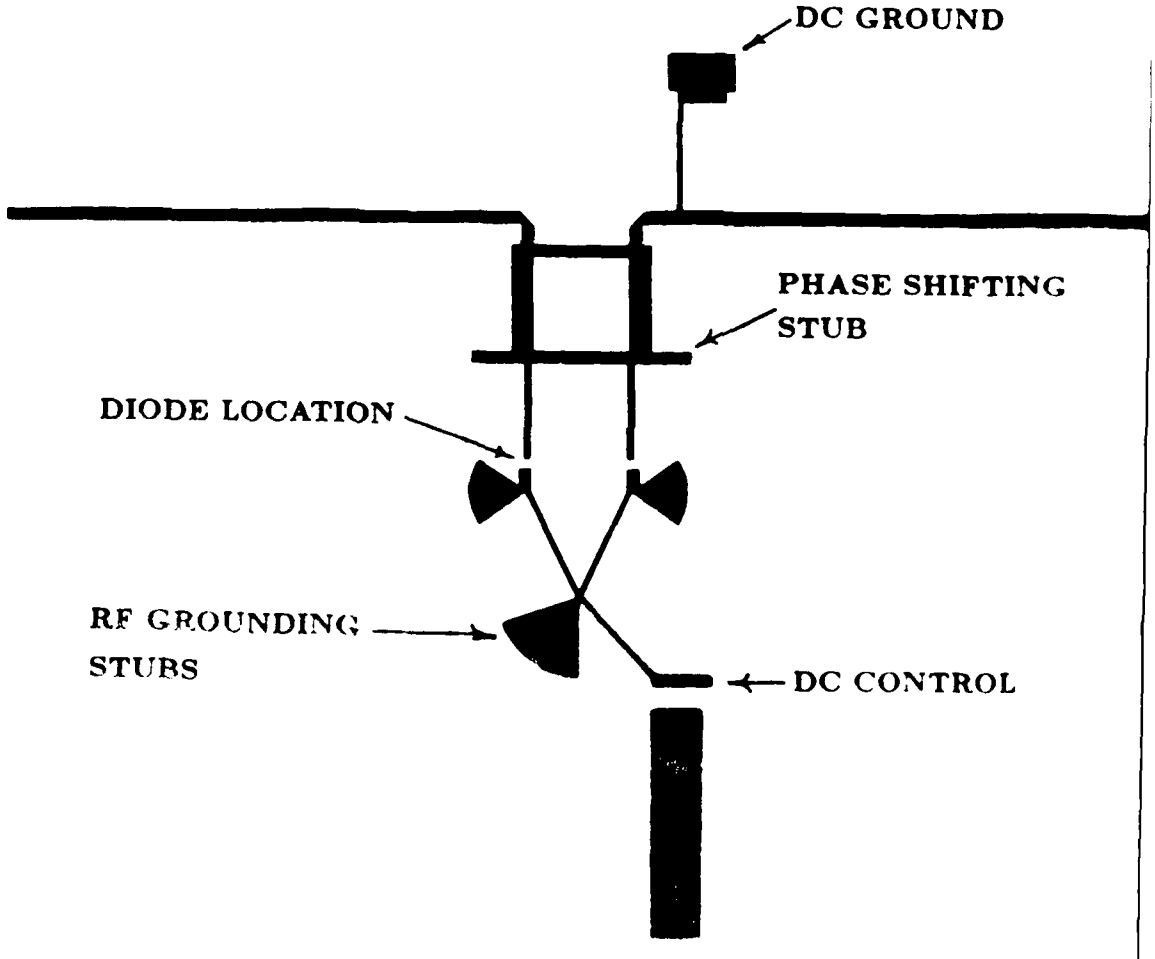

Figure 5.22 Branch line hybrid design used for prototype phase shifter

the application of a monolithic feed network. Also, [illegible] analysis of the design indicates higher sensitivity to the lengths of stray capacitances and inductances that should be desirable. Nevertheless several bits have been fabricated and tested. The best [illegible] with respect to phase shift are shown in Figure 3.22 where a rather large different insertion loss is observed. The inability to simultaneously achieve accurate phase shift and nearly equal insertion loss resulted in abandonment of the plans to demonstrate active beam steering. However, ongoing work at companies involved in millimeter wave devices and circuits indicates that monolithic phase shifters should be available for the next generation of phased arrays and the aperture coupled array should be a strong candidate for applications where a thin structure and high performance are required.

Chapter 6

THEORETICAL DEVELOPMENTS

As the reader may have gathered from the above discussions, a number of advancements in the analytical treatment of printed antennas and circuits were made during the course of this work, as summarized below:

1. Analysis of the scan characteristics of an infinite array of microstrip patches with idealized probe feeds [1].
2. Analysis of the scan characteristics of an infinite array of aperture coupled microstrip patches [2].
3. A current sheet model of the scan characteristics of a general printed phased array [3].
4. Analysis of finite phased arrays of printed dipoles [4], and microstrip patches [5].
5. Analysis of the aperture coupled patch element [6].
6. Analysis of microstripline gap and open-end discontinuities [13].

The above results are based on moment method solutions using the exact Green's functions for the appropriate dielectric slab geometry, and so surface wave effects (of particular interest for high-dielectric constant substrates at high frequencies) are included. Such solutions are sometimes referred to in the literature as "full-wave," or "spectral domain" solutions. We have found such techniques to be both rigorous and versatile. Each of these problems will now be discussed briefly, the reader is referred to the appropriate [illegible]

6.1 Analysis of the Scan Characteristics of an Infinite Phased Array of Microstrip Patches with Idealized Probe Feeds.

This work is described in detail in [1], and follows from earlier work on infinite arrays of printed dipoles [7]. It is relevant to the present effort because, as discussed in Chapter 2, an array of microstrip patches on a semiconductor substrate constitutes a potential geometry for a monolithic phased array. And even though we have discussed (in Chapter 2) a number of problems with such a geometry, as well as a number of interesting alternatives, the infinite array of probe-fed patches formed an important canonical problem which had not yet been treated.

The study of infinite arrays is important from a practical point of view because an infinite array can model quite well the behavior of elements in the central region of a planar array, and an infinite array solution is usually more tractable analytically than a finite array.

As derived in [7], the Green's function for a single infinitesimal dipole on a grounded dielectric slab can easily be extended to an infinite array of uniformly phased infinitesimal dipoles. This result is in the form of a double summation of Floquet modes, and does not involve any Sommerfeld type integrals (as does the isolated source). The infinite array solution then proceeds by using this Green's function in conjunction with a suitable set of expansion and weighting modes (entire domain modes, in this case), from which the current flow on the patches can be determined. The solution is periodic, meaning that the currents on adjacent patches differ only by a uniform phase factor. As shown in [1], calculations have been verified by measurements with a waveguide simulator. A few typical results from this type of analysis were presented in Chapter 2; additional results can be found in [1]. One problem with the above analysis is the feed model for the probe-fed patch element. The term "idealized probe feed" was used to indicate that the feed is not modeled

rigorously, but idealized as a uniform current element. This technique has been found to be useful for patches on thin substrates [8], and so is not without practical value. It is known to fail, however, for thick substrates. The improvement of the probe feed model is not an easy task, because the rapidly varying currents on the patch near the probe contact must be modeled accurately, together with the continuity of current condition. Such a solution could be carried out, but funding limitations of the present contract prevented this. In addition, the probe-fed patch may actually be of little interest for monolithic arrays because of the difficulty in fabricating via holes (as well as the electrical problems associated with a patch on a thick, high dielectric constant substrate).

Finally, we would like to respond to some technical comments made in [9], regarding our infinite patch array solution. In [9], the authors described a slightly different analysis of the infinite probe-fed patch array, and on page 166 of that paper, they made three comments which are addressed below:

a) "Failure to extract the rapid current variation of the patch current in the vicinity of the probes, causing slow convergence of the patch current solution." As discussed above, our model did not include the rapid variation of current near the feed point, but for patches on thin substrates this is not serious because the high-Q patch current of the resonant mode is dominant. Convergence is not slowed; just the opposite is true. In addition, such a model was verified for single patches on thin substrates by comparison with measured data in [8].

b) "The neglect of direct probe radiation influence on Z_a (in absence of patches) This contribution becomes important near the array blindness. As a result no leaky wave resonances are found. On the other hand, as a consequence of this

neglect, [our ref. 1] predicts H-plane total reflection at θ_{sw} which is not found in our solution."

We disagree with these conclusions. The direct probe radiation was neglected because our substrates were always thin, so the radiation resistance of the probes was quite small. We have since calculated this effect and found that the change in input resistance was at most a few tenths of an ohm. The effect of this is to reduce the reflection coefficient magnitude of unity at a scan blindness to a value on the order of 0.99 – obviously not a significant effect. (In [9], a number of results were presented for much thicker substrates than in [1], in which case this effect may be more significant.) The statement that our solution does not show leaky wave effects (the term 'resonance' here is debatable, since total reflection does not occur) is wrong. Our solution, being a 'full-wave' solution, does show leaky wave effects. We have calculated data for comparison with a number of cases in [9] where leaky wave effects are pronounced, and obtain good agreement. In most of these cases, the patch is operating well away from resonance; in [1] we concentrated on patches at resonance, where such effects are less obvious.

c) "Use of sinusoidal basis functions that do not explicitly enforce the edge condition. This choice increases the required size of the impedance matrix, and limits the practicality of the solution to thin, say $h/\lambda < 0.04$ substrates."

Over the years we have solved a variety of antenna problems by the moment method, and have usually found that the edge condition is not worth the cost in terms of added complexity and computer time. We do agree, however, that our solution is limited to thin substrates.

6.2 Analysis of the Scan Characteristics of an Infinite Array of Aperture Coupled Microstrip Patches.

This analysis has been completed but has not yet been published because we plan to perform some waveguide simulator experiments to verify the theory. It basically combines the infinite array analysis of [1] with a reciprocity-based treatment of the feed line coupling [10]. Thus, mutual coupling between the patches and both sides of the slots are accounted for; the feed lines are assumed to be localized to their respective coupling apertures, so no mutual coupling effects between them are included. This is a realistic treatment, and probably the only practical one since long feed lines would run into each other. So even though the aperture feed is in many ways more complicated than the probe feed, its analysis (at the present time) is more rigorous.

Figures 6.1 and 6.2 show results for an aperture coupled array geometry with an antenna substrate having ϵ_r=2.55 and d=0.02λ_o, and a feed substrate having ϵ_r=12.8 and d=0.05λ_o, thus simulating a possible monolithic array geometry. The feed substrate was intentionally made thicker than usual to show the surface wave resonances; a thinner substrate would move the feed resonance closer to endfire. Figure 6.1 shows the reflection coefficient magnitude versus scan angle, where surface wave resonances are seen to occur at 62° and at 86°. The former is due to surface wave excitation on the feed substrate, while the latter is due to surface wave excitation on the antenna substrate. The individual contributions of the patch and slot to this phenomenon are shown in Figure 6.2. The real and imaginary components of the patch and slot admittances as seen by the microstrip feed line are plotted versus scan angle for the same geometry as shown in Figure 6.1. The patch admittance, $G^P - jB^P$, is seen to have a resonance (zero real part) at about 86°. The slot looks into both the antenna substrate and the feed substrate, and so the slot admittance is separated into an antenna substrate component, $G^{sa} - jB^{sa}$, and a feed substrate component, $G^{sf} - jB^{sf}$. The former has a resonance (infinite susceptance) at 86°.

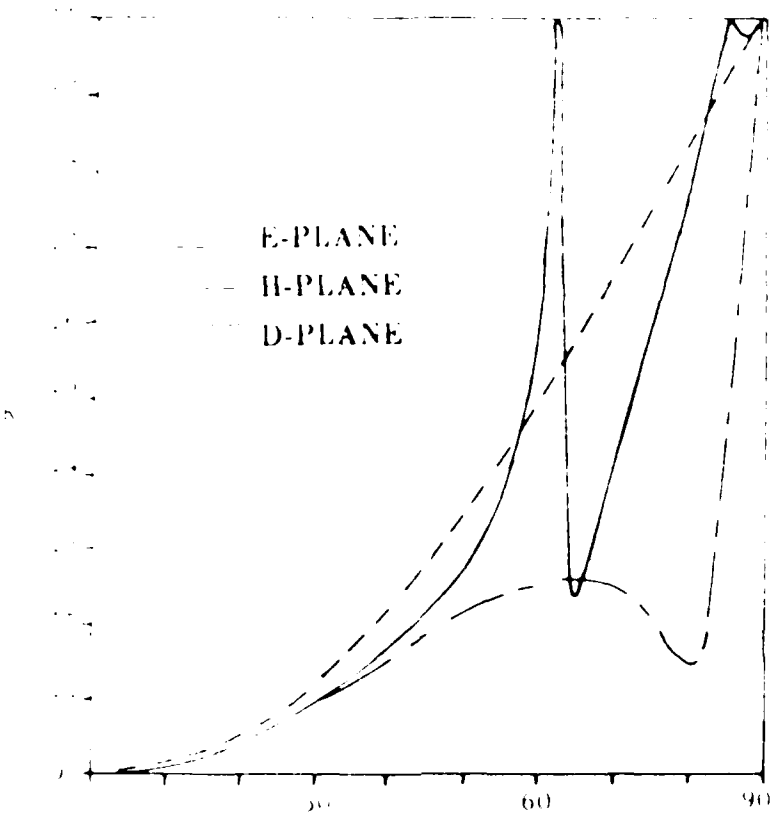

$\epsilon_{ra} = 2.55$ $\epsilon_{rf} = 12.8$

$\alpha_a = 0.02\lambda_o$ $d_f = 0.05\lambda_o$

$PL = 0.279\lambda_o$ $SL = 0.115\lambda_o$

$PW = 0.279\lambda_o$ $SW = 0.01\lambda_o$

$a = b = 0.5\lambda_o$ $W_f = 0.05\lambda_o$

$L_s = 0.075\lambda_o$

Figure 6.1 **Reflection coefficient magnitude of an infinite array of aperture coupled patches.**

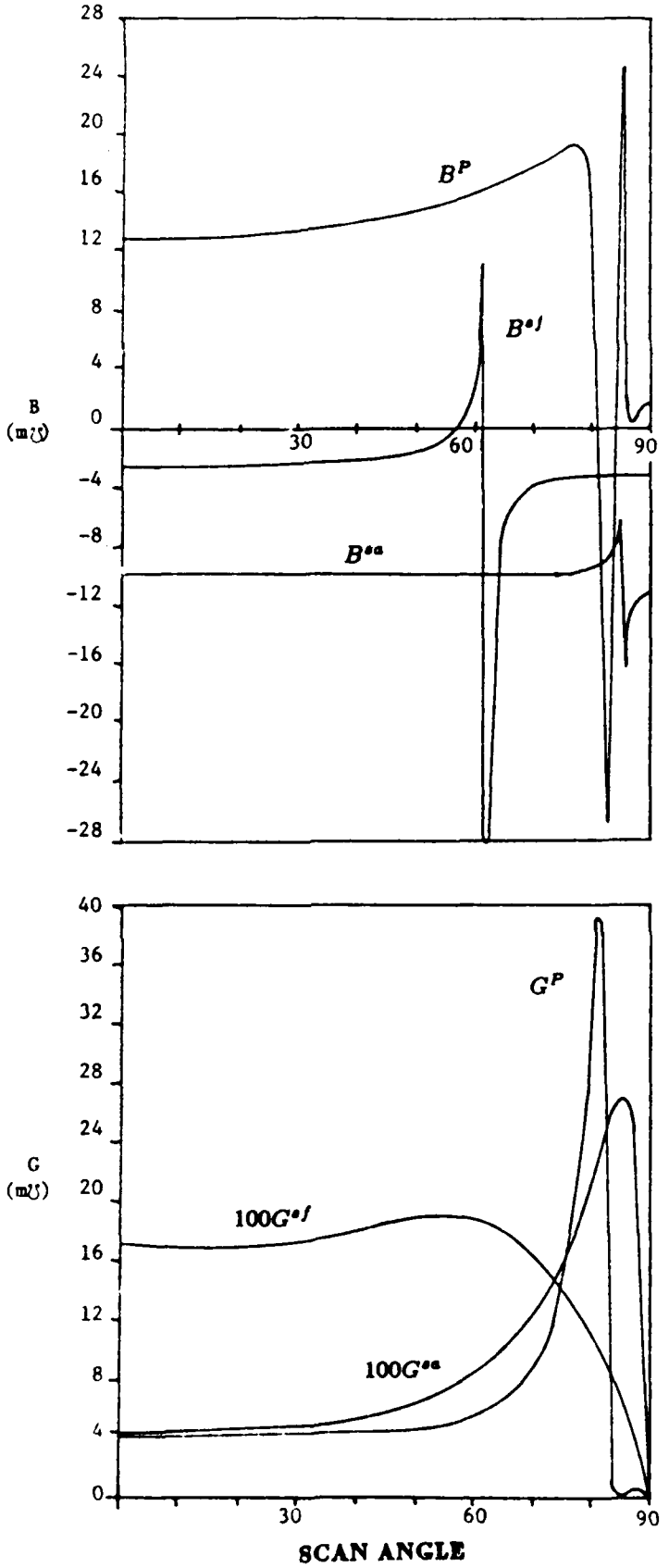

Figure 6.2 Active admittances of the patch and slot elements.

while the latter has a resonance (infinite susceptance) at about 62°. Thus, surface wave resonances are possible on the feed side of the substrate, due to slot coupling, but these resonances can be moved closer to endfire by making the feed substrate thinner.

6.3 A Current Sheet Model of the Scan Characteristics of a General Printed Phased Array.

After studying a number of different phased array geometries of dipoles and patches, it became evident that many of the dominant characteristics of printed phased arrays were controlled by the element spacing and substrate parameters, as opposed to the specific type of radiating element or feeding technique. This observation led to a current sheet model of a printed phased array [3], based on an extension of early work by Wheeler [11].

The purpose of this work, then, was not to generate a solution or data that was accurate for all printed phased arrays, or even for a specific phased array, but to derive an *analysis that predicted the major trends in the scanning* performance of a printed phased array. Such a result enhances our understanding of the operation of such antennas.

A number of results are shown in [3], comparing the current sheet model with rigorous solutions for dipole or patch elements from [7] and [1]. As an example, Figure 6.3 shows a comparison of the current sheet model with results from [7] for an infinite dipole array.

6.4 Analysis of Finite Phased Arrays of Printed Dipoles and Microstrip Patches.

While data for isolated printed dipoles or patches are useful, they are of limited value when a large array is being considered because mutual coupling must be taken into account. If it is very large, the central elements of a finite array may be modeled quite well by the infinite array approximation, which does include mutual coupling effects. The infinite array solution, however, does not account for edge effects in a finite array, and it is generally not known a priori how 'big' a finite array has to be before it can be reasonably

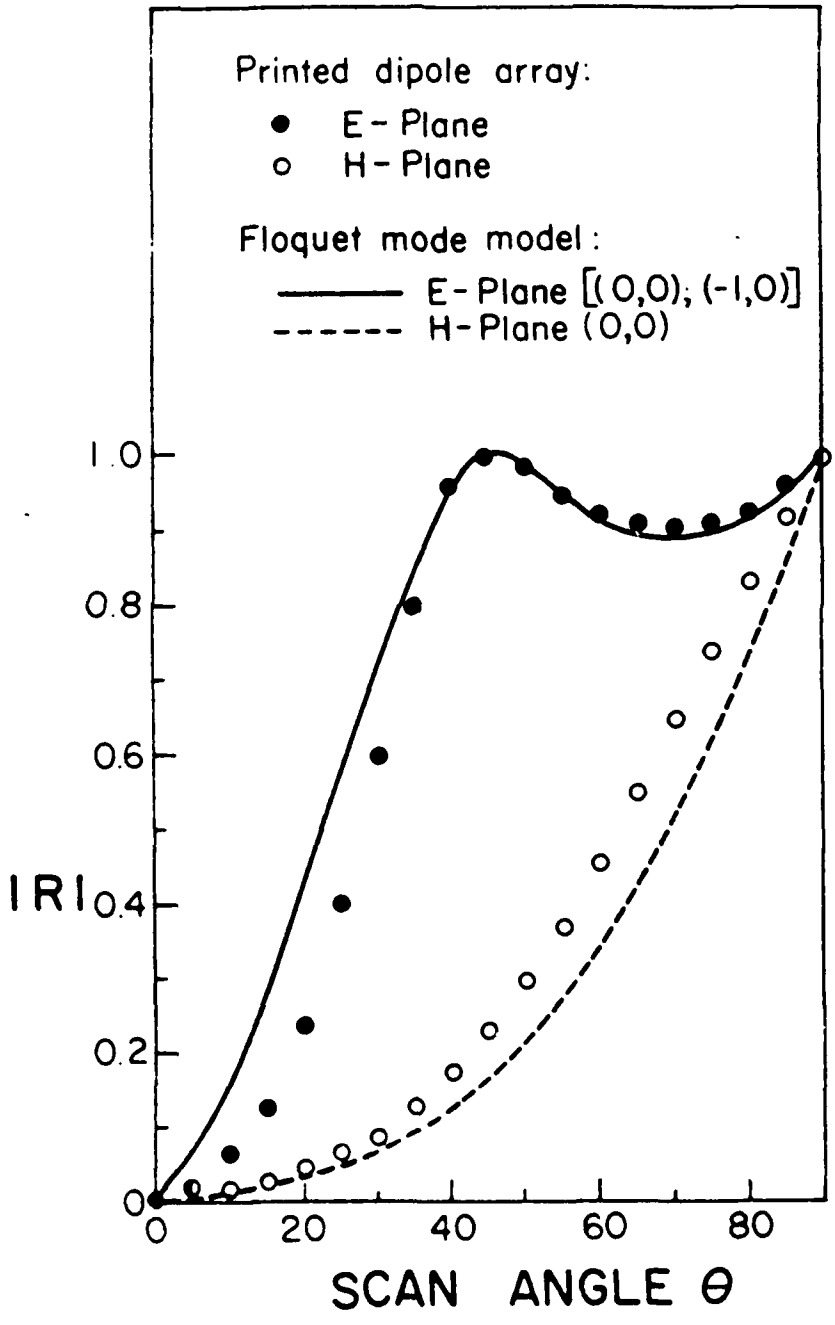

Figure 6.3. Comparison of the current sheet model with the results from the analysis.

modeled as infinite. Thus, the analysis of finite arrays may be of more practical utility than either the analysis of isolated elements or infinite arrays. The complexity of such an analysis, however, is somewhat more difficult than either the isolated element solution or the infinite array solution, due to the fact that mutual coupling between each pair of elements must be calculated, and the lack of periodicity across the array (as in the case of an infinite array).

Another reason for considering finite arrays of printed antennas concerns the role of surface waves. It has been shown that isolated printed antenna elements can convert significant fractions of their input power into surface waves, as opposed to radiated power [12]. On the other hand, surface waves cannot exist on infinite phased arrays except at certain critical angles (blindness angles) where all input power is converted to surface wave power, and no radiation leaves the surface of the array. The question then arises as to the effect of array size on the generation of surface waves. For example, will a finite array of printed dipoles excite more or less surface wave power than a single printed dipole on the same type of substrate, and how does this power vary with array size? It is also of interest to see how surface wave excitation varies with scan angle.

The work of [4] and [5] addresses the above questions by considering finite-sized arrays of printed dipoles and microstrip patches, respectively. The method of solution is basically the "element by element" approach, whereby the self and mutual impedance of the dipoles are calculated by the full-wave analysis of [8]. The active impedance for various arrays was calculated, and the efficiency (based on power lost to surface waves) is calculated. The solution also allows the active element pattern to be determined.

Figures 6.4-6.7 show a number of results for finite arrays of dipoles on a substrate with ϵ_r=2.55 and d=0.19λ_o. (The substrate was intentionally made thick to see the surface wave

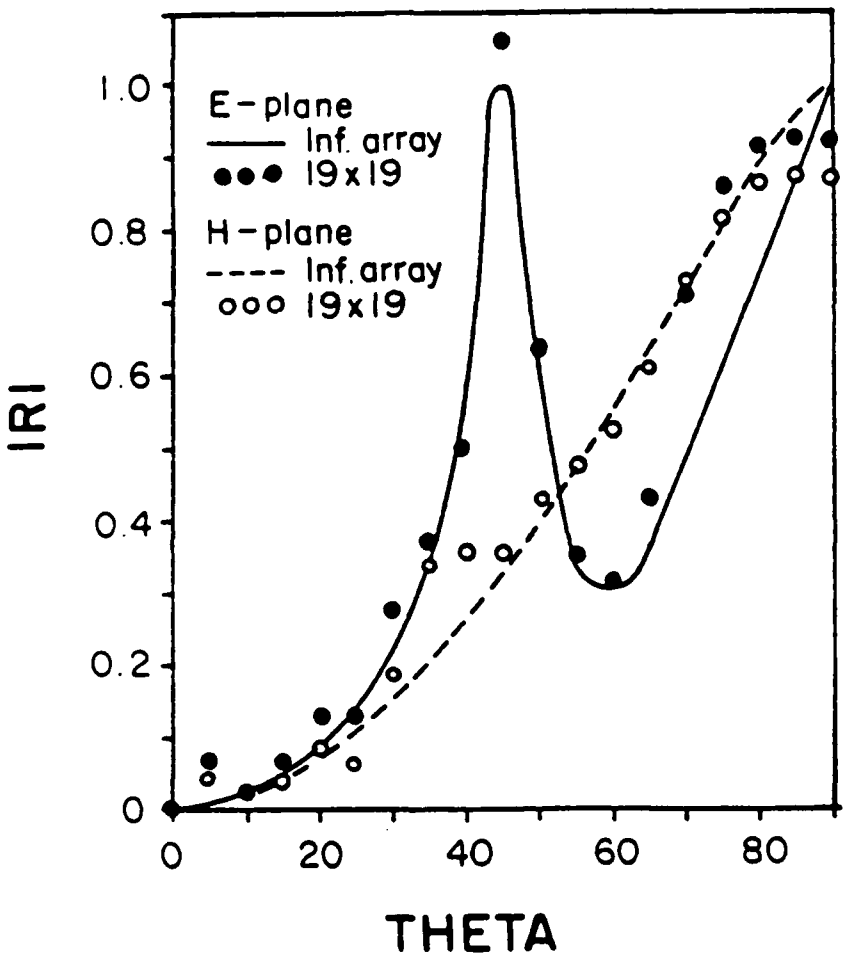

Figure 6.4 Reflection coefficient magnitude of a finite (19x19) planar dipole array.

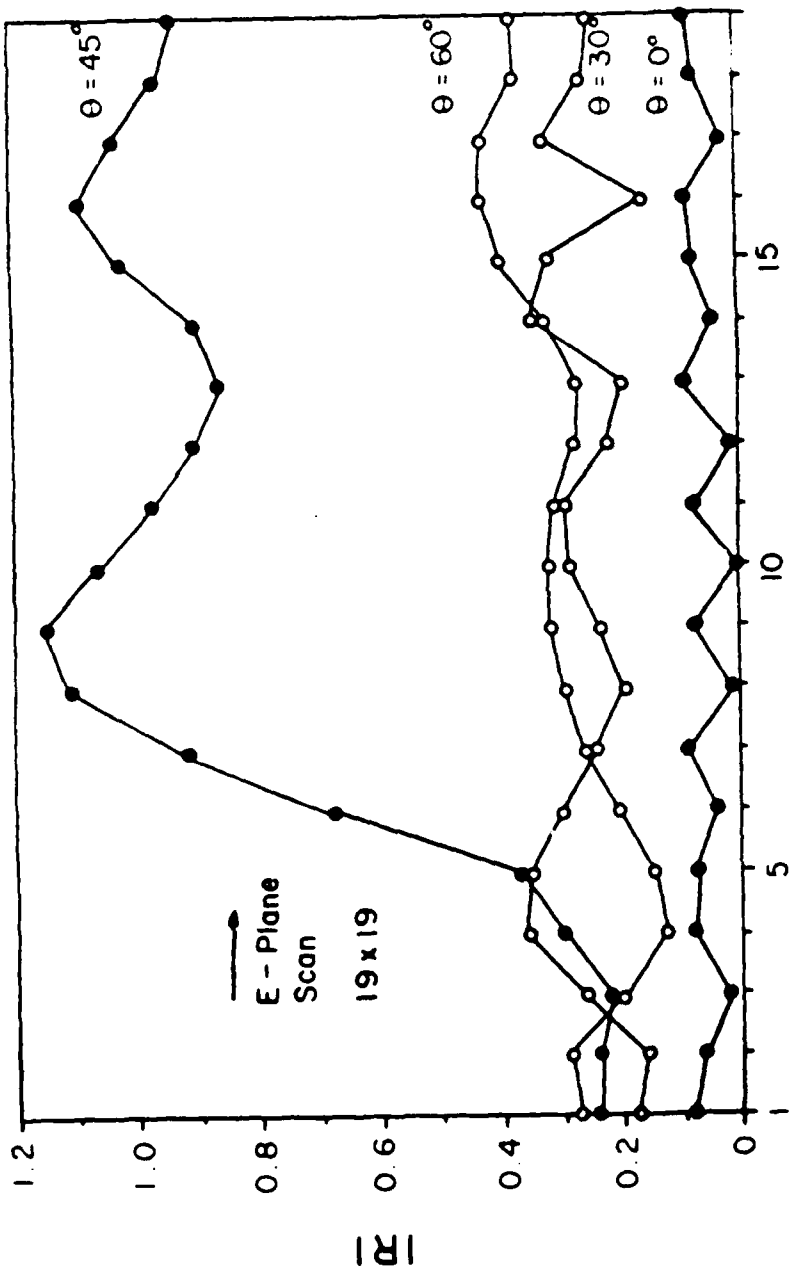

Figure 6.5 Variation of reflection coefficient magnitude with dipole position, for various scan angles.

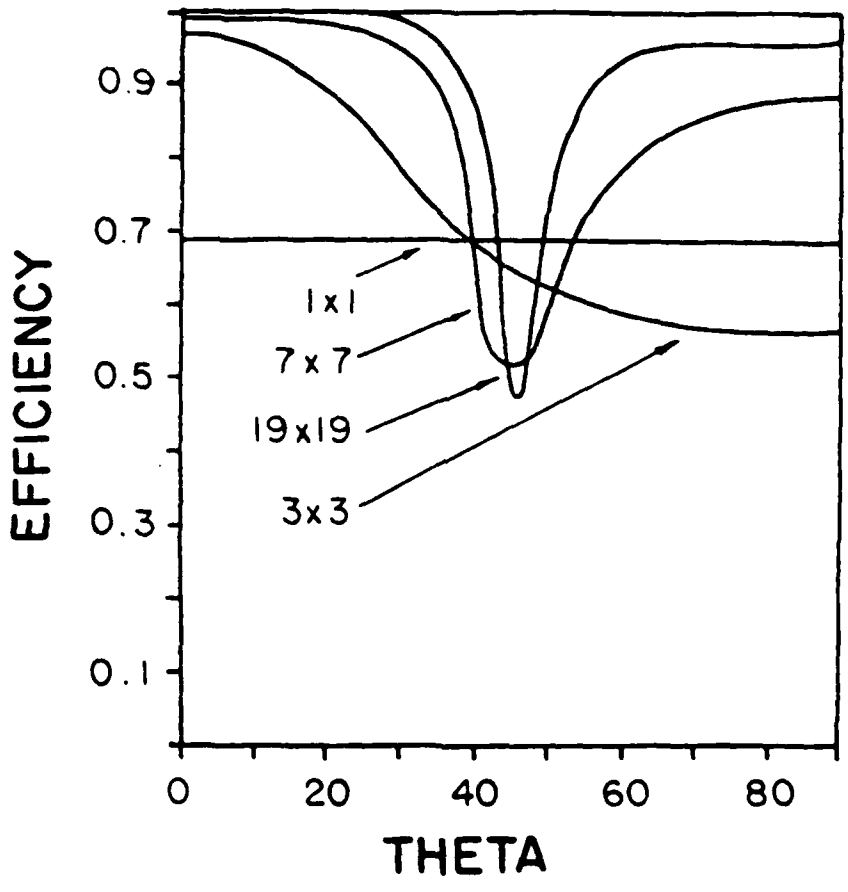

Figure 6.6 Efficiency (power lost to surface waves) for E-plane scan of finite planar dipole arrays of various sizes.

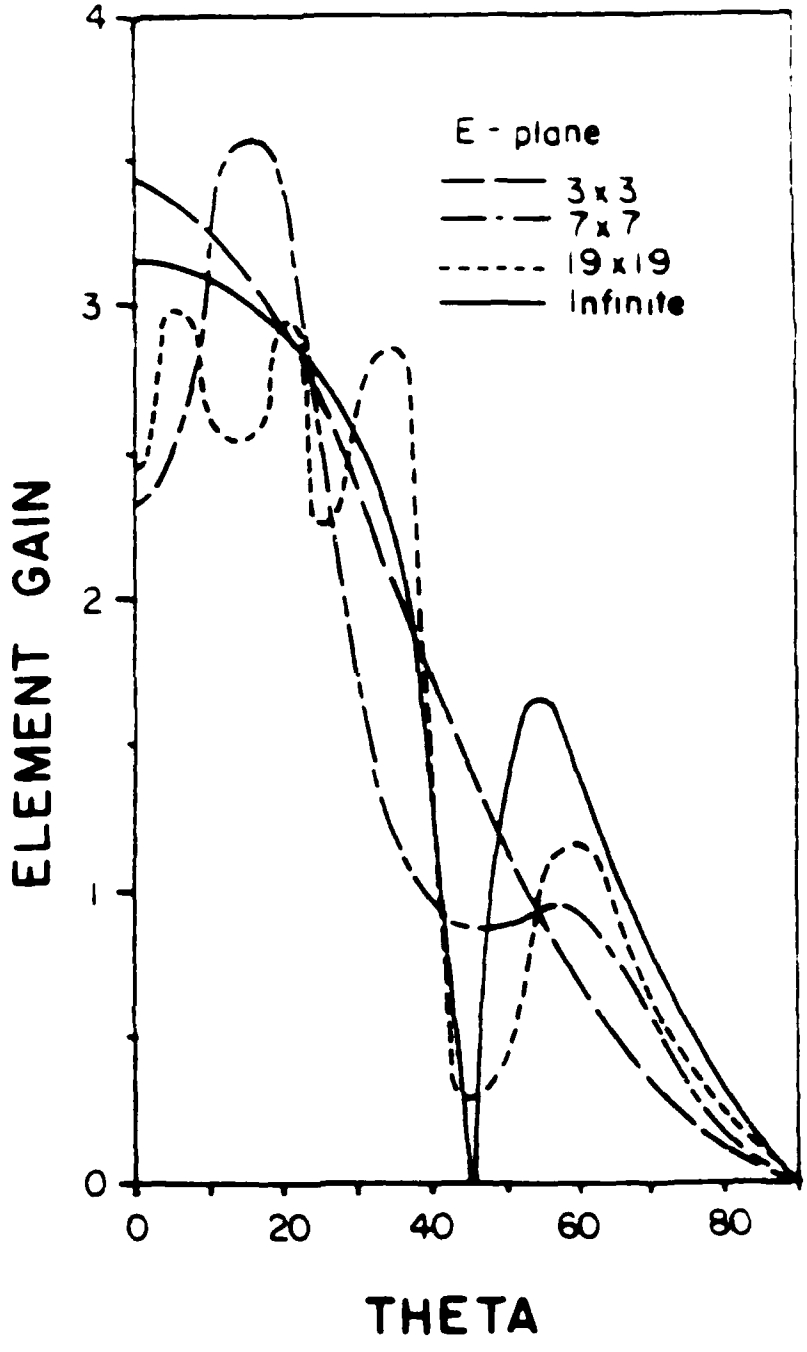

Figure 6.7a *E*-plane active element patterns of finite planar dipole arrays of various sizes.

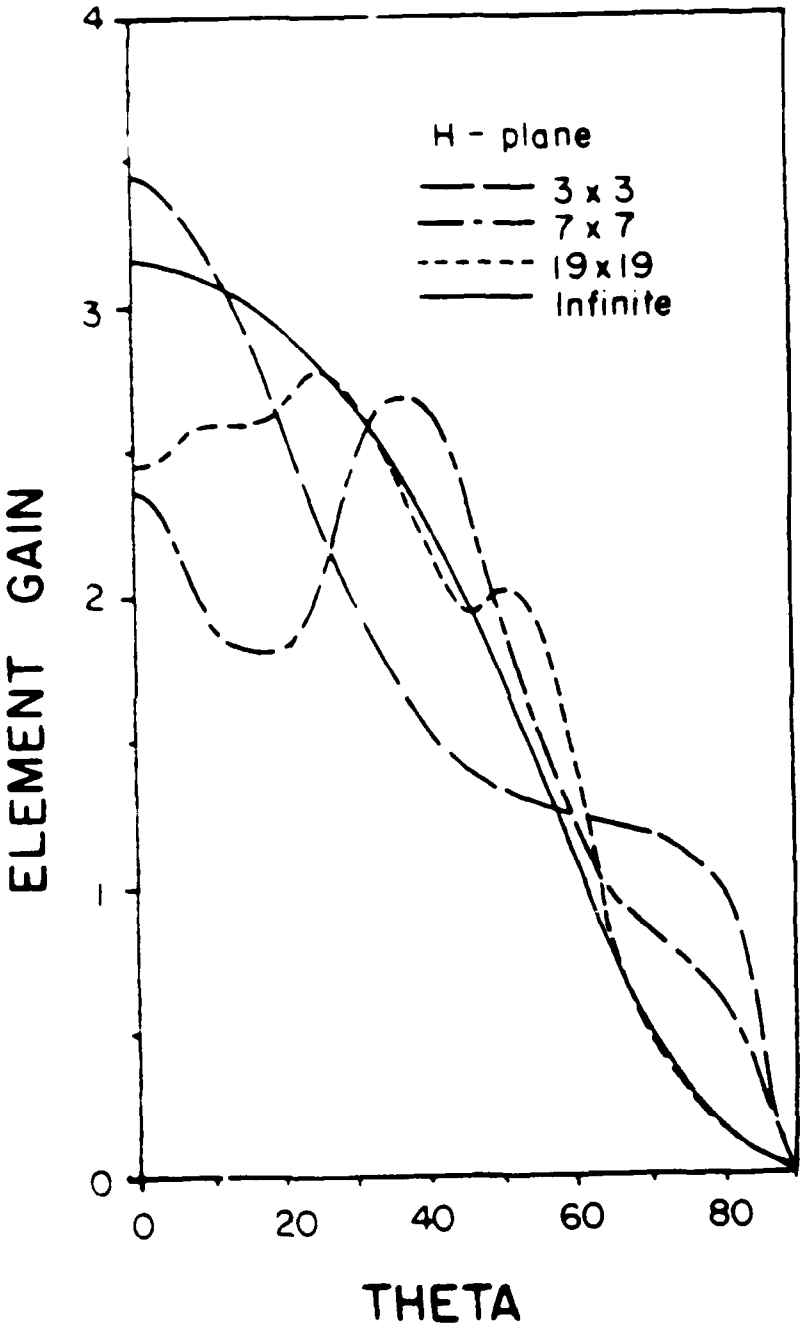

Figure 6.7b H-plane active element patterns of finite planar dipole arrays of various sizes

effects.) In Figure 6.4, the reflection coefficient magnitudes at the center elements of finite arrays of various size are shown, versus scan angle. Observe that the 19x19 array is large enough so that its reflection coefficient magnitude versus scan angle follows the result for the infinite array quite closely.

Figure 6.5 shows the reflection coefficient magnitude as a function of element position across the E-plane direction of a 19x19 dipole array, for various scan angles. Observe that there is substantial variation across the array, especially for scan angles away from broadside, and that the reflection coefficient magnitude may actually exceed unity in the vicinity of the blind spot. Power is conserved, however, because most of the ports are still absorbing power from the generators. These effects are due to the edges of the array, and would not occur in infinite array solutions.

Figure 6.6 shows the efficiency of finite arrays based on power lost to surface waves, versus E-plane scan angle. This is an interesting result, because it shows the role of surface waves in the transition from a single element to a finite array, and then to an infinite array. For a single dipole, about 22% of its input power is converted to surface wave power. For arrays, however, a significant variation of efficiency occurs with scanning. The general trend is that efficiency improves substantially for even modest sized arrays, and increases with array size at all scan angles except those near 46°, at which angle the efficiency decreases (more surface wave power) with increasing array size. This is the angle at which the infinite array has a scan blindness. If the efficiency of the infinite array were plotted in this figure, it would be unity at all scan angles except at 46°, where it would be zero.

Figure 6.7 shows E- and H-plane active element patterns for various sized dipole arrays. As the array size increases, the patterns tend to oscillate more around the infinite array element pattern, and the dip or null in the E-plane at 46° gets deeper.

Similar results are obtained for patches; results can be found in [5]. Also in [5], measurements of the active element patterns of a 7x7 array on a thin substrate were presented.

6.5 Analysis of the Aperture Coupled Patch Element

The aperture coupled patch antenna described in Section 3.1 has been analyzed by using a rigorous moment method technique. The analysis uses the Green's functions for grounded dielectric slabs so that it contains all radiation and surface wave effects. The problem is formulated in the spectral domain where the Green's functions can be represented in closed form. The moment method solution technique described in [6] then leads to a matrix equation wherein the matrix elements are obtained by numerical evaluation of a double infinite integral. This leads to rather lengthy computation times (on the order of 30 minutes per data point for a VAX 11/750), but the agreement between the calculations and experiment is quite good, as illustrated in Figure 3.2.

The formulation of the analysis proceeds as follows:

1. The equivalence principle is invoked to close the aperture and replace it by an unknown magnetic current $\bar{M}s$ to be determined as part of the solution (see Figure 6.8).
2. A known incident current $\bar{J}_{inc}$ and an unknown reflected current $\bar{J}_f$ are assumed on the feed line.
3. An unknown current $\bar{J}_p$ is assumed on the patch radiator.
4. The electric and magnetic fields due to each of these currents radiating in the presence of a grounded dielectric is calculated by using the appropriate Green's functions.
5. Boundary conditions on the total fields are enforced by a slightly modified Galerkin technique. The boundary conditions required to determine $\bar{M}_s$, $\bar{J}_f$ and $\bar{J}_p$ are (i) $\bar{E}^{tan}$=0 on the patch antenna, (ii) $\bar{E}^{tan}$=0 on the microstrip feedline, and (iii) $\bar{H}^{tan}$

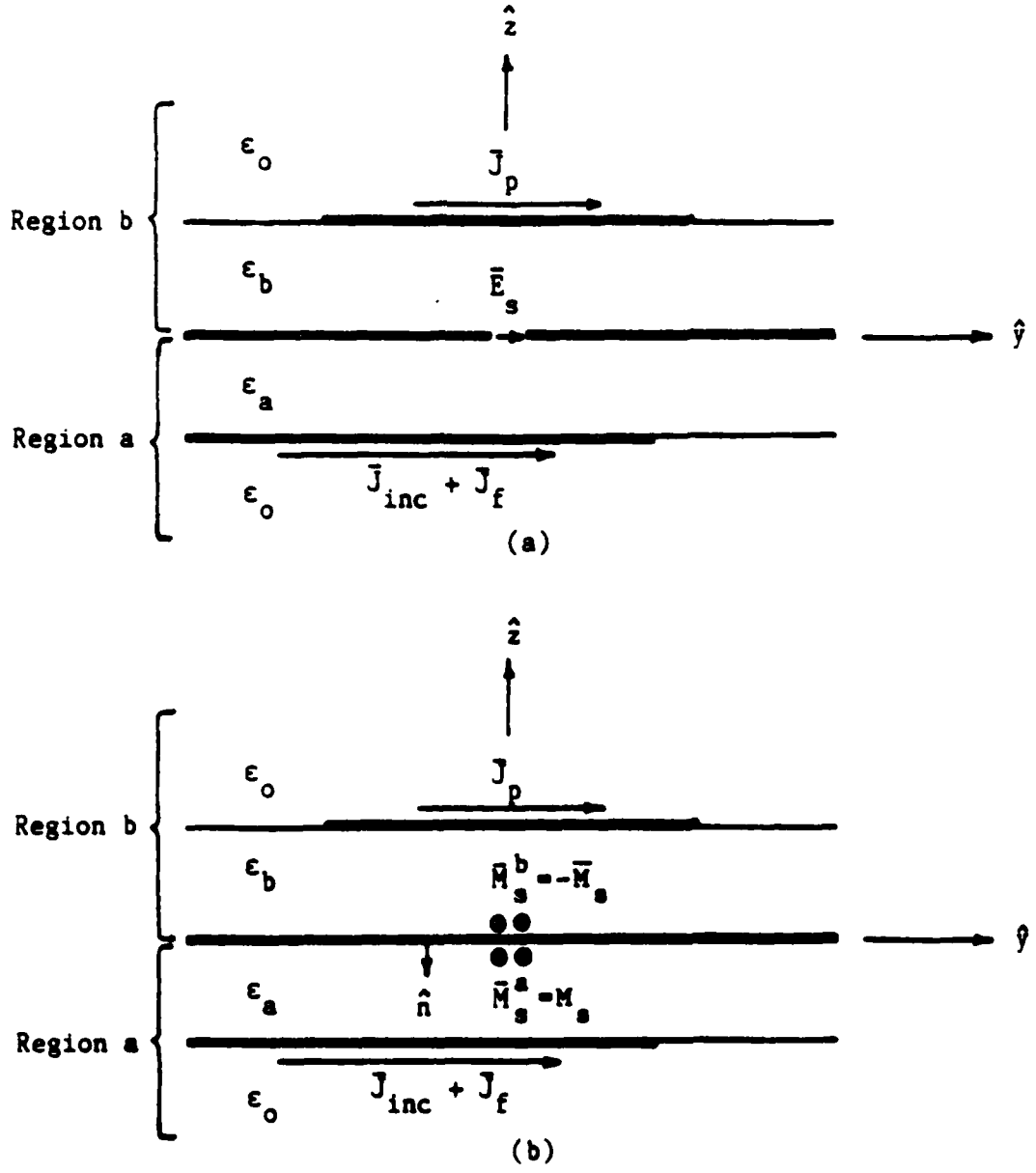

Figure 6.8 Antenna and feed with incident and induced currents. (a) Original problem. (b) Equivalent problem.

is continuous through the aperture. (Note that the assumption $\bar{M}_s^a = M_s^b$ ensures that $\bar{E}^{tan}$ is continuous through the aperture.

The formulation in [6] has achieved good results by assuming (i) only y-directed currents on the patch with piecewise sinusoidal variations in y and uniform in x, (ii) only x-directed magnetic current in the aperture with a single piecewise sinusoid in the x direction and uniform in the y direction, and (iii) only y-directed currents on the feed line with a combination of traveling wave and piecewise sinusoidal variations in y and uniform in x.

In addition to the results presented in Figures 3.2-3.5, the results in Figure 6.9-6.10 have been obtained to illustrate the control of impedance and the robustness of the design with respect to changes in the patch alignment over the aperture. The zero offset case is the L_s=2.0cm case in Figure 3.2, and comparisons of that case with the 0.5cm offset cases in Figures 6.9-6.10 show that a relatively large alignment error (more than 10% of the patch length) has a modest effect on the performance of the antenna. Finally, the reduction in coupling due to increasing the thickness of the feed substrate is illustrated in Figure 6.11. Some compensation for the reduction in coupling can be achieved by increasing the length of the aperture, but care must be taken to insure that the aperture does not approach resonant dimensions, where it will radiate on the feed side of the ground plane.

6.6 Full Wave Analysis of the Microstrip Open, Gap and Coplanar Waveguide Short

Three of the simpler discontinuities in integrated millimeter wave transmission lines were studied using the full wave analysis described in references [13], [14], and [15]. The discontinuities are the microstrip open end, the microstrip gap and the short circuit coplanar waveguide. Figure 6.12 illustrates these three.

The analysis used was rigorous in that it included all electromagnetic effects such as, for example, surface waves and radiation. The moment method technique was used

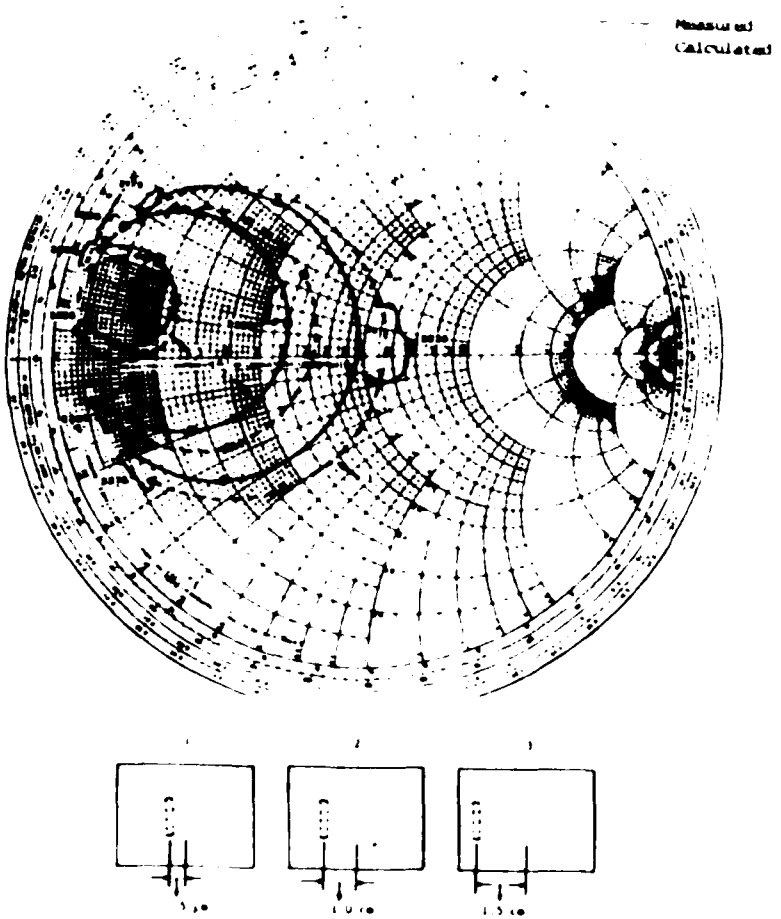

Figure 6.9 Measured and calculated input impedance as a function of patch offset in the direction of resonance. $L_s = 2.0cm$ and other antenna parameters are the same as Figure 3.2.

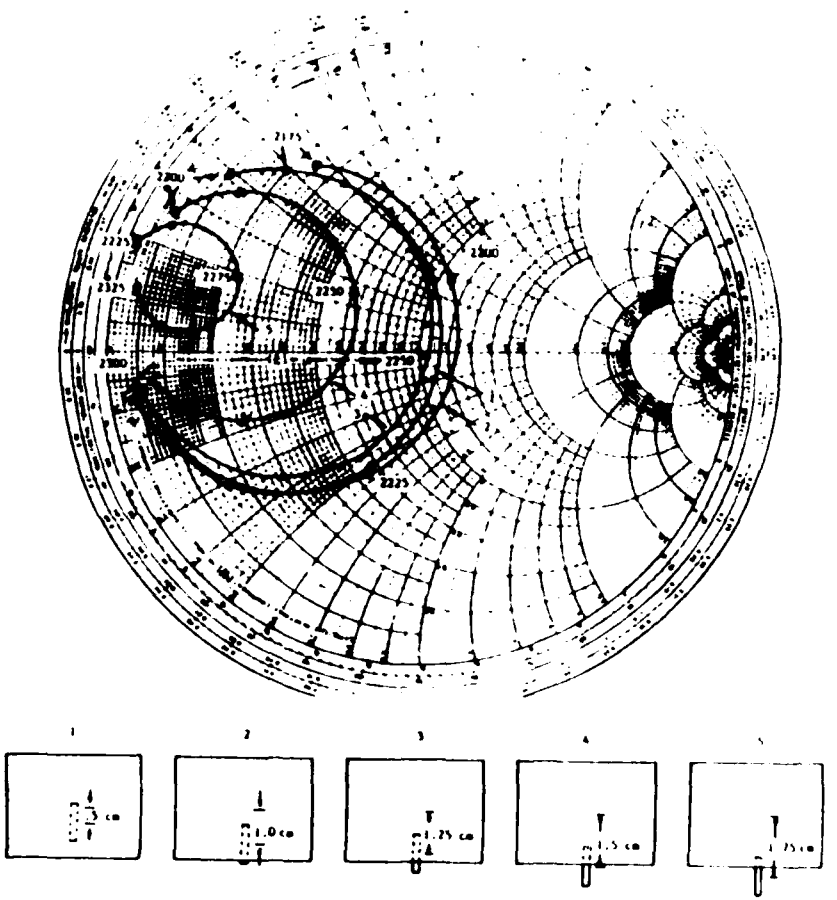

Figure 6.10 Measured input impedance as a function of patch offset in the direction othogonal to resonance. $L_s = 2.0cm$ and other antenna parameters are the same as Figure 3.2.

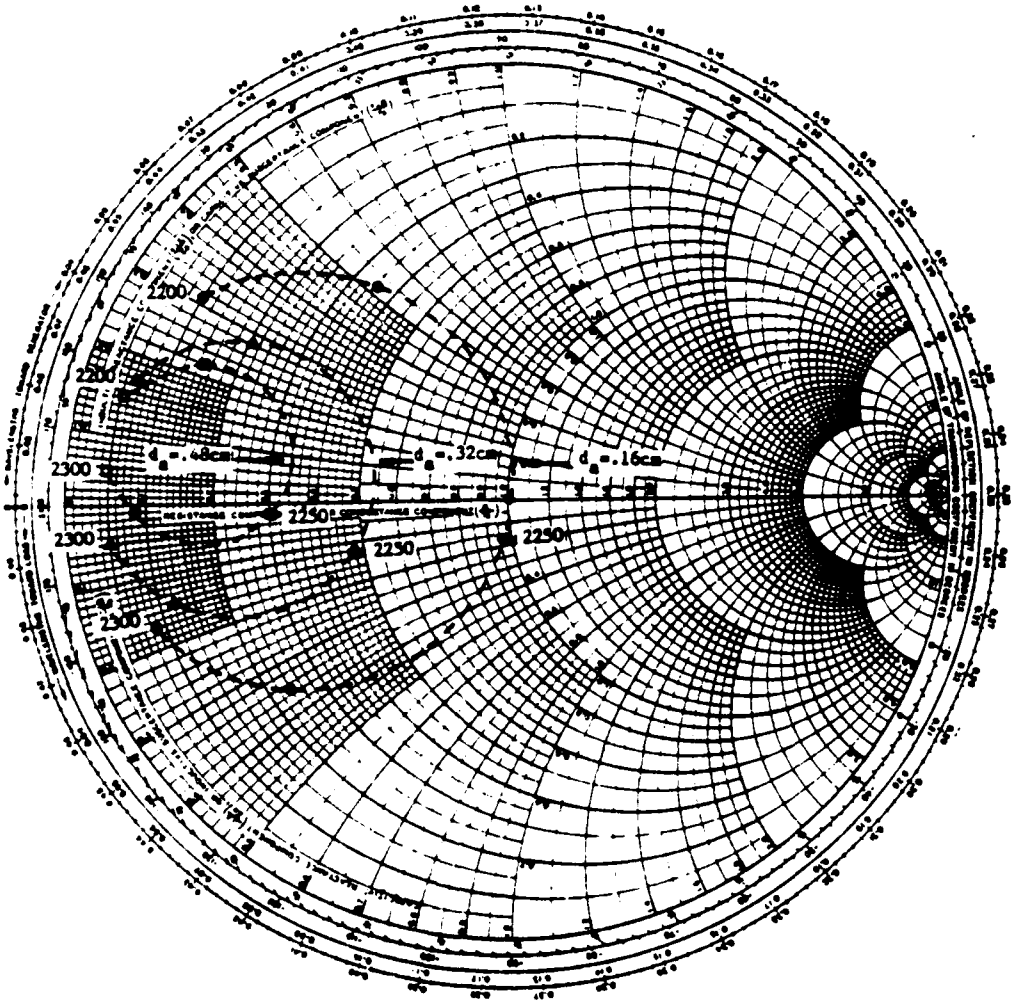

d_a	W_f	L_s
.16 cm	.173 cm	1.108 cm
.32 cm	.375 cm	1.083 cm
.48 cm	.613 cm	1.056 cm

Figure 6.11 Calculated input impedance as a function of feed substrate thickness. Tabular data give feedline width and stub length used to maintain 50Ω characteristic impedance and stub length of $0.22\lambda_f$ for each value of d_a. Other antenna parameters are $\epsilon_r^b = 2.54, d_b = 0.16cm, L_p = 4.0cm, W_p - 3.0cm, \chi_{0s} = 0.0cm, y_{0s} = 0.0cm, L_{ap} = 1.0cm, W_{ap} - 0.11cm, \epsilon_r^a = 10.2$.

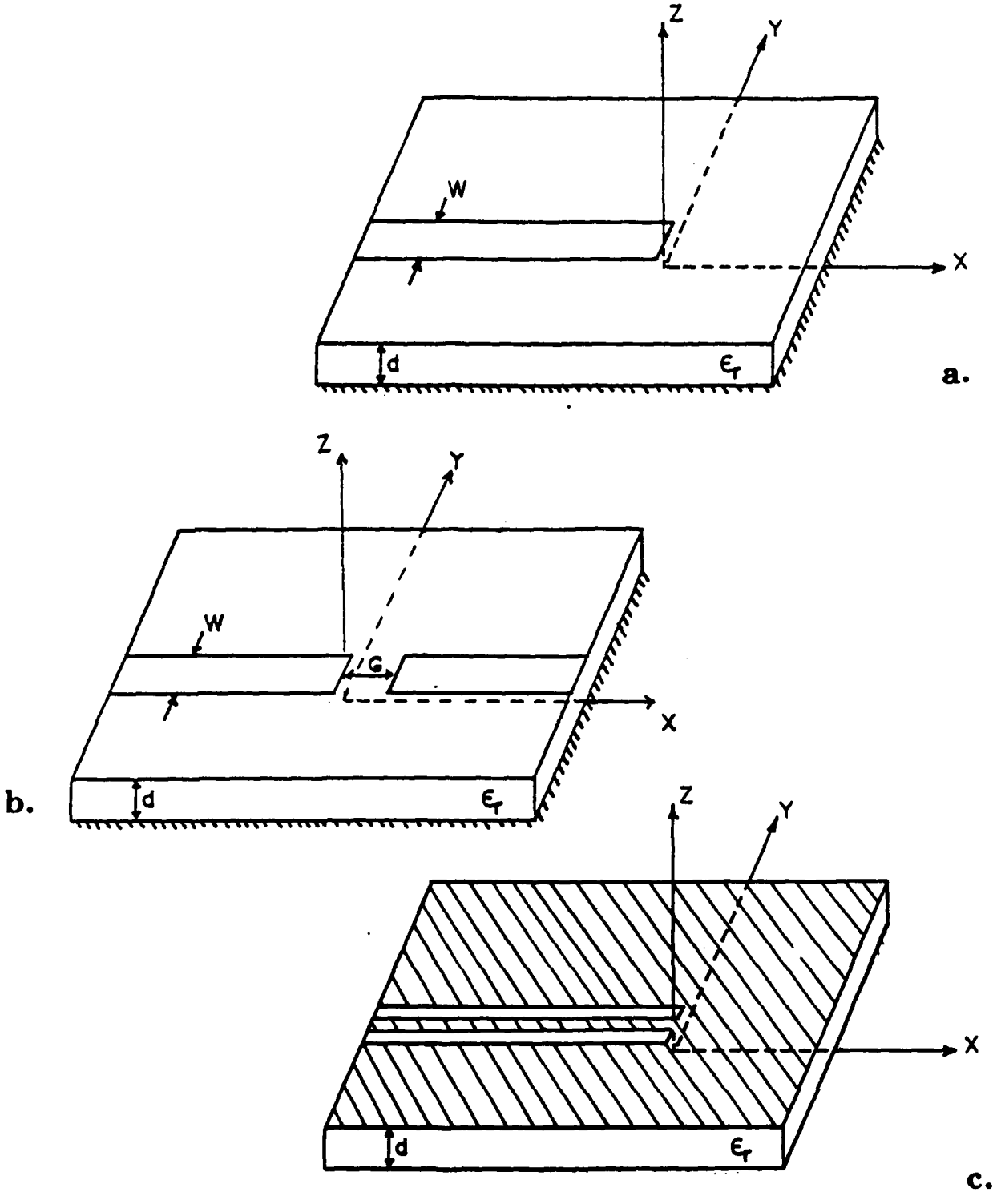

Figure 6.12 (a) Microstrip open end, (b) Microstrip gap, (c) Coplanar waveguide short circuit.

in conjunction with the grounded dielectric slab Green's function for the microstrip open end and gap. This Green's function is derived such that the boundary conditions at all surfaces are satisfied except where a microstrip line appears. Following the moment method procedure, the currents on the microstrip lines are expanded in terms of known functions multiplied by unknown constants. The electric fields tangent to the microstrip surface due to these currents can then be obtained via the aforementioned Green's function. The unknown are determined by forcing moments of the tangential electric field to vanish wherever a microstrip line is located. The number of moments taken depends upon the number of expansion currents used. All of this is done in the spectral domain.

For coplanar waveguide or slots, a Green's function is found which relates the electric field in a slot to the electric current on the perfectly conducting surface which holds the slot. All boundary conditions at the dielectric surface and the conducting surface are satisfied except where a slot is present. The moment method technique is then used to expand the fields in the slots and, by taking moments, determine the expansion coefficients necessary to insure that the electric currents in the slots are zero. This procedure is completely analogous to the microstrip analysis.

For the microstrip open end and the CPW short a large number of piecewise sinusoidal expansion functions are located near the ends. Each of these is a fraction of a wavelength long. Away from the ends the expansion functions were finite length sinusoids with wavelengths which were consistent with those determined by a full wave analysis of the infinite line. Each was two or three wavelengths long. One pair of finite sinusoids made up the known incident wave and one pair made up the reflected wave the complex amplitude of which was the desired quantity. Only longitudinal currents were assumed during this work. Later work funded by other sponsors showed that in most cases, transverse

expansion currents are not necessary. To solve for the microstrip gap, two additional finite length sinusoids are necessary to represent the transmitted wave.

Figure 6.13 shows representative results for the microstrip open end on a substrate with permittivity 12.8. The reflection coefficient magnitude is plotted and shows the loss of energy due to surface wave and space wave radiation. Figure 6.14 shows a similar result for the coplanar waveguide short circuit.

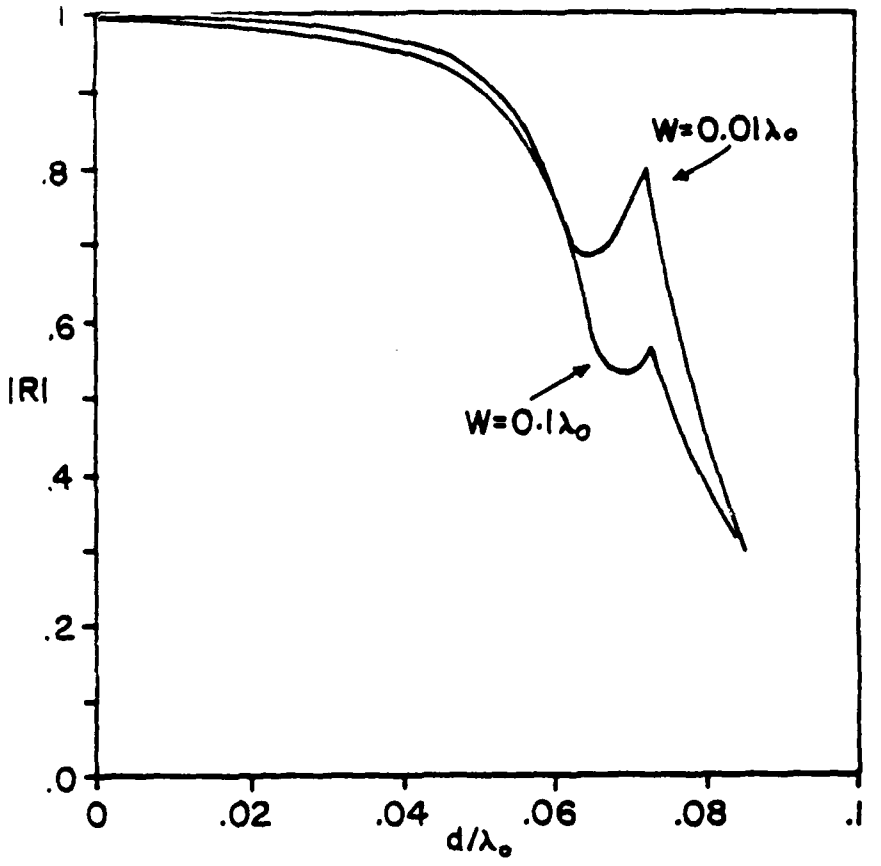

Figure 6.13 Reflection coefficient magnitude from microstrip open end on GaAs substrate.

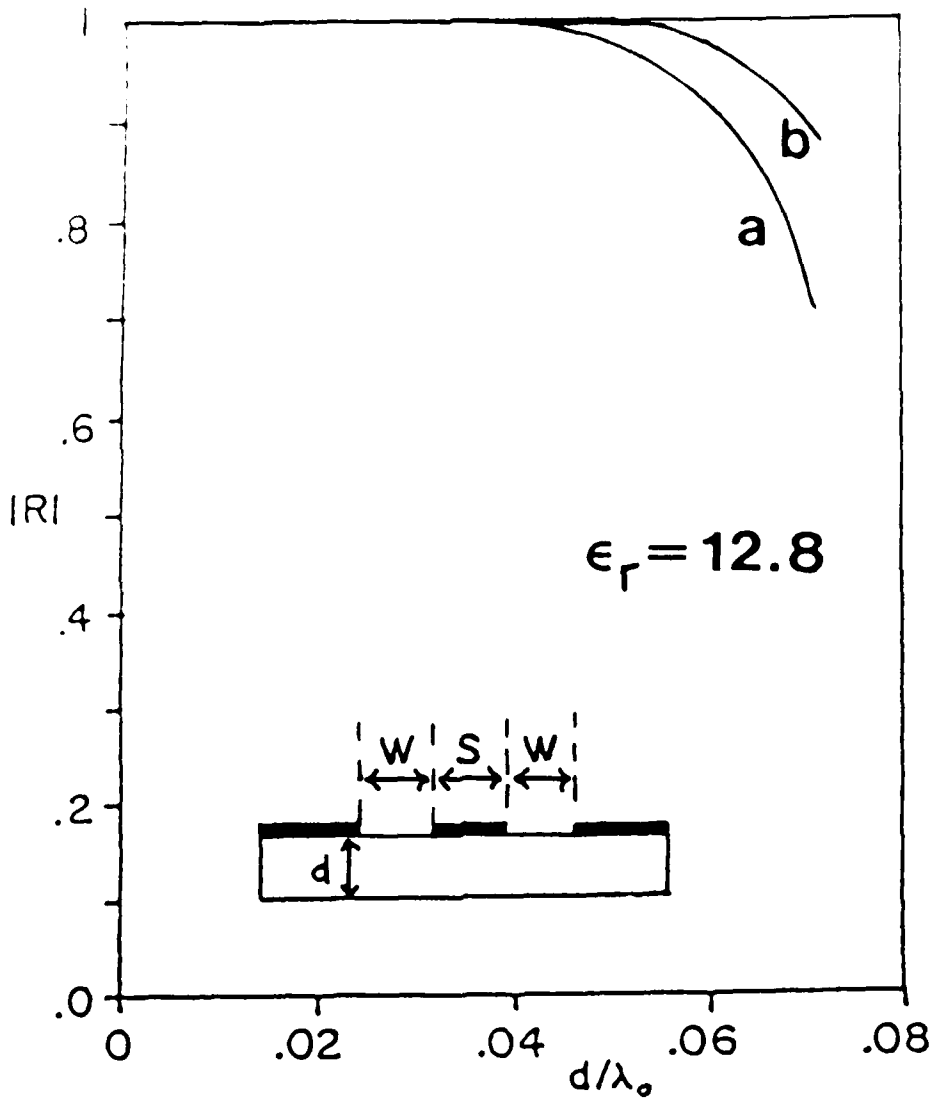

Figure 6.14 Reflection coefficient magnitude from coplanar waveguide short on GaAs substrate with (a) $S = 1.4d, W = d$, (b) $S = .7d, W = .5d$.

References for Chapter 6

[1] D. M. Pozar and D. H. Schaubert, "Analysis of an Infinite Array of Rectangular Microstrip Patches with Idealized Probe Feeds," IEEE Trans. Antennas and Prop., Vol. AP-32, pp. 1101-1107, October 1984.

[2] D. M. Pozar, Unpublished Work.

[3] D. M. Pozar, "General Relations for a Phased Array of Printed Antennas Derived from Infinite Current Sheets," IEEE Trans. Antennas and Prop., Vol. AP-33, pp. 498-504, May 1985.

[4] D. M. Pozar, "Analysis of Finite Phased Arrays of Printed Dipoles," IEEE Trans. Antennas and Prop., Vol. AP-33, pp. 1045-1053, October 1985.

[5] D. M. Pozar, "Finite Phased Arrays of Rectangular Microstrip Antennas," IEEE Trans. Antennas and Prop., Vol. AP-34, pp. 658-665, May 1986.

[6] P. L. Sullivan and D. H. Schaubert, "Analysis of an Aperture Coupled Microstrip Antenna," IEEE Trans. Antennas and Prop., Vol. AP-34, pp. 977-984, August 1986.

[7] D. M. Pozar and D. H. Schaubert, "Scan Blindness in Infinite Phased Arrays of Printed Dipoles," IEEE Trans. Antennas and Prop., Vol. Ap-32, pp. 602-610, June 1984.

[8] D. M. Pozar, "Input Impedance and Mutual Coupling of Rectangular Microstrip Antennas," IEEE Trans., Antennas and Prop., Vol. AP-30, pp. 1191-1196, November 1982.

[9] C. C. Liu, A. Hessel, and J. Shmoys, "Performance of Probe-Fed Microstrip-Patch Element Phased Arrays," 1985 Phased Arrays Symposium, Bedford, MA.

[10] D. M. Pozar, "A Reciprocity Method of Analysis for Printed Slot and Slot-Coupled Microstrip Antennas," to appear in the IEEE Trans. Antennas and Prop.

11 H. A. Wheeler, "Simple Relations Derived from a Phased-Array Antenna Made of an Infinite Current Sheet," IEEE Trans. Antennas and Prop., Vol. AP-13, pp. 506-514, July 1965.

12 D. M. Pozar, "Considerations for Millimeter Wave Printed Antennas," IEEE Trans. Antennas and Prop., Vol. AP-31, pp. 740-747, September 1983.

13 R. W. Jackson and D. M . Pozar, "Full Wave Analysis of Microstrip Open-End and Gap Discontinuities," IEEE Trans. on Microwave Theory and Tech., October 1985.

14 R. W. Jackson and D. M. Pozar, "Surface Wave Losses at Discontinuities in Millimeter Wave Integrated Transmission Lines," 1985 Microwave Theory and Techniques Symposium.

15 R. W. Jackson, "Considerations in the Use of Coplanar Waveguide for Millimeter Wave Integrated Circuits," IEEE Trans. on Microwave Theory and Tech., December 1986.

Chapter 7

SUMMARY

This project has included investigations of architectures and radiating elements for integrated phased arrays and of FET oscillators and amplifiers that could be used in these arrays. Many analyses have been developed and several prototype elements and subarrays have been fabricated and tested. All of these investigations have contributed to an understanding of the technical issues that control the performance of integrated phased arrays. For example, scan blindnesses associated with surface waves on printed antenna substrates and competition for limited surface area have prompted consideration of architectures and element designs that take advantage of integration without restricting the array to be monolithic. Experimental and analytical studies have shown that efficient electromagnetic coupling from feed lines to radiating microstrip patches can be achieved through small apertures in an intervening ground plane. This promises array architectures that use the best substrate for each function (radiation or active circuit) with the added advantages of reliable fabrication and shielding of feed network radiation. Some of the aperture coupled configurations also may be advantageous from the point of view of cooling and module assembly or replacement.

Injection locked oscillators using FETs and microstripline or coplanar waveguide circuits have been developed as a means of providing phase controlled sources for transmitters or local oscillators. These circuits could be integrated into modules that interface with a variety of radiators and control/distribution networks. A coplanar waveguide FET amplifier similar to the one studied during this project could be used as a low noise amplifier in an integrated receiving array.

The technology developed during this project was intended for application to millimeter wave phased arrays. However, much of it is applicable at lower frequencies, as demonstrated by the scale models fabricated during the project. Also, much of the technology can be integrated in ways that have not yet been explored. These could include the use of optoelectronic controllers and exotic substrates to achieve performances beyond those described in this report. Further work in these areas is certainly needed.

MISSION
of
Rome Air Development Center

RADC plans and executes research, development, test and selected acquisition programs in support of Command, Control Communications and Intelligence (C³I) activities. Technical and engineering support within areas of technical competence is provided to ESD Program Offices (POs) and other ESD elements. The principal technical mission areas are communications, electromagnetic guidance and control, surveillance of ground and aerospace objects, intelligence data collection and handling, information system technology, solid state sciences, electromagnetics and electronic reliability, maintainability and compatibility.

Printed by
United States Air Force
Hanscom AFB, Mass. 01731

END

8-87

DTIC